SANDIA REPORT
SAND2008-8084
Unlimited Release
Printed December 2008

Plastic Neutron Detectors

F. Patrick Doty, Douglas A. Chinn, Tiffany M. S. Wilson, and
Michael J. King

Prepared by
Sandia National Laboratories
Albuquerque, New Mexico 87185 and Livermore, California 94550

Sandia is a multiprogram laboratory operated by Sandia Corporation,
a Lockheed Martin Company, for the United States Department of Energy's
National Nuclear Security Administration under Contract DE-AC04-94AL85000.

Sandia National Laboratories

Issued by Sandia National Laboratories, operated for the United States Department of Energy by Sandia Corporation.

Available to DOE and DOE contractors from
U.S. Department of Energy
Office of Scientific and Technical Information
P.O. Box 62
Oak Ridge, TN 37831

Telephone: (865) 576-8401
Facsimile: (865) 576-5728
E-Mail: reports@adonis.osti.gov
Online ordering: http://www.osti.gov/bridge

Available to the public from
U.S. Department of Commerce
National Technical Information Service
5285 Port Royal Rd.
Springfield, VA 22161

Telephone: (800) 553-6847
Facsimile: (703) 605-6900
E-Mail: orders@ntis.fedworld.gov
Online order: http://www.ntis.gov/help/ordermethods.asp?loc=7-4-0#online

SAND2008-5267816
Unlimited Release
Printed December 2008

Plastic Neutron Detectors

F. Patrick Doty, Tiffany M. S. Wilson, and Michael J. King
Engineered Materials Department
Sandia National Laboratories
P.O. Box 969 Livermore, CA 94551

Abstract

This work demonstrated the feasibility and limitations of semiconducting π-conjugated organic polymers for fast neutron detection via n-p elastic scattering. Charge collection in conjugated polymers in the family of substituted poly(*p*-phenylene vinylene)s (PPV) was evaluated using band-edge laser and proton beam ionization. These semiconducting materials can have high H/C ratio, wide bandgap, high resistivity and high dielectric strength, allowing high field operation with low leakage current and capacitance noise. The materials can also be solution cast, allowing possible low-cost radiation detector fabrication and scale-up. However, improvements in charge collection efficiency are necessary in order to achieve single particle detection with a reasonable sensitivity. The work examined processing variables, additives and environmental effects.

Proton beam exposure was used to verify particle sensitivity and radiation hardness to a total exposure of approximately 1 MRAD. Conductivity exhibited sensitivity to temperature and humidity. The effects of molecular ordering were investigated in stretched films, and FTIR was used to quantify the order in films using the Hermans orientation function. The photoconductive response approximately doubled for stretch-aligned films with the stretch direction parallel to the electric field direction, when compared to as-cast films. The response was decreased when the stretch direction was orthogonal to the electric field. Stretch-aligned films also exhibited a significant sensitivity to the polarization of the laser excitation, whereas drop-cast films showed none, indicating improved mobility along the backbone, but poor π-overlap in the orthogonal direction.

Drop-cast composites of PPV with substituted fullerenes showed approximately a two order of magnitude increase in photoresponse, nearly independent of nanoparticle concentration. Interestingly, stretch-aligned composite films showed a substantial decrease in photoresponse with increasing stretch ratio. Other additives examined, including small molecules and co-solvents, did not cause any significant increase in photoresponse.

Finally, we discovered an inverse-geometric particle track effect wherein increased track lengths created by tilting the detector off normal incidence resulted in decreased signal collection. This is interpreted as a trap-filling effect, leading to increased carrier mobility along the particle track direction. Estimated collection efficiency along the track direction was near 20 electrons / micron of track length, sufficient for particle counting in 50 micron thick films.

This page intentionally left blank.

Contents

Tables

Figures

Summary

Conductive polymers have been intensively developed over several decades and are now in use for applications including light emitting devices, displays, and photocathodes for xerography. This project was undertaken to investigate the feasibility of exploiting these materials for detection of nuclear radiation. These materials typically exhibit very high resistivities and dielectric strengths, as well as low dielectric constants, which promise low noise operation with respect to leakage currents, breakdown, and capacitive effects, respectively. Furthermore, because of their hydrogen content and low photoelectric cross sections for x- and gamma radiation, they are particularly interesting as neutron conversion/detection media.

Strides have been made in the chemistry of conjugated organic systems over the years, but questions remain about the fundamental physics of charge generation and transport in these materials. Therefore, one objective of this work was to elucidate relationships between the polymer molecular ordering and transport of positive and negative carriers excited by radiation. Accurate physical models for electrical properties and their dependence on structure and processing observables will enable prediction of device performance and could also lead to model-informed discovery of new materials for challenging applications such as photovoltaic power conversion.

At the outset, this project was divided into three major tasks: New synthesis of ordered polyacetylene through ring opening metathesis polymerization (ROMP), long-range ordering of poly(paraphenylene vinylene) derivatives (PPVs) via phase separation techniques, and long range ordering through stretch-orientation of PPV. The latter approach was found to be the most viable, and relationships between structure, processing, environmental effects, and charge collection were thoroughly investigated for this system.

Using novel methods of stretching Teflon substrates supporting thick PPV films cast from styrene solutions, we showed a functional relationship between order measured by IR dichroism and the fast component of the photocurrent. We also quantified large improvements in photoconductivity by addition of fullerenes and by optical pumping with sub-bandgap light. Proton beam studies were used to relate the photoconductive response to recoil proton response, and to quantify tolerance of these materials to fast protons. Our results clearly showed that proton beam dosimetry is a feasible commercial application, and that stretch-ordered PPV may be viable for use as a neutron counting detector.

This page intentionally left blank.

1. Polymers for Radiation Detection

1.1 Materials selection

A single polymer was chosen for detailed studies. The selection was made on the basis of air stability, commercial availability, dielectric properties, and resistivity. The ability to process stretched films was also considered, and preliminary investigations were made to stretch-align a number of polymers. The family of poly(*p*-phenylene vinylene)s, or PPVs, seemed to work the best. We had also found a unique solvent enabling concentrated solutions of PPVs, and therefore casting into thick films from solution. Very thick films would be necessary to efficiently interact with neutrons. This was in line with other requirements, since PPVs are known to be reasonably air stable and have mobilities in the range of 10^{-5} cm^2/Vs to $1x10^{-2}$ cm^2/Vs. To improve the sensitivity to fast neutrons, a high ratio of hydrogen to carbon was necessary, which could be achieved with long, hydrogenous side chains. Therefore poly[2,5-bis(3′,7′-dimethyloctyloxy)-1,4-phenylenevinylene], as shown in Figure 1, was chosen for study. This material was commercially available from at least two suppliers and reasonably soluble in the polymer state. It was also found to have some of the highest hole mobility for a highly branched PPV. This will hereafter be referred to as OC10PPV.

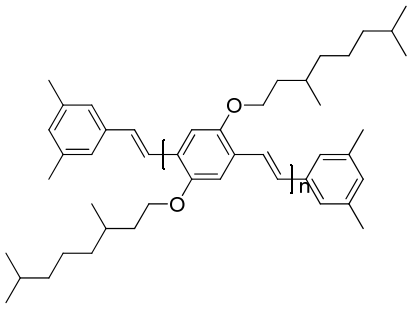

Figure 1. Chemical structure of OC10PPV.

1.2 Figure of merit

The quality of semiconductors for radiation detectors is ranked by their μτ products, with μ being mobility and τ being the trapping time referred to deep states. Subscripts of e and h are commonly used to denote electrons and holes. For a uniform electric field and negligible de-trapping, charge collection efficiency (CCE) can be given by the Hecht equation:

$$CCE = \frac{Q}{Q_o} = \frac{\tau_e \mu_e E}{L}\left[1 - \exp\left(-\frac{(L - x_o)}{\tau_e \mu_e E}\right)\right] + \frac{\tau_h \mu_h E}{L}\left[1 - \exp\left(-\frac{x_o}{\tau_h \mu_h E}\right)\right] \qquad 1\text{-}1$$

Q is the total charge collected, Q_0 is the total charge created, L is the detector thickness, x_o is the distance from the cathode to the point of charge creation, and E is the applied electric field. Due to the low mobility of polymers, $\mu E << x_o$, and the exponential terms go to zero. Therefore for a hole transport polymer:

$$CCE \approx \frac{\tau_h \mu_h E}{L} \qquad 1\text{-}2$$

This equation implies that CCE scales linearly with both field and channel width, therefore new figure of merit can be defined by:

$$FOM = \frac{CCE \times L^2}{V} \qquad 1\text{-}3$$

where L is the device width and V is the applied voltage. This figure of merit has dimensions of $\mu\tau$, but it is not strictly a material property since experimentally it varies with device geometry, field, and integration time. However, it affords a convenient means to rank materials and evaluate processing effects on transport.

2. Conductivity Transients

2.1 Experimental Setup

OC10PPV was obtained from American Dye Source in Quebec, Canada and used without further processing. The polymer was spun-cast or applied after stretching onto substrates of interdigital transducer (IDT) structures with gold electrodes on glass, as shown in Figure 2. The electrode gap could be varied from 4, 8, 16, 32, or 64 μm, and the electrode width was 4 μm.

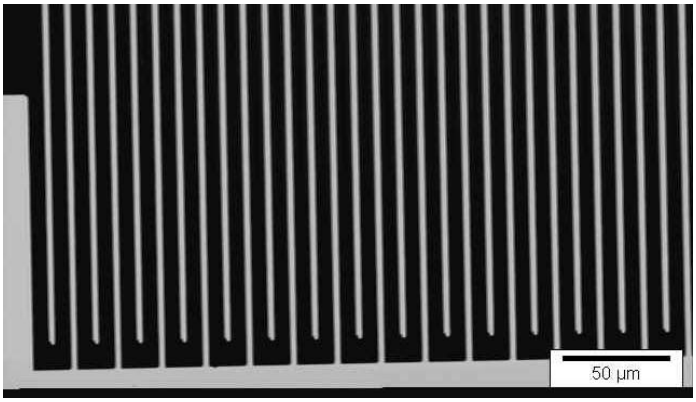

Figure 2. Portion of IDT. For the one shown, electrodes are nominally 4 μm (light) and spacing between is nominally 16 μm (dark).

The electronic setup for both proton and photoconductivity testing was used as diagrammed in Figure 3. The photoconductivity stimulus used a 337 nm nitrogen laser, shifted to 590 nm with a rhodamine dye cell. The laser could be linearly polarized, and then rotated if chosen. It was then focused on the back of the IDT. The charge was collected for 10 μs.

For proton exposure testing, a 3 MeV tandem accelerator was used. The pulsed beam was swept past a variable slit in order to vary the total exposure. For proton exposure testing, the sample was held under vacuum and for photoconductivity testing, the sample was in air. All experiments were performed at room temperature.

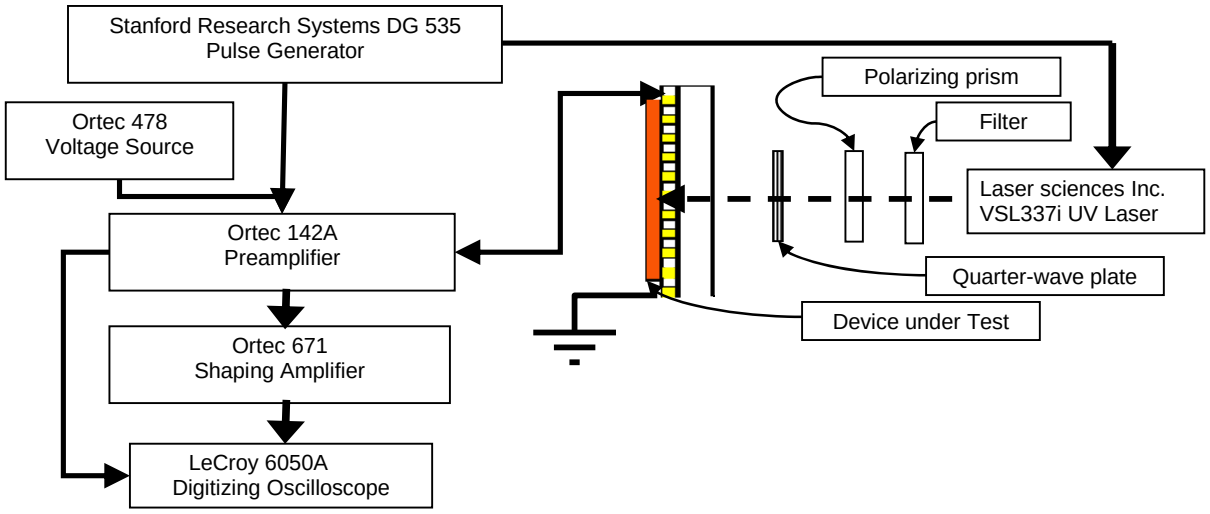

Figure 3. Diagram of setup for photoconductivity testing.

Example photoconductive traces are shown in the figure below. The time base is 500 μs per division. The lower trace is the direct preamplifier output, and the upper trace is the output from the 671 spectroscopy amplifier with a 10 μs shaping time. A significant portion of the charge can be integrated within the first 10 μs, but clearly mobile charge continues to be collected over a greater time scale. The preamp output is seen to be rising for 100 μs, where the waveform is clearly distorted by the 400 μs resistive reset time constant of the amplifier, and the shaping amp output is non-Gaussian, and does not return to baseline for several milliseconds. For particle counting however 10 μs was determined to be a practical shaping time, and this setting was used throughout the study.

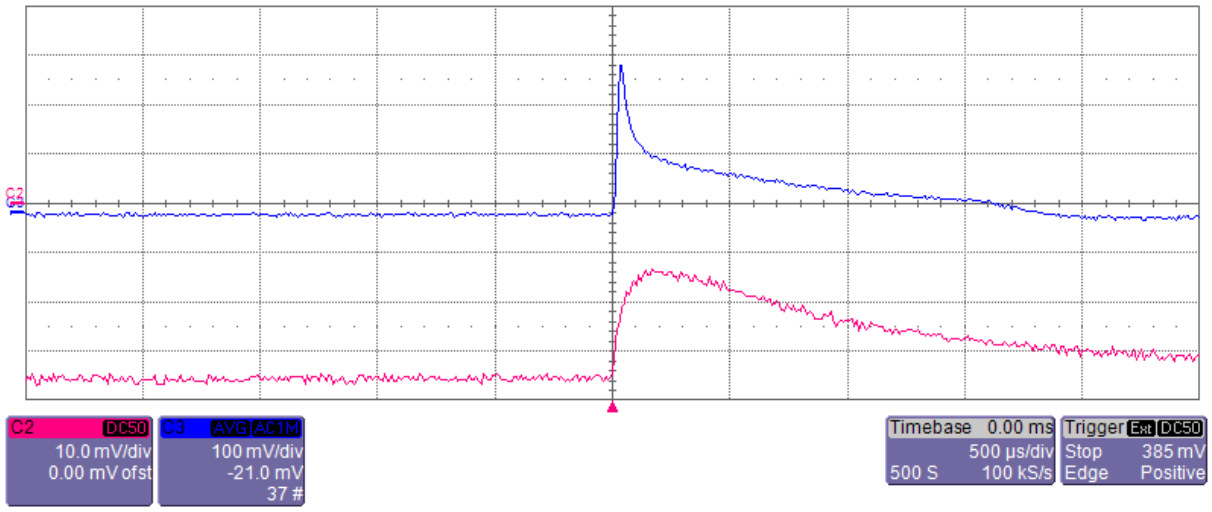

Figure 4. Oscilloscope traces.

2.2 Comparison of photon and proton stimuli

Transient response of spin-cast PPV films is seen below. Photoconductive (PC) response was compared with the fast-proton sensitivity was determined using Sandia's 3 MeV tandem proton accelerator in Livermore, CA. A 0.6 μm thick film of OC10PPV showed a distinct ion-induced conductivity transient response, as shown in Figure 5. For comparison, the photoconductivity transient results are also shown for a similar sample, using a 590 nm laser. The charge collection efficiency was calculated assuming 1000 ion pairs per micron of track length, a polymer band gap of 2.5 eV, and the observation that 3 times the gap energy is required to produce an ion pair in typical semiconductors [4]. For photoconductivity calculations, a quantum efficiency of 0.1 was used, based on published estimates.

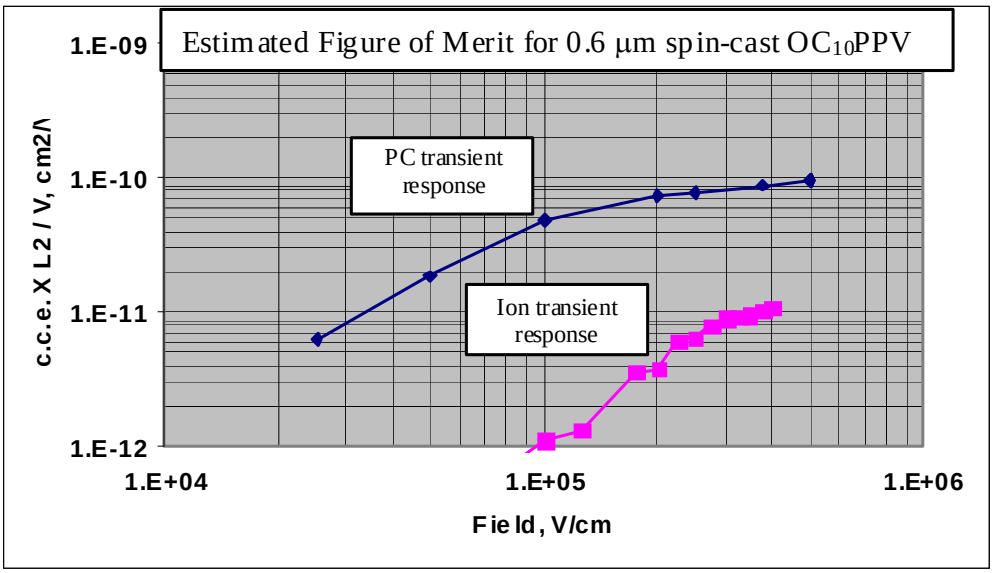

Figure 5. Figure of merit using 3 MeV proton beam stimulus, showing photoconductive (PC) transient with 590 nm laser for comparison, based on a 10 μs collection time.

The two curves are well correlated, indicating that the PC method can be used as a surrogate for evaluating effects of structure and processing variables. This is beneficial as photoconductivity testing is far less involved and less costly for routine material testing. A particle gain can be defined for this device in terms of electrons collected per proton subtending the 0.6 μm thick film detector. This gain is plotted in Figure 6 below.

The above encourages further evaluation of this material for radiation detectors. It indicates that direct electronic detection of single fission neutrons may be feasible in conjugated polymer-based detectors using standard laboratory electronics at room temperature, though thicker devices will be necessary.

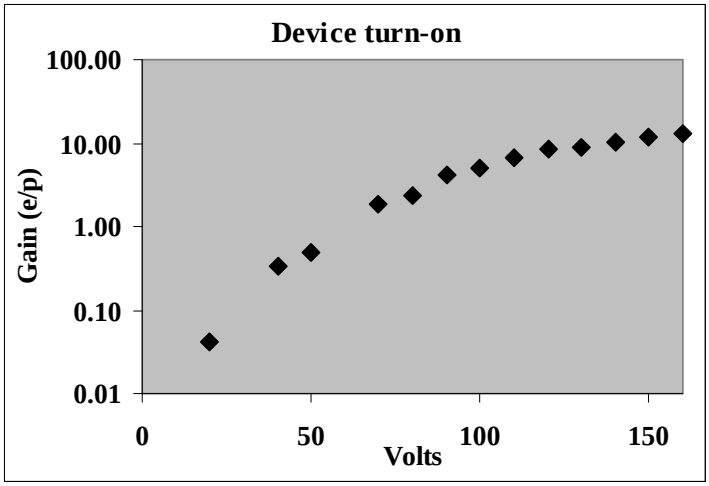

Figure 6. Gain as a function of bias voltage for a 0.6 μm thick film of OC10PPV in a proton beam.

2.3 Total dose sensitivity

The polymer film was tested for ion-induced degradation of the response, and the results are displayed in Figure 7 for two different IDTs, normalized to the maximum response for each. Dose and dose rate were increased by a factor of two between each data point by doubling the rep rate for a fixed period of time. The rate was then lowered to 10 Hz to test the response. The onset of degradation appears to occur at a total absorbed dose of about 1 Mrad, which is similar to the dose degradation that is typically seen in plastic scintillators.

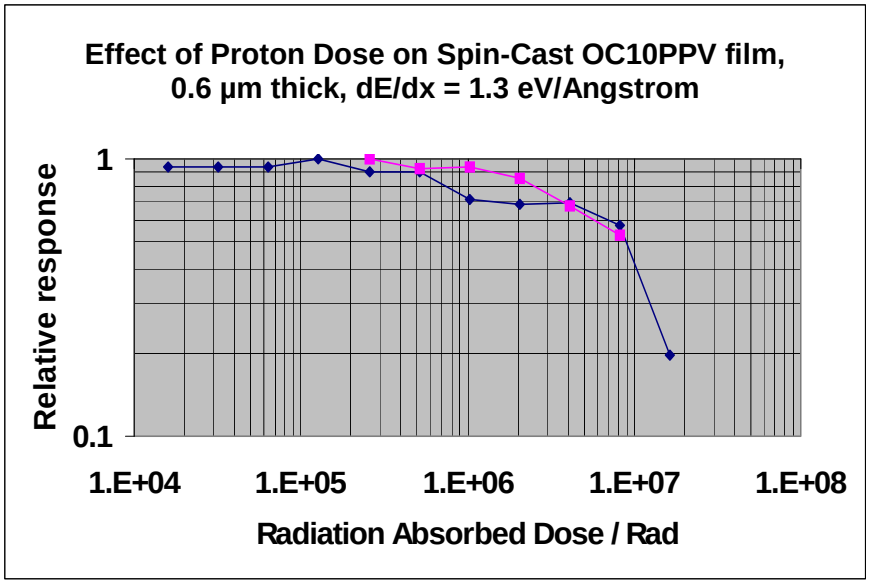

Figure 7. Proton radiation tolerance of OC10PPV device, tested in two locations.

3. Environmental Sensitivity

Environmental characterization was done using a branched PPV, poly[2-methoxy, 5-(2-ethylhexoxy)-1,4-phenylene vinylene], commonly referred to as MEHPPV. MEHPPV is readily available and is the most commonly used PPV for solar applications.

Using interdigitated gold electrode structures (IDT)s similar to those used for proton exposure testing, films were cast from a solution of 3 wt% MEHPPV onto a 32 μm IDT structures to test for electrical properties, transient effects, and environmental sensitivity. Testing was done in an enclosed box for electrical and light shielding. Background noise for a 2 Gohm resistor was found to be less than 100 fA. The only light included was the room light that could come in a 1 cm diameter hole in the lid of the test box, which was also closed off unless otherwise stated. Initial testing was for sensitivity to low intensity light such as room lighting to see how much this could affect measurements. Figure 8 shows the resistance in GΩ of the same sample measured, but once exposed to a blue LED and the other time with the LED turned off, but not moved. Other light exposure to the sample was negligible. This effect appears to be transient, perhaps with traps filling due to previous light exposure. The sampling rate was the same for both tests, just one was stopped earlier. Even with a low intensity light that is not at an optimum energy to excite the material, this is clearly an important variable to consider for electrical testing, and future tests need to be done in complete darkness.

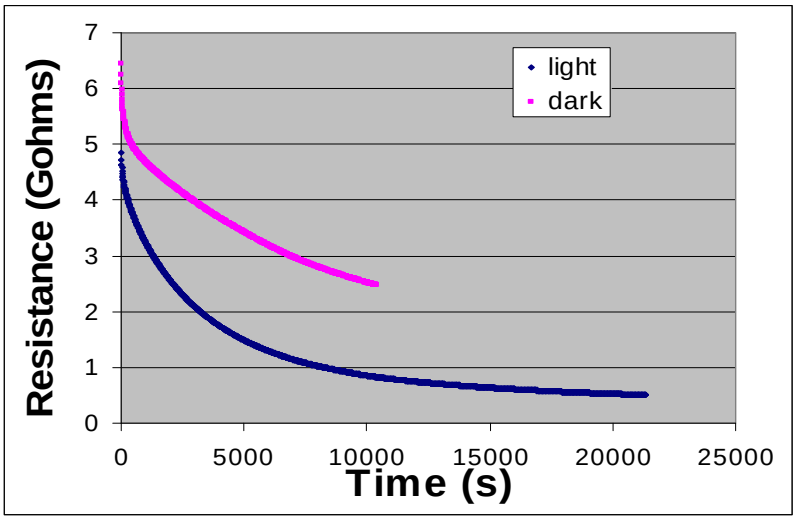

Figure 8. Resistance across a 32 μm IDT of MEHPPV, with or without a blue LED, with 3 V bias.

The next test examined the effects of pulse frequency of the same LED, which could be related to the trap filling and release rate. As shown in Figure 9, the resistance drops as the LED frequency increases within the pulse frequency range that was measured, from 0.05 to 0.4 Hz. This could mean that traps are continually being filled and that the time between pulses is not long enough for the traps to empty to a greater degree than they are filled with each pulse. It is also possible that the net energy given off with the LED is higher at a higher frequency and this was not measured for control.

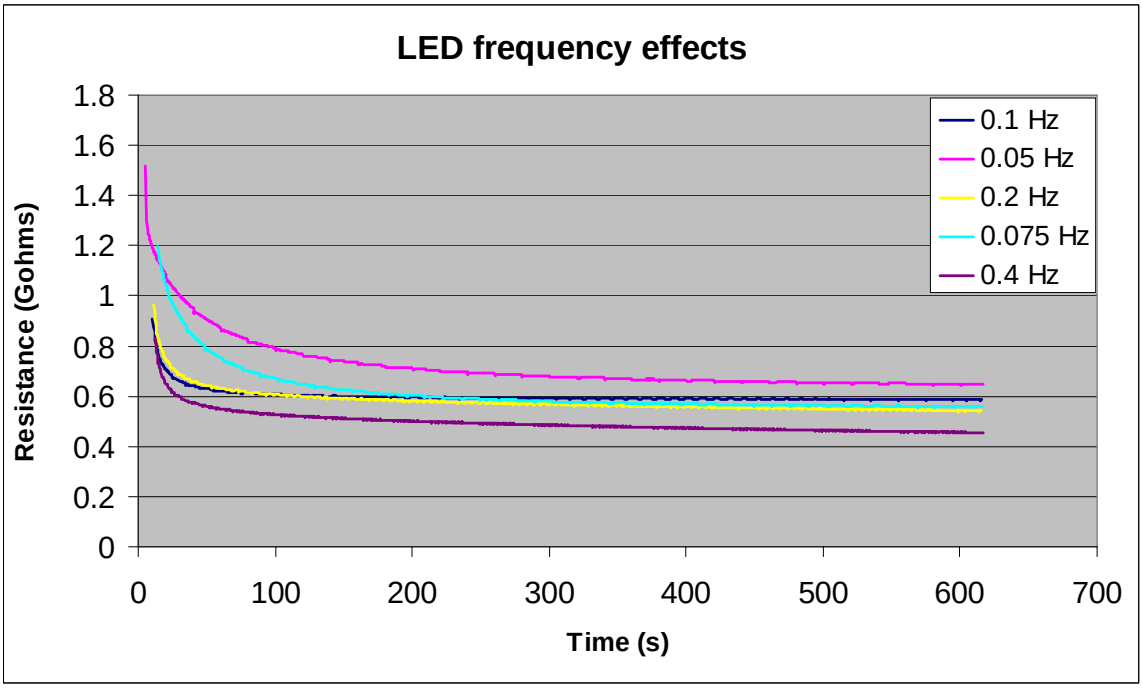

Figure 9. Sensitivity to LED pulse frequency of 32 μm IDT of MEHPPV, with 3 V bias.

It is also important to evaluate the sensitivity of the material to environmental variables such as air, moisture, and temperature. The current was monitored over long periods of time while monitoring or changing environmental conditions. This was again done using a drop cast film of MEHPPV on an IDT with 32 μm gap spacing and done in complete darkness. Figure 10 is quite interesting, showing an overlay of the monitored IDT current and room temperature. The thermostat control of the laboratory was excellent, with the total temperature varying only 1 °C over three days, but this was still enough to cause current fluctuations across the IDT of approximately 10 pA. This was done with a bias of only 1 V across the sample so the effect likely could have been drowned out by high current at higher bias, but it is important to note that the sample response is distinctly, consistently sensitive to small fluctuations in temperature. There are literature reports of thermally activated photocurrent and increases in current with increasing temperature in MEHPPV, which would tend to agree with this data [1, 3]. The general trend of increasing current with increasing temperature is not surprising, but what is surprising is the sensitivity to such small temperature changes. As the laboratory does not have a method for such precise temperature control, this is a potential source of error in future measurements. However, this is much less of a concern at the higher fields used for radiation detection. The general trend of decreasing current is likely due to the slow loss of the effect of previous light exposure as the sample was tested in darkness.

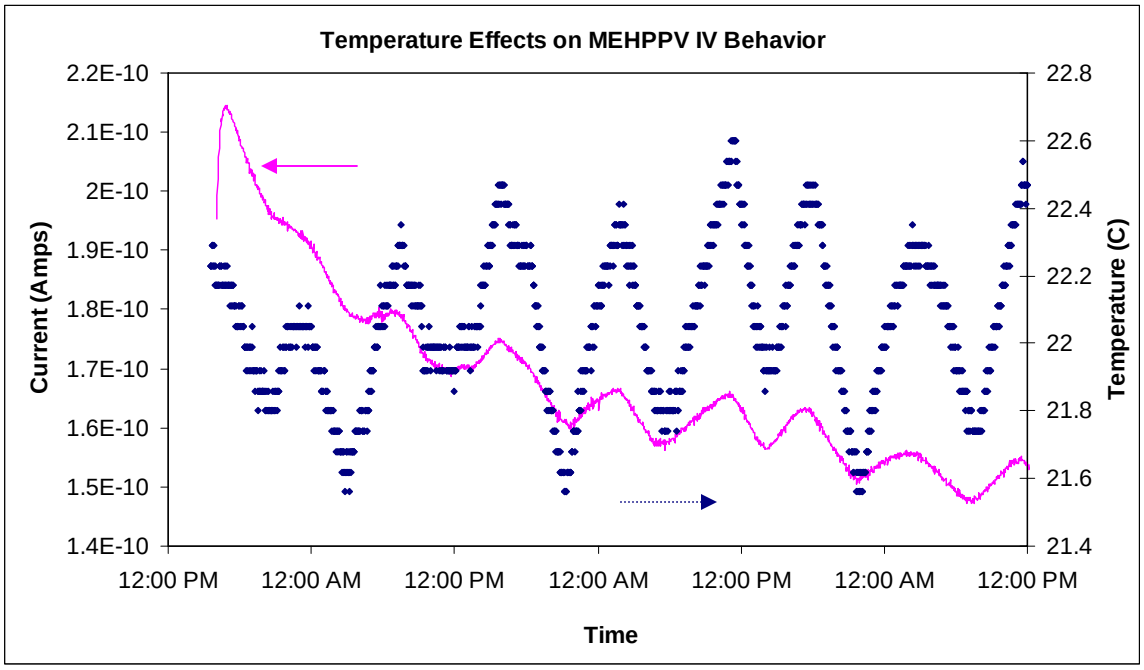

Figure 10. Overlay of room temperature (blue dots) and current (pink line) for MEHPPV 32 μm IDT with 1 V bias in room air.

Next, the effects of ambient air and dry air were monitored and the results are depicted in Figure 11 below. In order to partially reduce temperature effects, a slightly higher bias of 3 V was used for these tests. The sample was first tested with a 3 V bias in ambient air over 60 hours to allow the resistance across the IDT to completely stabilize in the given conditions. Dry air conditions were then achieved by placing desiccant packs in the bottom of the electrical testing box. After a day with the desiccant pack the test chamber was measured to have less than 1% relative humidity. Resistance of the MEHPPV across the IDT was monitored again over 60 hours in the dry air conditions. There is some initial transient, likely due to remaining effects of room lighting and possible remaining humidity, so the test was repeated in the dry atmosphere without opening the chamber. This helped assure that the sample was dry and the chamber was as dry as possible. The resistance was very repeatable and the transient effect was reduced. The desiccant packs were then removed and some time was allowed for the chamber and the sample to return to ambient conditions.

The transient test was then repeated to determine if the effects were reversible and indeed it does appear do be completely reversible. The large transient present in the initial test is not present in the repeat test. However, this is more likely due to the increased amount of time that the sample was allowed to rest with the chamber closed and in the dark, rather than to any effect of the humidity. The inset is shown zoomed in to better show the stabilized resistance after a long settling time, which is the more important data. There is some instability, which could be temperature fluctuations, but the overall trend is still quite clear, with the dry tests both showing resistance across the IDT of approximately 0.2 GΩ, and the ambient tests, both before and after the dry air tests showing resistance of approximately 0.4 GΩ.

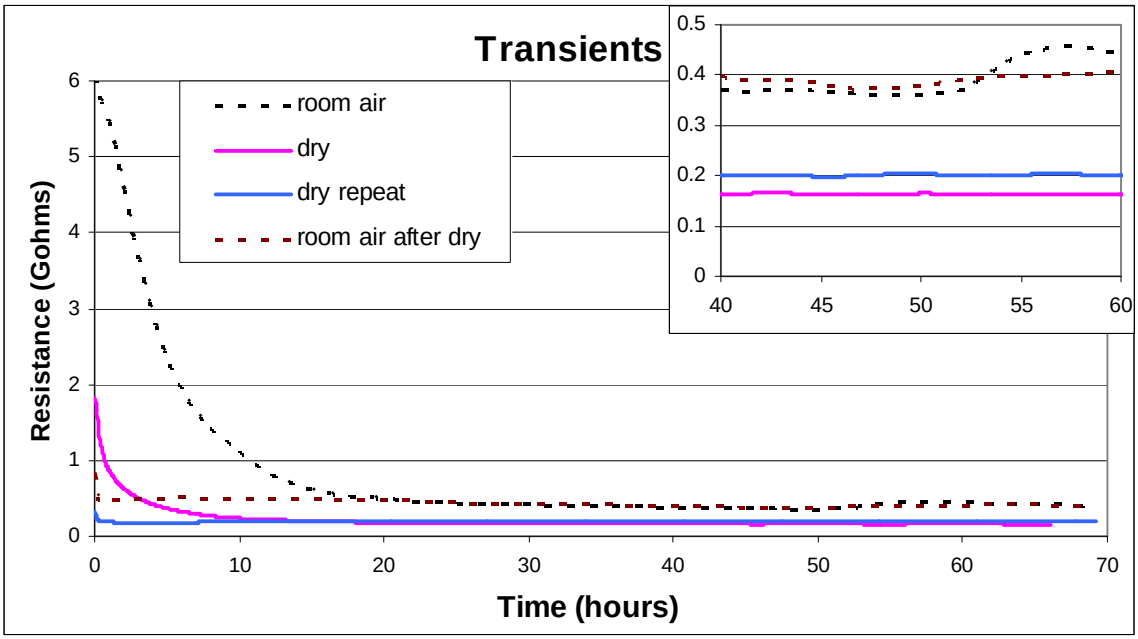

Figure 11. Resistance of 32 µm MEHPPV IDT in room air (black dashes) and dry air (pink, repeated in light blue), then returned to room air (dark red dashes), measured with a bias of 3 V (inset: close-up of stabilized resistance at long time scale).

The sample chamber was then purged with dry nitrogen while the sample resistance was monitored. As shown in Figure 12a, the resistance rather quickly increased over the first seven hours, then appeared to be leveling off. Interestingly, this indicates that there is more of an effect than just the humidity effect that was seen with the dry air test, as this is trending in the opposite direction of the dry air, which showed lower resistance than room air. The sample was left in the sample chamber under dry nitrogen flow and monitored for the next two weeks, and the results are shown in Figure 12b. Note that there is some time lag between the short time scale plot in Figure 12a and the long time scale figures, so the resistance at the start of Figure 12b is initially higher. The large dip on day six was from an experiment with an increase in the nitrogen flow. The nitrogen flow may have had additional effects such as altering the temperature. Other local variations could also be due to temperature as previously discussed. Another perturbation at day 10 was tested when the nitrogen purge was briefly removed, exposing the sample to room air, then re-inserted. This portion of the data is shown expanded in Figure 12c. Upon removal of the nitrogen purge and exposure to ambient air, the resistance quickly decreased at a rate of 0.18 Gohms/min. The nitrogen purge was then replaced and the resistance slowly restored to previous values at a rate of 0.05 Gohms/min. This is difficult to analyze since the concentrations of various gases in the surrounding environment are not well known, but it is intriguing how different the two rates of change are, indicating this may not be simple diffusion effects. The data for Figure 12 was taken at a bias of 0.1 V except the perturbation at day 6, which was taken at 4 V.

(a)

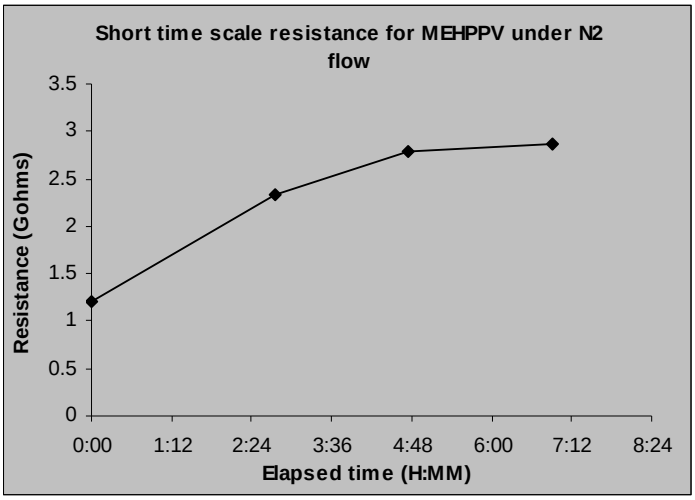

(b)

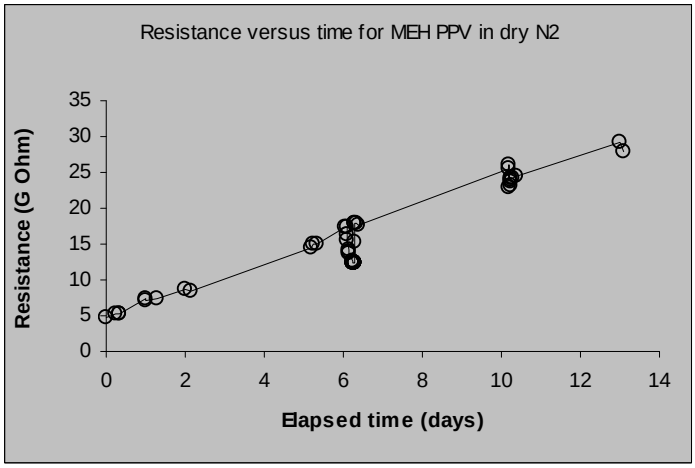

(c)

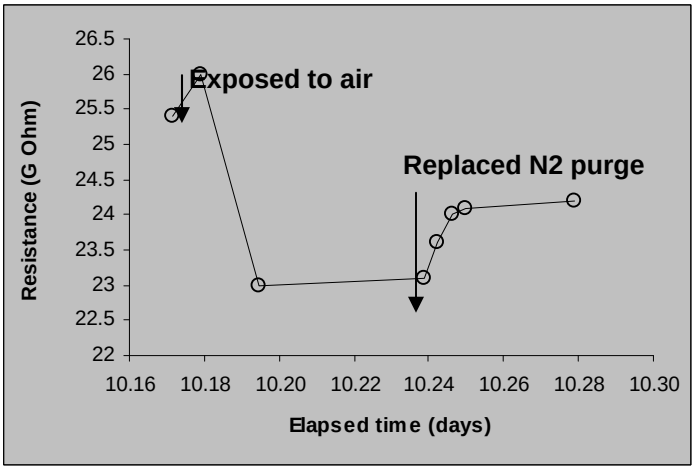

Figure 12. (a) Short time scale resistance across a MEHPPV 32 µm IDT upon exposure to dry nitrogen. (b) Long time scale resistance under dry nitrogen flow for MEHPPV 32 µm IDT. (c) Close-up of day 10 perturbation when nitrogen purge was removed and replaced.

In order to best visualize the dramatic difference in the environmental impacts on MEHPPV, Figure 13 shows an overlay of the ambient air, dry air, and dry nitrogen transient resistance data.

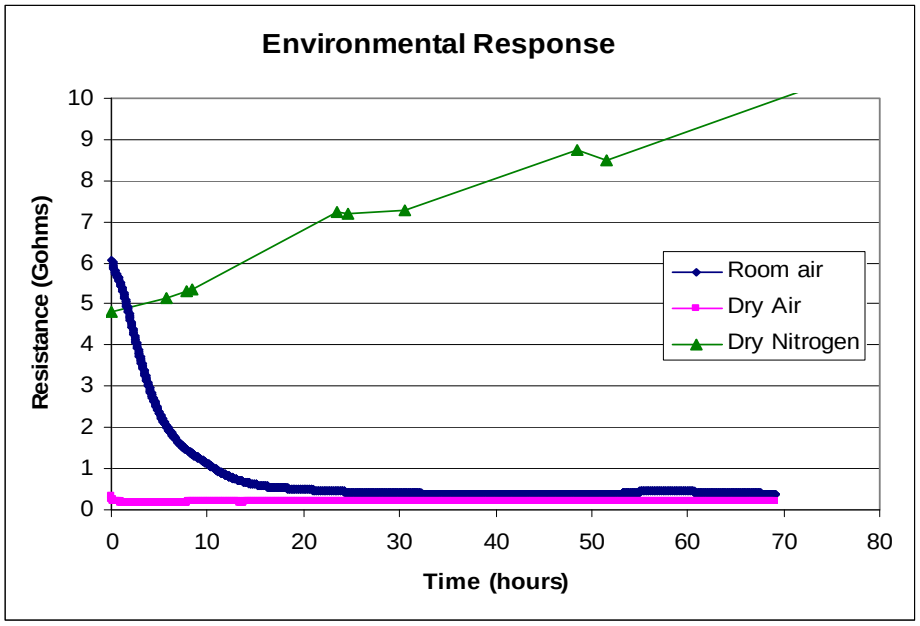

Figure 13. Resistance of MEHPPV IDT in room air, dry air, and dry nitrogen environments.

By comparison, similar tests were also performed on OC10PPV films, and the polymer was not nearly as sensitive to environmental conditions, particularly the dry nitrogen effect seen with MEHPPV. Figure 14 shows transient tests done on a 16 μm IDT of OC10PPV with a 3 V bias under conditions of ambient air, dry air, and dry nitrogen. The small fluctuations in each test are likely due to room temperature changes.

Optical properties of the films were also important, and how they were impacted by the environment. Two MEHPPV films were prepared on glass slides; one was stored in room air and one in a nitrogen purged glovebox for several weeks. They were then tested for their excitation and emission spectra. As shown in Figure 15, their overall spectra did not change dramatically between the two samples, but the absolute intensities of different peaks changed significantly. Peaks did not generally appear or disappear, but did change in relative intensities. For the sample stored in air, the peak at 589 nm is the strongest excitation, but for the sample stored in the glovebox, the peak at 467 nm has a stronger excitation.

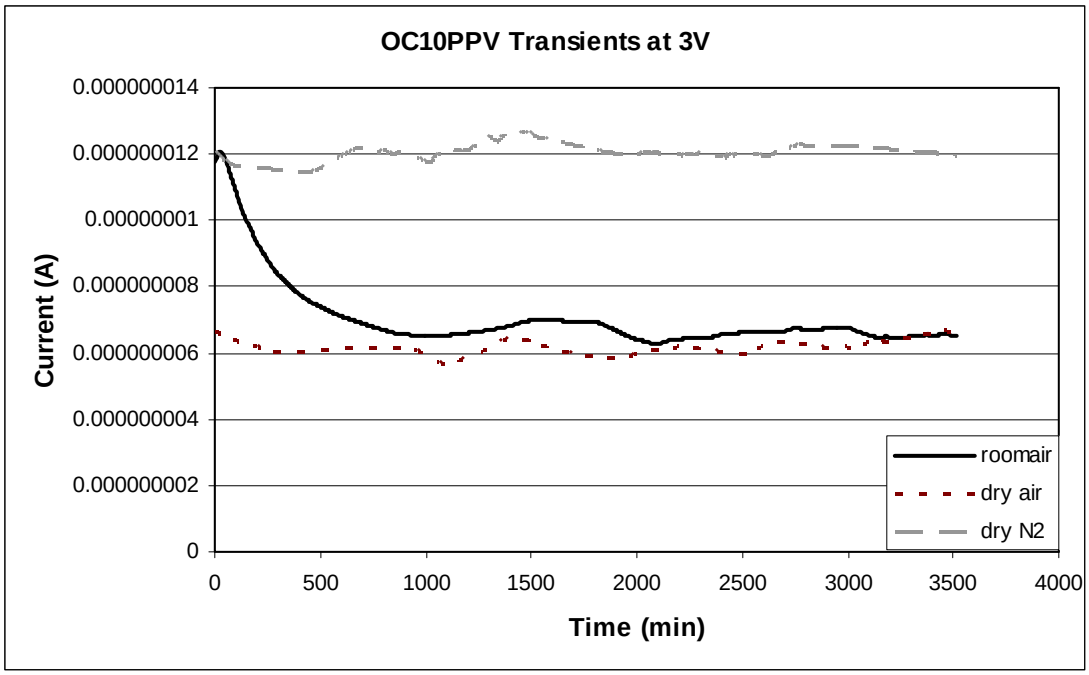

Figure 14. Transient current tests with 3 V bias across 16 μm OC10PPV films in ambient air, dry air, and dry nitrogen.

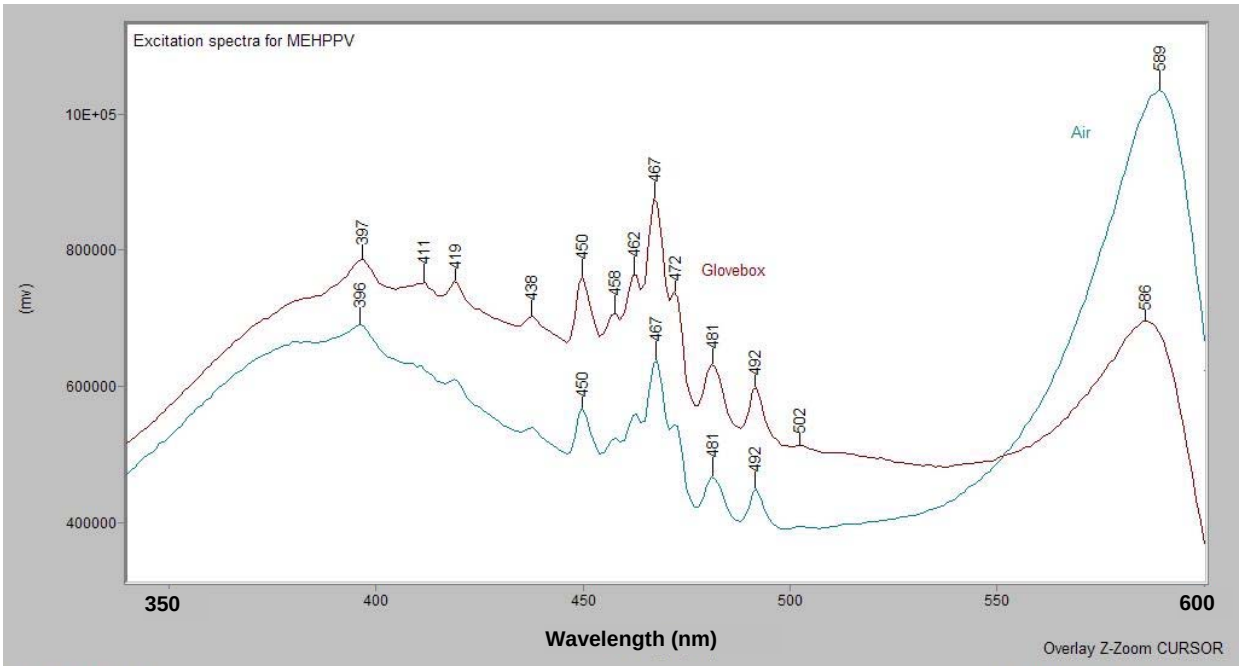

Figure 15. Excitation spectra for two films of MEHPPV, one stored in air (green) and one in a nitrogen purged glovebox (red).

Emission spectra were then taken, using both 467 nm and 590 nm as the excitation wavelengths. Figure 16 shows the emission spectra excited at 467 nm. The sample stored in the glovebox shows a higher overall intensity, which is logical since this was the wavelength of its peak excitation. More interesting though is that the sample stored in air exhibits a shoulder and the sample stored in the glovebox shows minimal if any sign of a shoulder. Figure 17 shows the emission spectra excited at 590 nm. The sample stored in air is correspondingly more intense, but this time the two samples show nearly identical shape and structure.

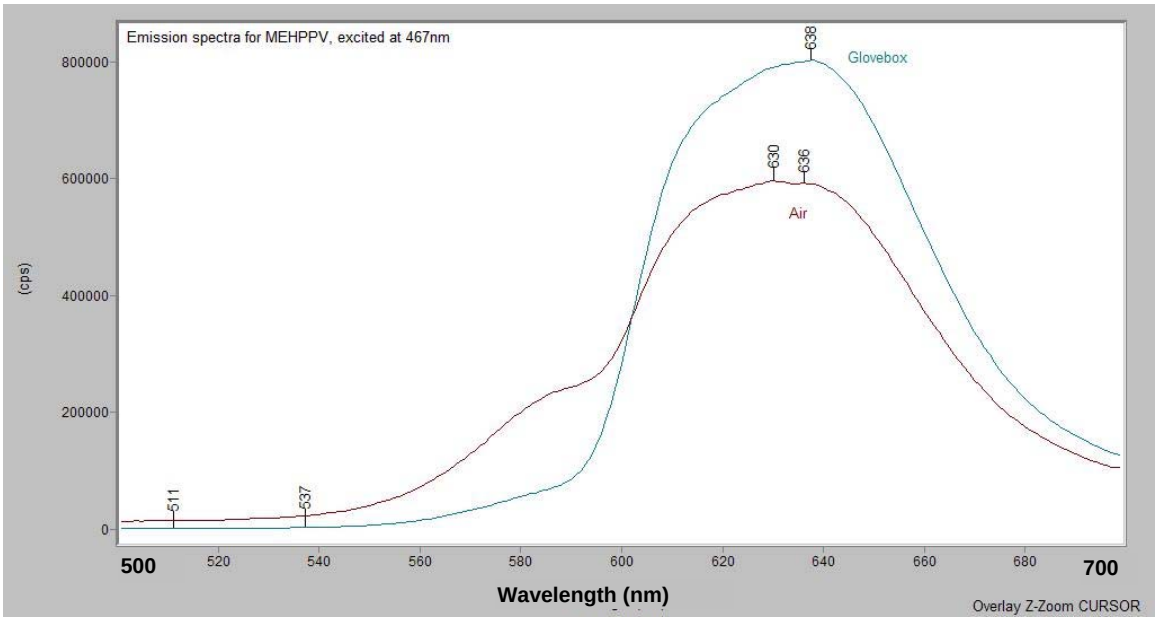

Figure 16. Emission spectra for MEHPPV, excited at 467 nm, for samples stored in air (red, bottom) and in a nitrogen glovebox (green, top).

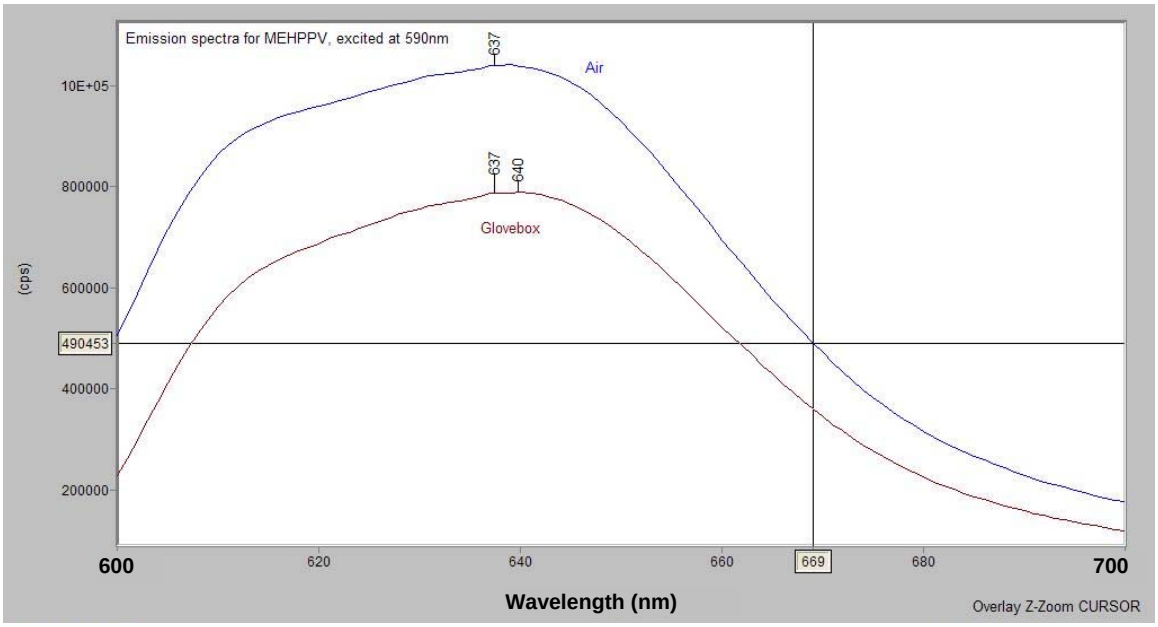

Figure 17. Emission spectra for MEHPPV, excited at 590 nm, for samples stored in air (blue, top) and in a nitrogen glovebox (red, bottom).

This page intentionally left blank.

4. Stretch-Orientation

4.1 Experimental setup

Post-polymerization mechanical stretching was used to align bulk polymer films. The apparatus used for stretch-alignment was designed and built by Sandia and is diagrammed in Figure 18. Ten-mil-thick polytetrafluoroethylene (PTFE) tape was applied to the stretcher with the edges rolled under and clamped. The tape was pre-stretched ¼" to provide a flat surface. The edges of the tape were marked and measured. Solutions were drop cast onto the top (non-sticky side) of the tape on the stretcher and the solvent allowed to evaporate until the film was just visibly dry. The tape was then stretched using a screw mechanism and rotary motor with adjustable speed. Because of some slipping of the tape during stretching, the markings on the tape were used to determine the final stretch ratio, rather than the movement of the clamps. Operations were performed in a glovebox purged with dry nitrogen.

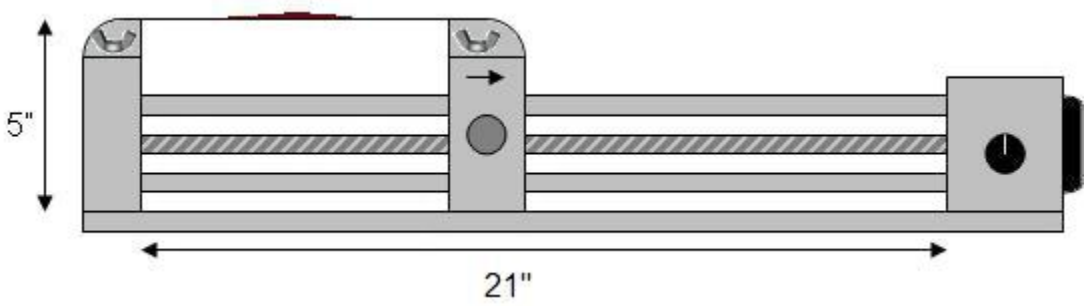

Figure 18. Diagram of stretching apparatus.

4.2 Method comparison

The polymer films were processed in varied ways and ordered through the stretch-aligning process. A method was needed to quantify the order in the films, ideally without destroying the films since the polymer is relatively expensive and it is convenient and minimizes error to characterize the same sample over multiple tests. Therefore, several methods were examined in order to determine what measurement technique is best suited for measuring order in these polymer films. Polarized infrared (IR) spectroscopy has been shown to give quantitative agreement with X-ray diffraction and birefringence methods for appropriate samples. X-ray diffraction is non-ideal because it is not strongly sensitive to amorphous order. Differential scanning calorimetry, or DSC, has a similar weakness, and is not ideally suited for measurement of films. Additionally, DSC is destructive to the film.

Atomic force microscopy can show surface order, but not true bulk order of the entire film. Scanning electron microscopy is not as quantitative and can be destructive to the sample and

have very difficult sample preparation, especially with soft materials such as PPV. Polarized UV-Visible spectroscopy is very similar to polarized infrared spectroscopy, but in this case the absorption peaks are much broader and thus more difficult to quantify. Additionally, these films are very absorbent in the visible range so using this technique would be difficult for thick films as the absorbance would become higher than the accurate range of the spectrometer. This was tested with several samples and found to be the case.

Due to the aforementioned weaknesses with these other methods and relative ease of FTIR, infrared dichroism was chosen as the more ideal measurement method. Infrared dichroism is simple and non-damaging to the film, while providing a quantitative measure of order.

4.3 Infrared dichroism background

By exposing a polymer film to polarized light, the vibrations will be preferentially excited at the polarization that is closest to the transition dipole for that vibrational excitation. By comparing the absorbances at orthogonal polarizations, a measure of the material order can be derived. Since it is calculated as a ratio, the thickness does not need to be measured for each sample.

The dichroic ratio, *R*, is calculated separately for each absorbance peak. It is defined as the ratio of the integrated absorbance with the sample orientation parallel to the polarization, $A_{\parallel}$, to the absorbance with the sample orientation orthogonal to the polarization, $A_{\perp}$. A material that is purely amorphous or randomly oriented will have a dichroic ratio of one, as all directions appear the same; perfectly ordered, aligned materials will typically tend away from one. The dichroic ratio is a function of the angle of the transition dipole for each mode relative to the chain axis, α. A transition angle of 54° results in a dichroic ratio of 1, and as α for a specific absorbance peak departs from 54°, the mode will show greater dichroism. An absorbance band with a dichroic ratio of greater than one is referred to as a pi band, and a band with a ratio less than one is a sigma band [2]. As the order of the material is increased, the dichroic ratios will change in a quantifiable manner. From the measured dichroic ratio, it is possible to calculate the Hermans orientation function. This calculation treats the polymers as rigid rods oriented preferentially in the stretch direction, but with some distribution of angles about the stretch direction. The measured dichroic ratio is first related to α and the orientation parameter, *s*, according to equation 4-1.

$$R = \frac{2\cos^2\alpha + s}{\sin^2\alpha + s} \qquad 4\text{-}1$$

The angle α is generally not known, but can sometimes be estimated theoretically or from similar molecules reported in the literature. For a PPV film, the vibrational mode at 966 cm^{-1} is an out-of-plane CH vibration, which is expected to have a moment of 90° for a planar molecule. Experimental results have determined the value of α to be 82° to 84°. We now have an estimate of α for at least one absorbance peak, so *s* can be calculated from equation 4-1, and used to calculate the Hermans orientation function, *f*, using equation 4-2.

$$f = \frac{2}{3s+2} \qquad 4\text{-}2$$

For a completely ordered sample, the Hermans orientation function will approach one and for a perfectly disordered sample, it will approach zero. The dichroic ratio will be different for most peaks unless they have the same transition angle, but the orientation function should agree within reasonable error for all peaks. Reports on PPV precursor ordering have published a Hermans orientation function of as high as 0.96, reaching a plateau with a draw ratio of 5-7.

Kratky proposed a model for the orientation mechanism in a drawing process such as the one reported here, beginning with an unoriented sample and ending with a distribution function about the draw direction [3]. This mechanism assumes a constant density, and thus it has been shown to be inaccurate for drawn PPV precursor, which loses volume as it is converted to polymer during the thermal elimination process [5, 9]. However, since in this case there is no thermal elimination, the stretch orientation should be close to constant density, and the Kratky model should hold. For a constant density, the Kratky model is thought to be an upper bound, as orientation is more often limited by melting or softening and viscous flow limiting the actual degree of orientation [3]. The Kratky model, *F*, was derived from equations found in Zbinden, section V.4 [3] to be equation 4-3, with *v* defined to be the draw ratio l/lo.

$$F = 1 - \frac{v^3}{v^3 - 1} + \frac{v^3}{\left(v^3 - 1\right)^{3/2}} \cos^{-1}\left(v^{-3/2}\right) \qquad 4\text{-}3$$

4.4 FTIR spectrum

Infrared spectra were obtained using freestanding films and a Digilab FTS 7000 with nitrogen purge and a KRS-5 wire grid polarizer with 0.4 μm spacing, when applicable. The polarizer was obtained from International Crystal. It provides polarization in the range of 2 – 35 μm, with 99% polarized at 10 μm and >88% at 3 μm according to the manufacturer specifications. A sample spectrum taken with no polarizer of a film of OC10PPV is shown in Figure 19. Table 1 lists selected peaks and their likely origin.

Based on the absorption and likely origin, the peaks near 1256, 1206, and 966 wavenumber will be followed for analysis. The absorbances at 1256 and 1206 cm^{-1} are very distinct and respond in opposite directions to polarization, making them of interest. For a PPV film, the vibrational mode at 966 cm^{-1} is an out-of-plane CH vibration expected to have a moment of 90°, making this a good choice to follow [6]. Experimental values of 82° and 84° have been reported.

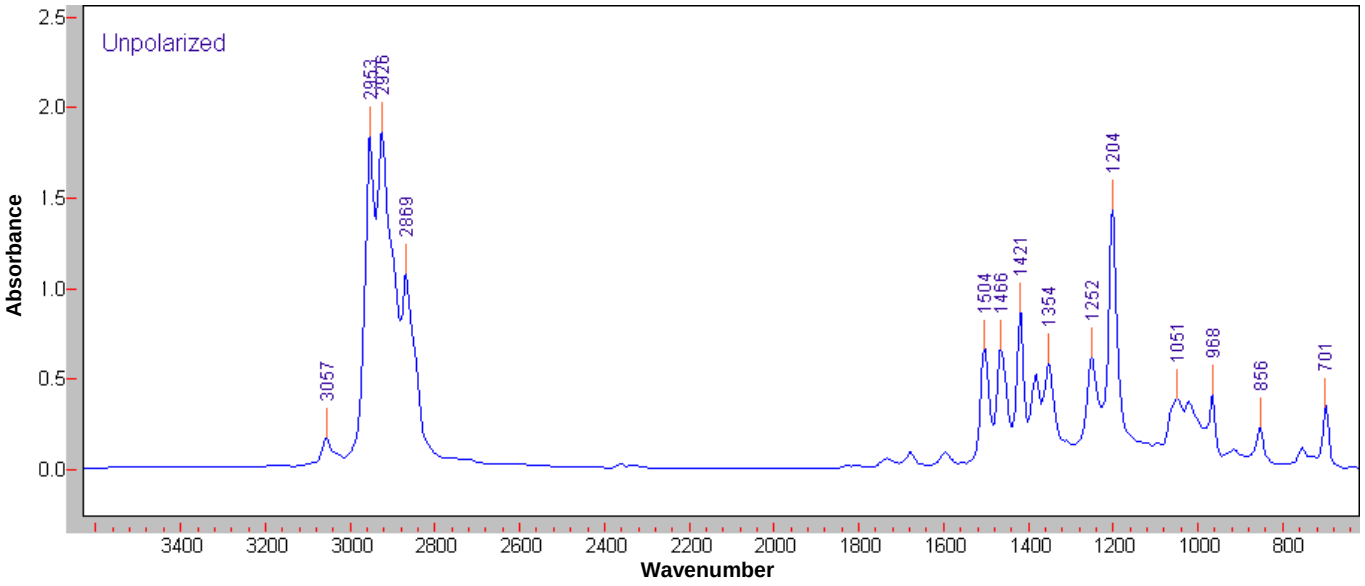

Figure 19. Absorbance of a film of OC10PPV.

Table 1. Likely origin of selected peaks in OC10PPV spectrum.

Wavenumber (1/cm)	Relative Absorbance	Likely Origin
2955	2.06	Aromatic C-H Stretch
2926	2.05	Vinylene C-H Stretch
1469	0.78	C-C ring stretch
1256	0.75	C-H in-plane bend
1206	1.74	C-H bend
966	0.58	C-H out of plane wagging vinylene
856	0.35	C-H out of plane wagging phenylene

4.5 XRD results

X-ray diffraction scans were taken on stretched and unstretched films of OC10PPV. Both showed a nearly identical, very broad peak centered around two theta equal to 22 degrees, as shown in Figure 20. The location of this peak agrees well with ordered, unsubstituted PPV previously studied by XRD [11]. It is possible that the films resulted in nearly equal intensity because the stretched film was thinner than the unstretched film. Since the method was not chosen as the analysis method, this was not investigated further. This would have also resulted in the necessity to accurately measure the film thickness for each sample in order to quantify the order, adding an unnecessary and time-consuming step. The data was taken in steps of 0.05 degrees with a 5.0 minute dwell. Although it is difficult to see, the slightly lower intensity peak, tape 16a, is actually the stretched film. Tape 17a was unstretched and is slightly higher intensity.

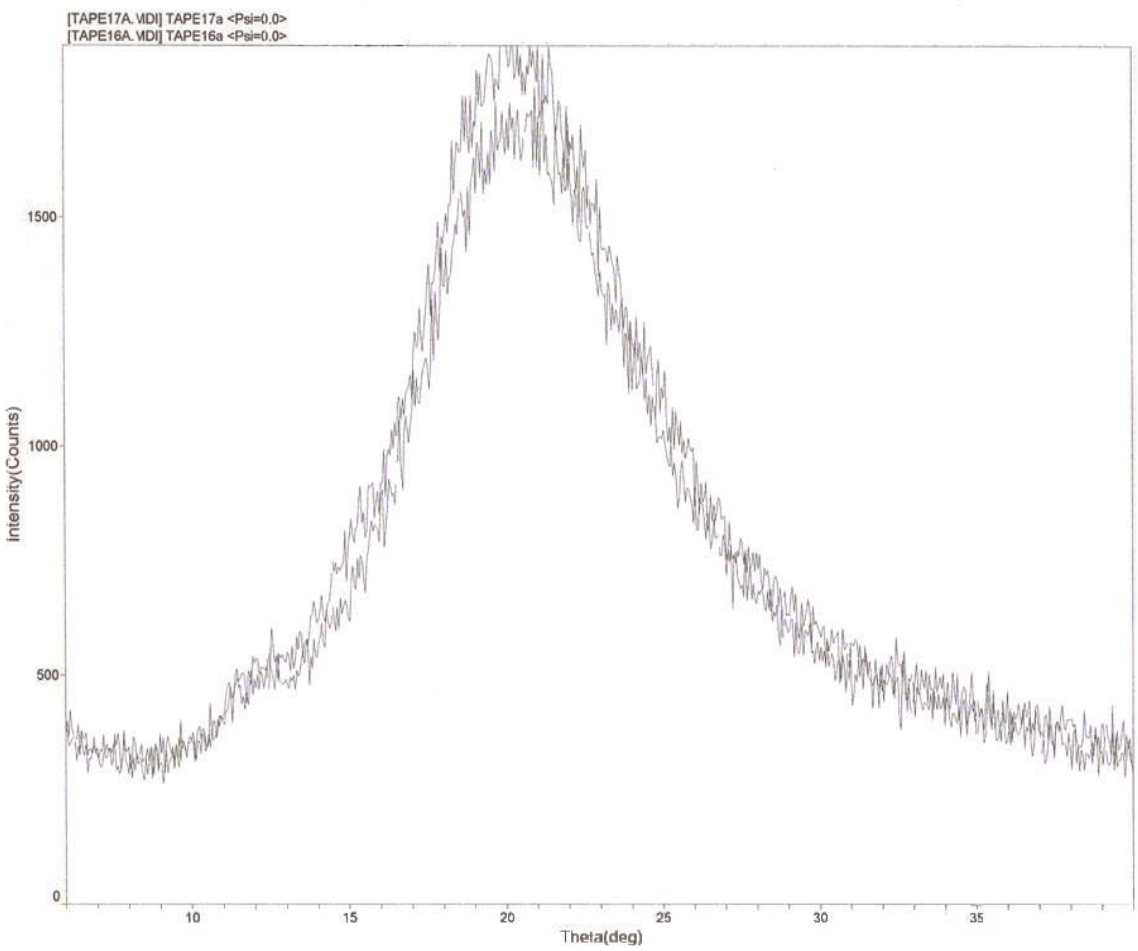

Figure 20. XRD of stretched and unstretched films, overlaid.

4.6 DSC results

Differential scanning calorimetry (DSC) was performed on stretched and unstretched films of OC10PPV that were otherwise prepared identically. For the stretched film, there is a sharp, exothermic peak at 119°C, as shown in Figure 21. The unstretched film exhibits a much lower intensity peak, and a slight shift to higher temperatures. In both cases, the peak does not appear on a second run of the same sample, nor is it present in a powdered sample. This peak is likely due to crystallization of the polymer, with the increased order induced by stretching allowing an increase in the amount of crystallization. Additional DSC tests performed on different equipment on other samples have shown an upward shift in this peak to as high as 132°C.

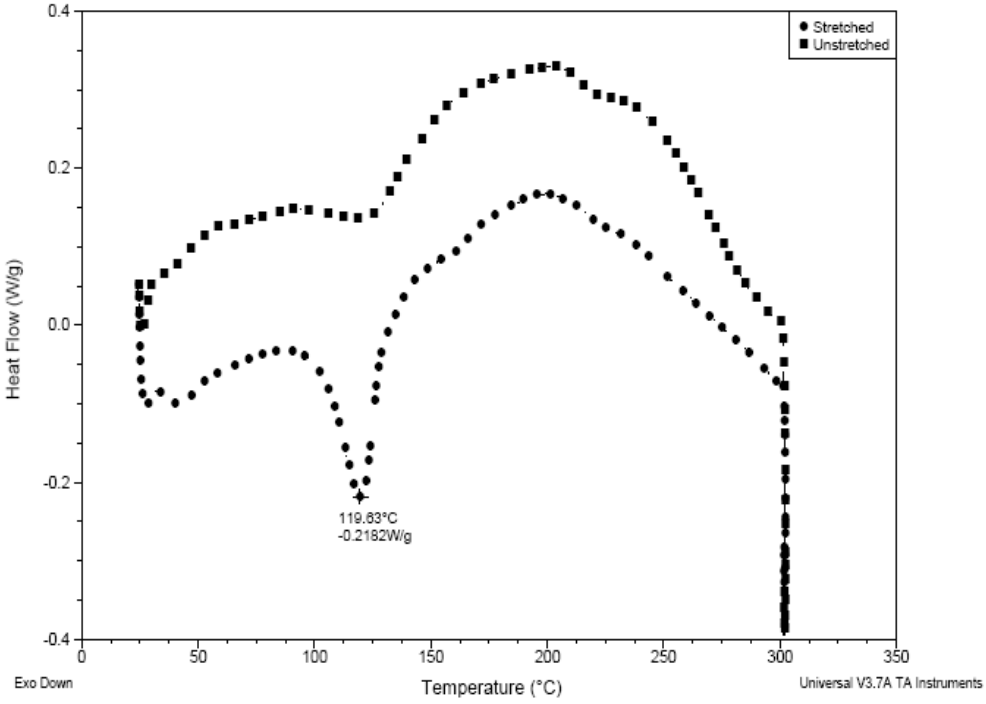

Figure 21. Differential Scanning Calorimetry of OC10PPV, stretched (circles) and unstretched (squares).

5. Processing Effects

5.1 Polymer/repeatability

Unfortunately, purity in semiconducting polymers is not anywhere near that of inorganic semiconductors, and the impurities can affect the behavior of the polymer. To minimize the impacts of impurities, all testing was done from one batch of polymer. While the impurities may still be having a significant effect on the results, it should be reasonably uniform across all of the testing. The polymer was purchased from American Dye Source in Quebec, Canada. The supplier quoted the polymer as having an average molecular weight Mw (by gel permeation chromatography, GPC) of 210,000, and a polydispersity of 5.9.

Perhaps due to the high molecular weight of the chosen batch, or perhaps due to some impurities, there were often some visible chunks on films. For this reason, the solution was generally run through a 1 μm PTFE filter prior to use. Figure 22 shows representative microscope images of the edge of drop cast films before and after filtering, taken at the same magnification. GPC data taken in house on samples showed an Mw prior to filtration of 208,000 and polydispersity index, PDI, of 3.97, and an Mw after filtration of 154,000 and PDI of 2.65. This indicates that the filtration was removing some less soluble high molecular weight components. The difference in initial measurement between the supplier and the measured value may also be due to low solubility of high molecular weight components.

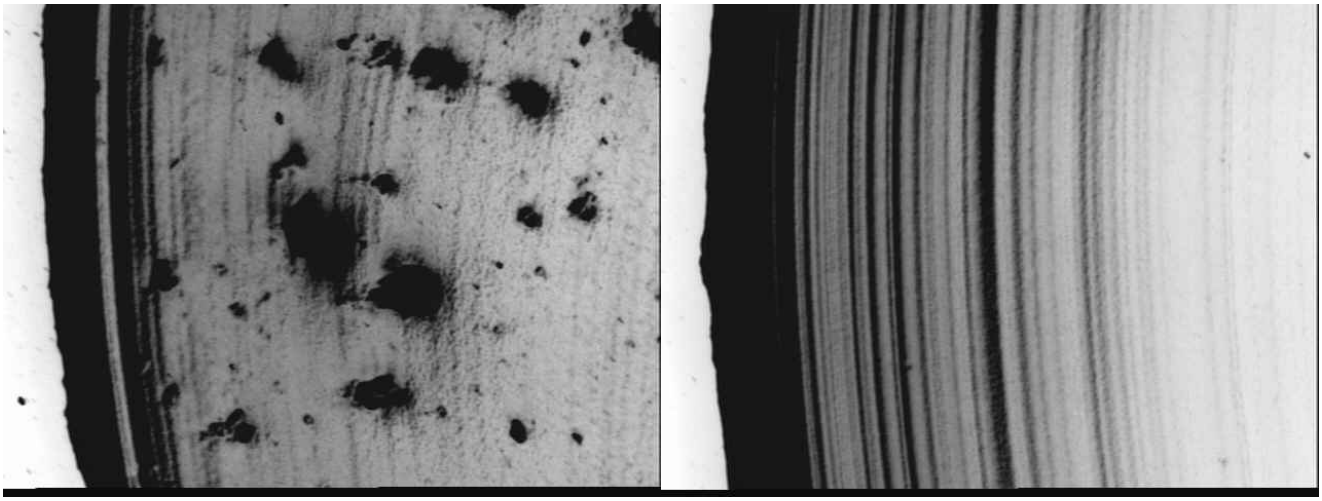

Figure 22. Microscope images showing particles in unfiltered film (left) compared to filtered film (right) at same magnification.

5.2 Processing variables

The primary processing variation that was examined was post-processing stretch-alignment, as previously detailed. First, it was necessary to determine if this was indeed imparting increased order on the films. Since the published literature generally focuses on alignment of oligomers or alignment during polymerization, this was a break from convention. It is well known that polymers respond to shear, but it was not known if this mechanism was imparting enough shear on the polymer to induce order. Polarized FTIR spectra of films stretched to three times their original length are shown in Figure 23, shown at orthogonal polarizations. For comparison with a control, Figure 24 shows orthogonally polarized spectra of an unstretched film of OC10PPV.

Clearly, post-polymerization substrate stretching can induce order into the polymer. It was then necessary to determine which processing variables impact the order. However, in order to know if a variable has impacted the order, one must first have an idea of the sample to sample variation in dichroism. Four samples were processed similarly to a stretch ratio of three and tested for infrared dichroism. Since the infrared spectrometer does so much sample averaging, the same sample variation tested on different days is negligible compared to sample to sample variation. Figure 25 shows the averages and range of the dichroic ratio for the samples for the three absorbance peaks that were chosen to follow. Samples stretched to a lower value may vary slightly less, but when looking at variables other than stretch, samples were generally either drop cast or stretched to l/lo=3.

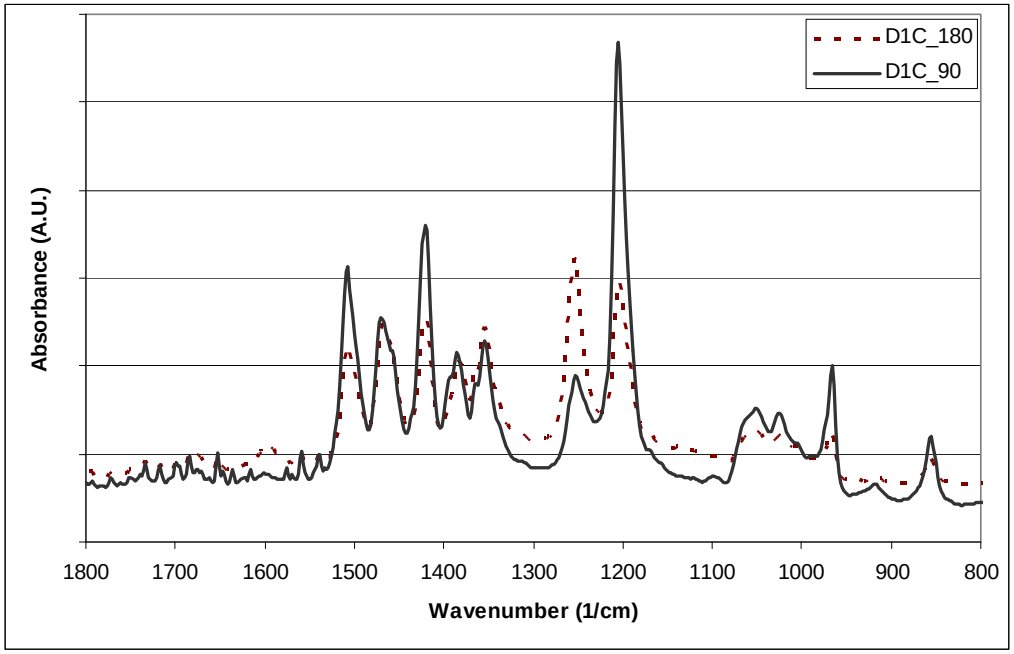

Figure 23. Infrared spectra for l/lo=3, solid line $A^{\perp}$, dashed line $A^{\parallel}$.

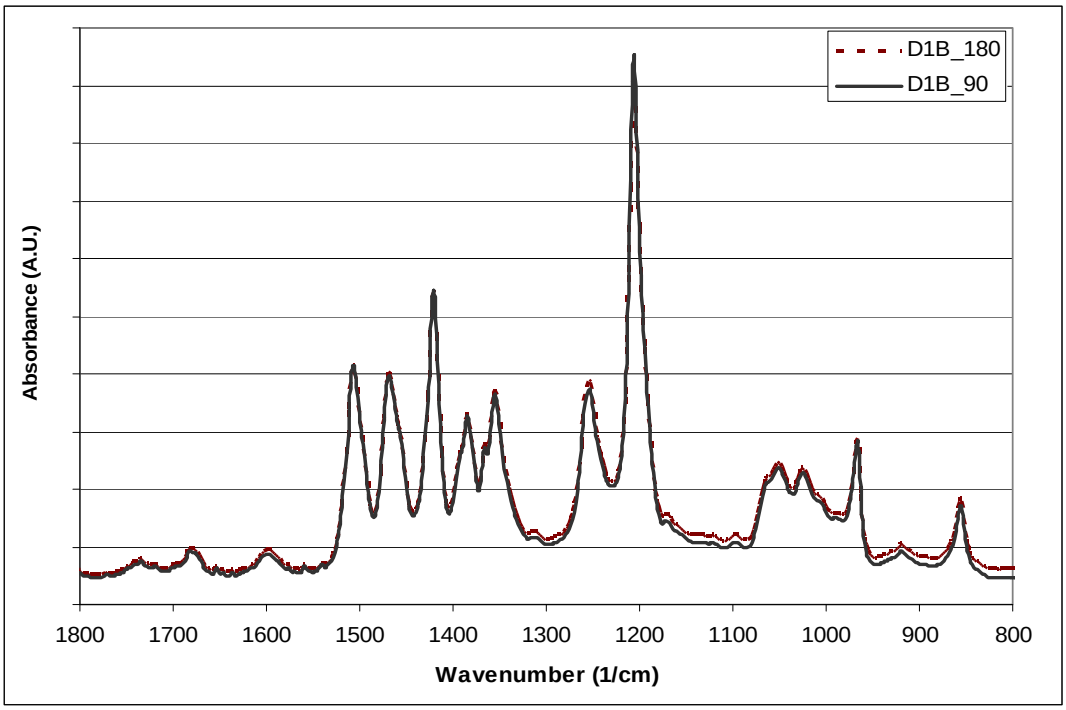

Figure 24. Infrared spectra for I/Io=1, solid line $A^{\perp}$, dashed line $A^{\parallel}$.

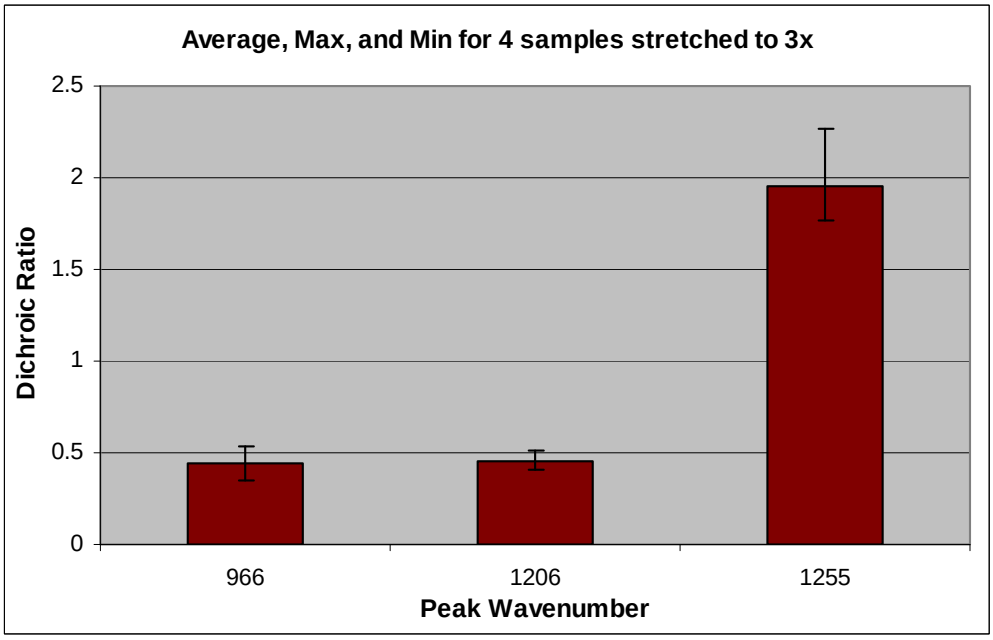

Figure 25. Dichroic ratio average and range for 4 samples stretched to 3x.

The next control test was to verify that the material is modified by the actual stretching, and this is not simply induced order from the ordered substrate, as has been reported for a rubbed polyimide substrate. Films were drop cast onto three different substrates of varying order. Substrates used were a standard PTFE substrate with very little order, a skived PTFE substrate with some degree of order, and a PTFE tape that had been pre-stretched to the equivalent of a 3x film, which had a high degree of order. As shown in Figure 26, no dichroism was observed with any of the unstretched films, even from a substrate that was highly ordered. In all cases, the dichroic ratio is within error of one. It is clearly the actual act of stretching that is ordering the polymer, not simply the order in the substrate.

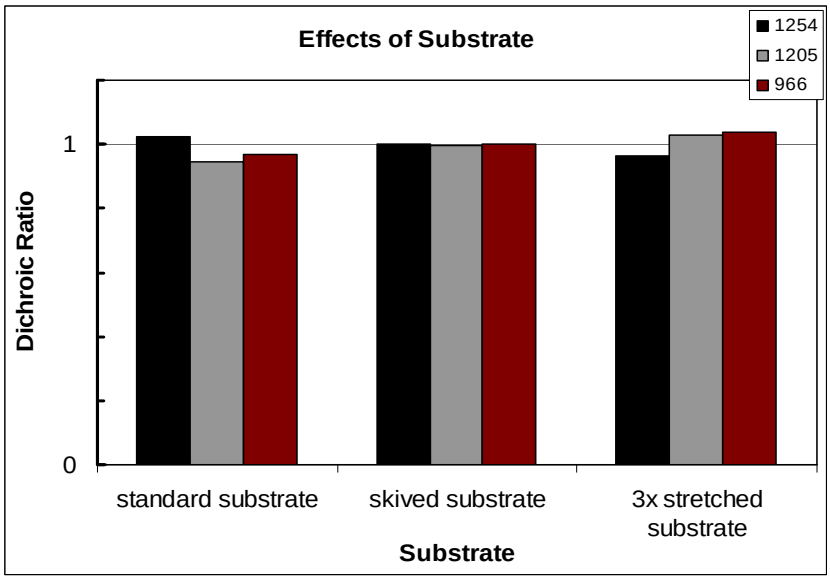

Figure 26. Dichroic ratio of unstretched OC10PPV films cast onto different substrates.

The most likely processing variable to have a significant impact on order is the stretch ratio. With all other variables held constant, the stretch ratio (l/lo) was varied from one (unstretched) to four, and the dichroic ratio was measured for the three absorbances being followed, as shown in Figure 27. The dichroic ratio for the absorbance at 1254 cm^{-1} (a pi band) increases from essentially one to a high of 2.13 at a stretch ratio of 3.7. The absorbance at 966 and 1205 cm^{-1} are both sigma bands and decrease from one to minimums of 0.28 and 0.33, respectively.

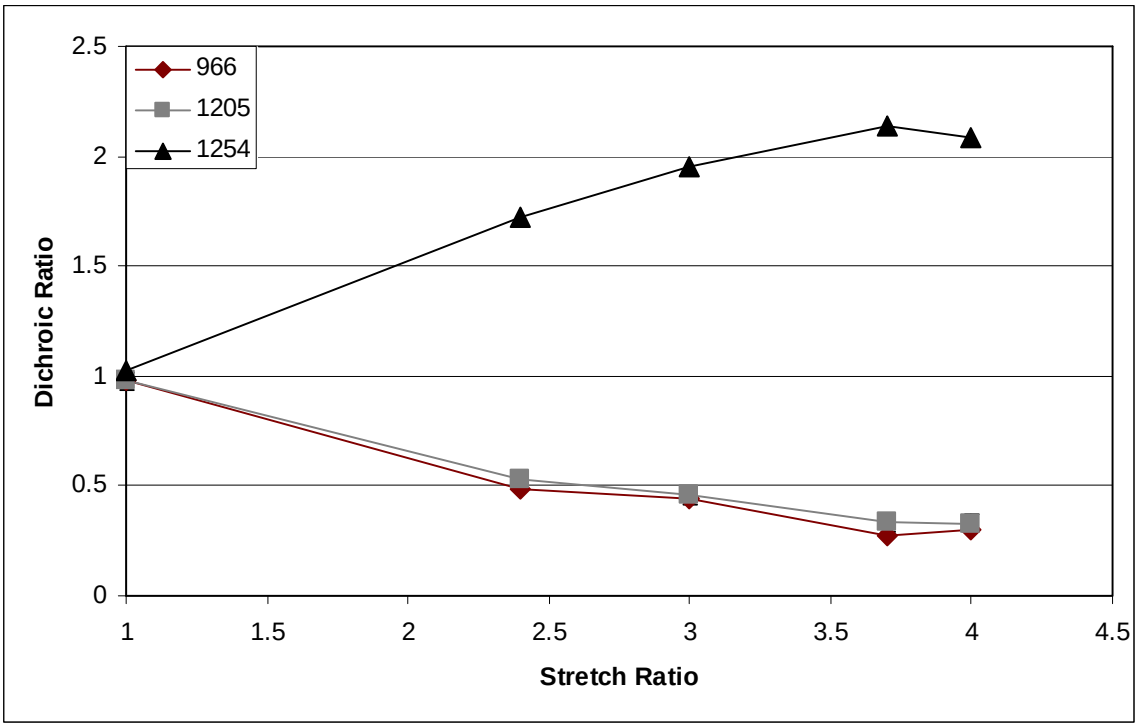

Figure 27. Dichroic ratio as a function of stretch ratio.

Using this data, the orientation function was calculated as previously detailed, and this is plotted in Figure 28. Calculations were based on the absorbance peak at 966 cm^{-1}, and an estimated angle of 84°. The values are plotted as a function of stretch ratio l/l_o, increasing from zero for an unstretched sample, $l/l_o=1$, indicating negligible order, to 0.66 at $l/l_o = 3.7$, near the elongation limit of the stretching apparatus, where the order parameter appears to approach a limiting value. Published reports from other groups who aligned PPV precursor without side chains show similar plateau behavior. For visual reference, the range of the repeats at l/lo=3 is shown on the plot. The Kratky model is depicted as the solid line on the plot.

The orientation function is approaching the values predicted by the Kratky model, thought to be a theoretical limit for orientation of a polymer without a change in volume. Some additional optimization of parameters may get the orientation function closer to the Kratky line, but this indicates that for this case, in which the sample is likely operating at nearly constant density, the orientation is approaching the theoretical limit of the orientation parameter. At this point, the data appears to plateau, so additional improvements by stretching are minimal. This stretch ratio is also nearing the limits of the current stretching apparatus.

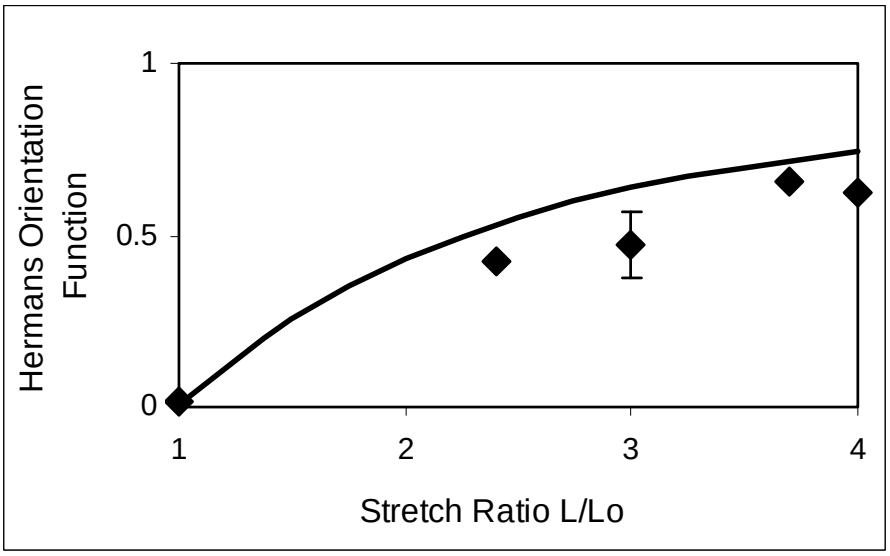

Figure 28. Hermans orientation parameter as a function of stretch ratio, based on 966 1/cm. The solid line represents the Kratky model.

More importantly, the stresses on the film at high stretch ratios become important and the films become thinner so the film quality starts to become problematic, particularly since this is for electrical applications. At a stretch ratio of four, small pinholes were sometimes developing in the films, which depending on the design of the electrical device could easily result in electrical shorts. Even for less demanding electrical applications, the mechanical integrity of the films was less impressive at higher stretch ratios. Increasing the initial volume of solution deposited seemed only partially able to compensate for this.

The next obvious variable to test was the stretch rate. Samples were all stretched to a final stretch ratio of three, but at jaw movement rates varying from 0.28 to 3.8 inches per minute. As previously noted, there is some slippage during stretching, so the sample does not experience that exact rate, but it did experience a rate change of roughly an order of magnitude. The dichroic ratio for the three chosen absorbance peaks was monitored and is plotted in Figure 29. There is no clear trend with stretch ratio in this range of stretch rates. Unless otherwise noted, all other tests were performed at a jaw movement speed of approximately one inch per minute.

An interesting variable to examine that is perhaps not as obvious is light. Since we know these materials absorb visible light, some experiments were performed to see if light had any impact on the stretch alignment. Stretch alignment was performed in nearly complete darkness, in standard room lighting, and with a high intensity flashlamp shined onto the film. Interestingly, those stretched with the flashlamp almost completely delaminated from the tape before completion of the stretching, those in room lighting may have had some very slight delamination, and those in darkness had essentially no delamination.

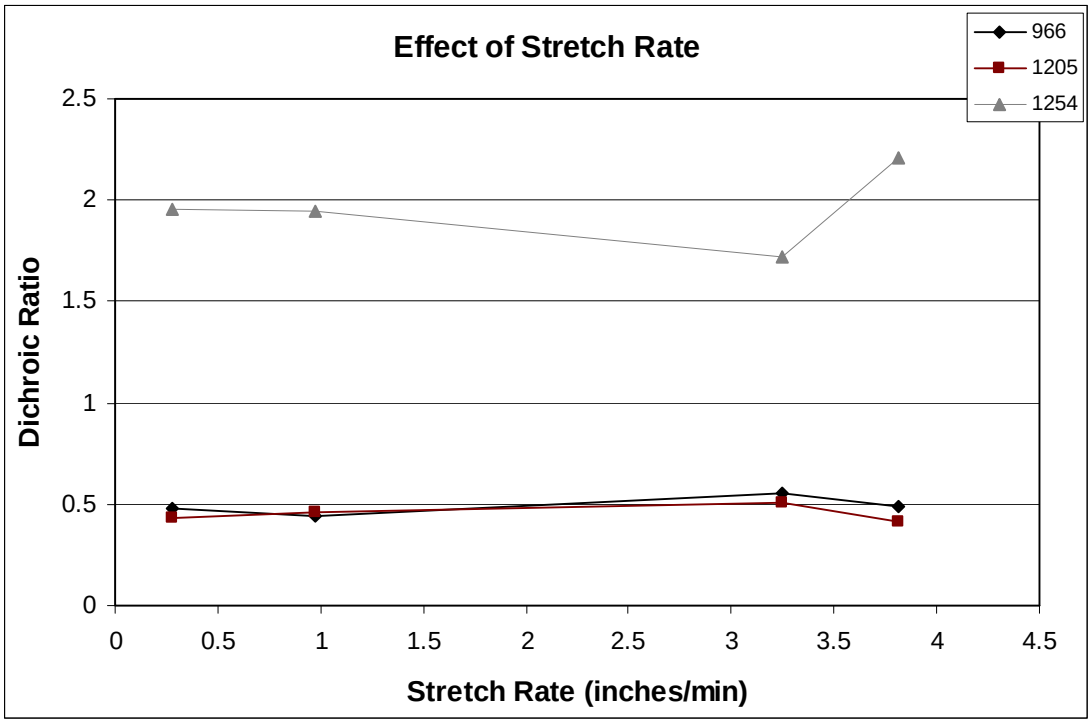

Figure 29. Dichroic ratio as a function of stretch rate, with I/Io=3.

It is possible that the films were partially crosslinking due to the high intensity light, but it is also likely that the light may have just increased the speed of solvent evaporation and the solvent acts as a plasticizer during stretching. Although the films were stretched once visibly dry, there was certainly residual solvent at this point. These films were not tested for dichroism since delaminated films do not experience the stretching, but from this point, films were stretched with minimal room lighting on.

Another relevant processing variable is temperature. Unfortunately, the laboratory did not have the ability to controllably alter the temperature while stretching, which could have been very interesting. However, based on the DSC results, and published literature reporting interesting results with post-processing annealing, this was examined. Films were stretch-aligned and tested for dichroism, then annealed at 135°C for 10 minutes in a vacuum oven. The same samples were then tested again for dichroism. Because this was done with the same samples, rather than samples processed similarly, the error is much lower. It should also be noted that the films appeared somewhat damaged by the heating, so perhaps a slightly lower temperature could be tried in the future. A matrix of time and temperature variables was not examined. The results are shown in Figure 30 for three samples with different stretch ratios. For each sample, the dichroism appears to decrease very slightly after annealing (approach one). The solid colors in the figure are prior to annealing, and patterned are after annealing.

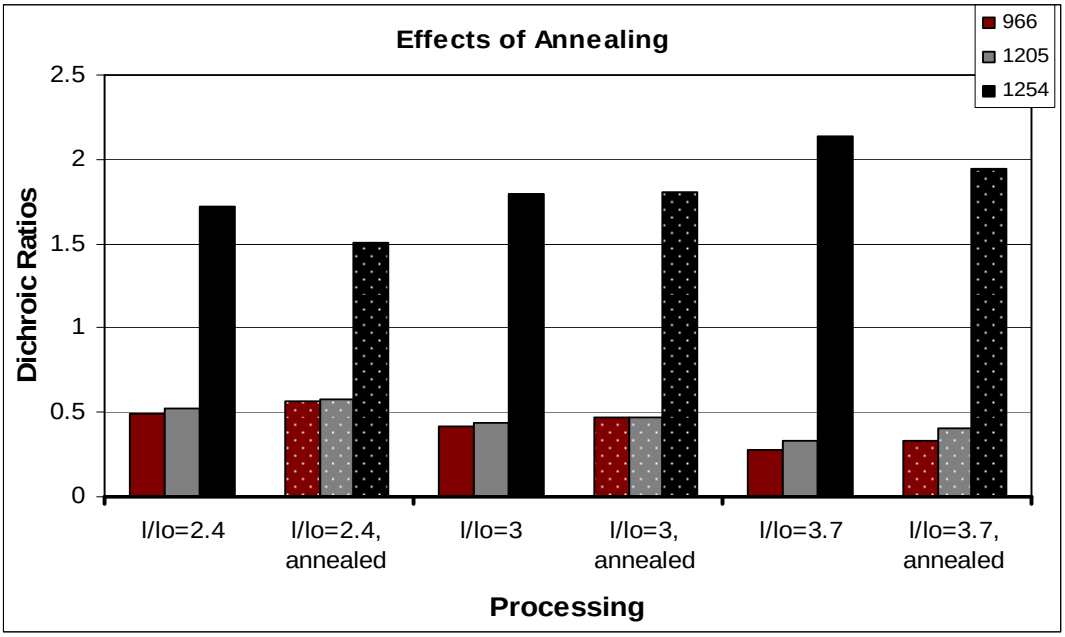

Figure 30. Dichroic ratios before (solid) and after (patterned) 135 °C anneal.

5.3 Additives

A number of additives were investigated, but the most significant was a nanoparticle additive known as [6,6]-PCBM, or simply PCBM, introduced in Chapter 1. As will be shown in the next chapter for electrical tests, this could be mixed up to 50 percent by weight with OC10PPV. However, these films were of poor physical quality and could not support themselves for infrared testing. The highest PCBM concentration that could be mixed in and still achieve a freestanding film of sufficient quality for infrared examination was 20 % by weight. All composites were achieved by mixing separate solutions of PCBM in solvent with polymer in solvent in proper proportions. The composite films were stretch aligned similarly to pure polymer films, as previously discussed. As shown in Figure 31, 15 % and 20 % by weight PCBM did not appear to interfere with the bulk alignment of the polymer during stretch alignment, as the dichroic ratios appear to be within error of the pure polymer for samples stretched to l/lo=3. Again, the average and range is depicted for the pure polymer sample. This result is actually somewhat surprising as one might expect that the pure mechanical interference may have caused a slight decrease in the effectiveness of the ordering, but perhaps due to the small size of the particles, this does not appear to be the case.

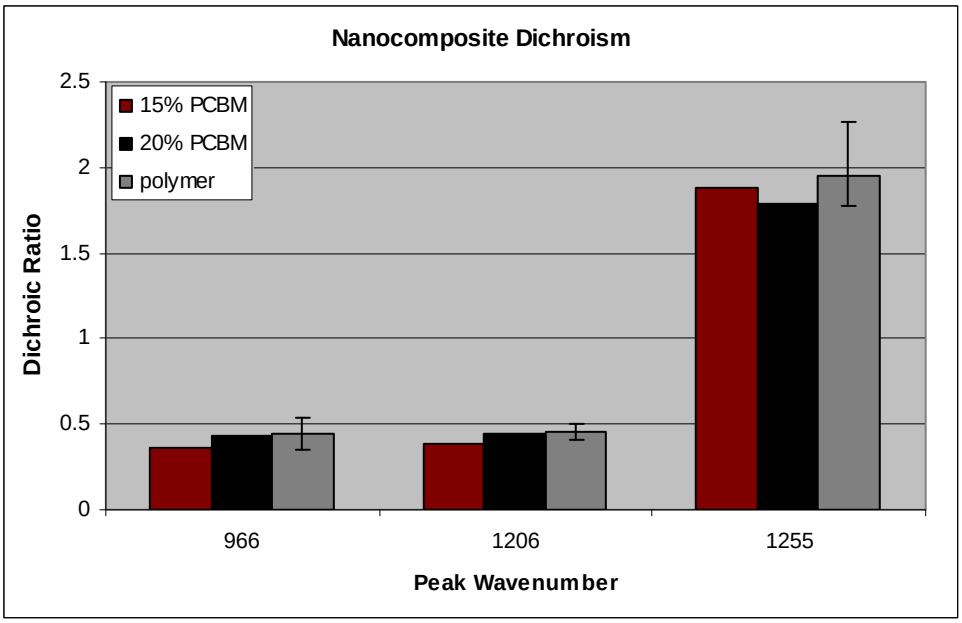

Figure 31. Dichroic ratio of polymer and composites with 15% and 20% nanoparticles by weight stretched to l/lo=3.

Solvent vapors were not screened in depth, but dry methanol vapor was examined. If only one solvent were to be chosen for maximum possible effect, this would probably not be it, but it was available in a dry form so the moisture would not contaminate the glovebox and would minimally solvate the polymer, perhaps opening up the chains enough to plasticize the polymer and increase the effectiveness of the stretching. While the polymer solution was drying and while the film was being stretched, large quantities of dry methanol were evaporated in the glovebox in the vicinity of the film in an effort to expose the film to as much methanol vapor as possible. The film was stretched to a final stretch ratio of three and tested for dichroism. Figure 32 shows the average and range of the dichroic ratio for the standard film repeats and for the film stretched while exposed to methanol vapor, which is within the range of the standard samples. Other solvents may work better, but it is important to choose a solvent that does not act as any form of ionic dopant, increasing the conductivity of the film. This was not pursued in greater depth due a few reasons. The first was a perceived lack or reproducibility of the experimental method of the solvent exposure. The second was a concern of exposure of other samples in the glovebox to potentially harmful solvents and moisture.

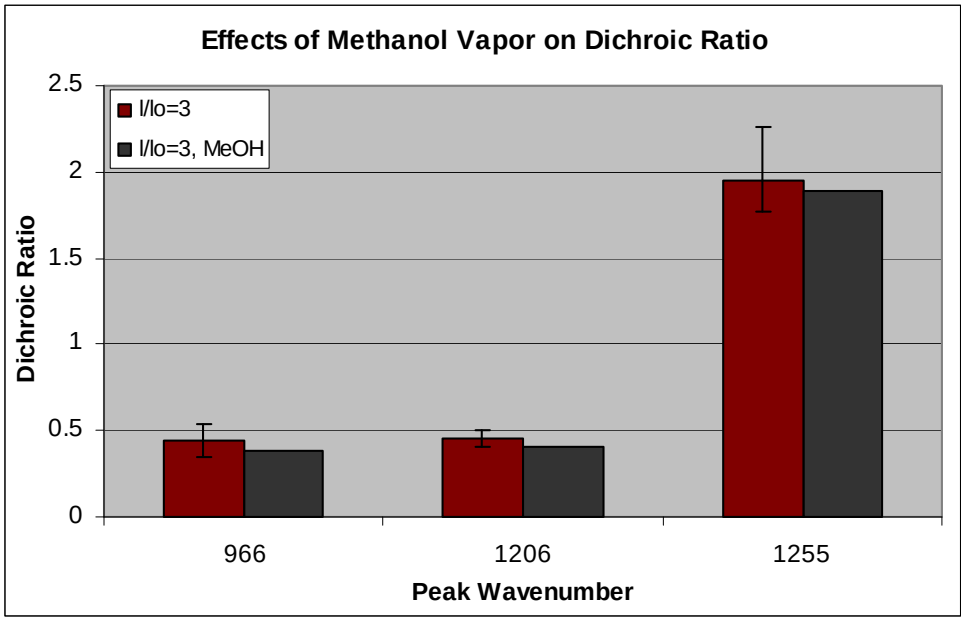

Figure 32. Dichroic ratio for OC10PPV films with and without exposure to methanol vapor before and during stretching.

This section demonstrates a useful, non-destructive method for measuring order in amorphous conjugated polymer films. Using post-polymerization stretch alignment, bulk order was successfully induced into films of OC10PPV, resulting in a Hermans orientation function as high as 0.66, as measured by polarized FTIR, approaching the Kratky model. The stretch ratio was a dominant factor in the dichroism, but the stretch rate had no substantive effect, nor did a methanol vapor exposure during stretching. Post-stretching annealing caused a possible, though very slight decrease in order in the films. PCBM nanoparticles up to 20% by weight did not interfere with the ordering in the polymer.

6. Structure–Property Relationships

The bulk order induced by various processing parameters on OC10PPV films was discussed above. This section will show the effects of the processing parameters on the electrical properties. Several additional processing parameters will also be shown that were not screened for order, but only for electrical effects.

6.1 Experimental setup

Unless otherwise noted, experiments were performed on IDT array structures with a 16 μm gap spacing and 4 μm electrodes. A 3 Hz pulsed nitrogen laser tuned to 581 nm was directed through the back of the device. Amplification was performed with an Ortec 142A charge sensitive pre-amplifier and an Ortec 570 shaping amplifier with 10 μs shaping time, averaged over at least 100 pulses. The laser was linearly polarized and the polarization could be rotated with a quarter-wave plate. Charge collection was calculated based on a 10% quantum efficiency, as found by Moses. Imposed fields were used in the range of 104–105 V/cm.

Testing for dark current and transients were performed in a separate testing station in a semi-sealed box. Tests could be performed at ambient conditions, with desiccant packs to test in dry air conditions, or under slow flow of dry nitrogen. The box could be sealed to test in complete darkness, or a microscope illuminator could be inserted through a hole in the center of the lid. Unless otherwise noted, the center hole was covered with metal tape and tests were done in complete darkness. The sweep rate is generally noted separately for each test. High bias measurements were taken with a Keithley 6517A electrometer and programmed manually. For measurements up to 10 V, a Keithley 6487 picoammeter was used, controlled by ExceLINX, an add-in to Microsoft Excel written by Keithley. In both cases, the bias was supplied by the instrument.

Stretch-aligned films were peeled from the PTFE tape and applied gently to the IDT test structure. A drop of isopropyl alcohol was used to flatten and smooth the film using a paintbrush as the alcohol evaporated. The alcohol does not dissolve the polymer. The IDT was then clamped to a glass slide covered in PTFE and placed in a nitrogen purged drybox to allow full drying of the sample for at least 24 hours after stretching prior to any additional testing. Unless noted, the stretch direction was applied parallel to the field direction.

6.2 Stretched films

Since noise in a radiation detector is dramatically increased by dark current, initial tests were to ensure that the processing is not significantly increasing the dark current in stretched films. If the mobility is increasing, as desired, then some increase is expected, but this should be checked. Current-voltage sweeps were performed on IDTs of drop cast films and films stretched to l/lo=3 and the results are shown in Figure 33. A sweep rate of 0.2 V/ 300 s was used. This relatively slow sweep rate was used to minimize the effects of the long transients as commonly seen with these films. In fact, even at this slow rate, there are still likely some transient effects.

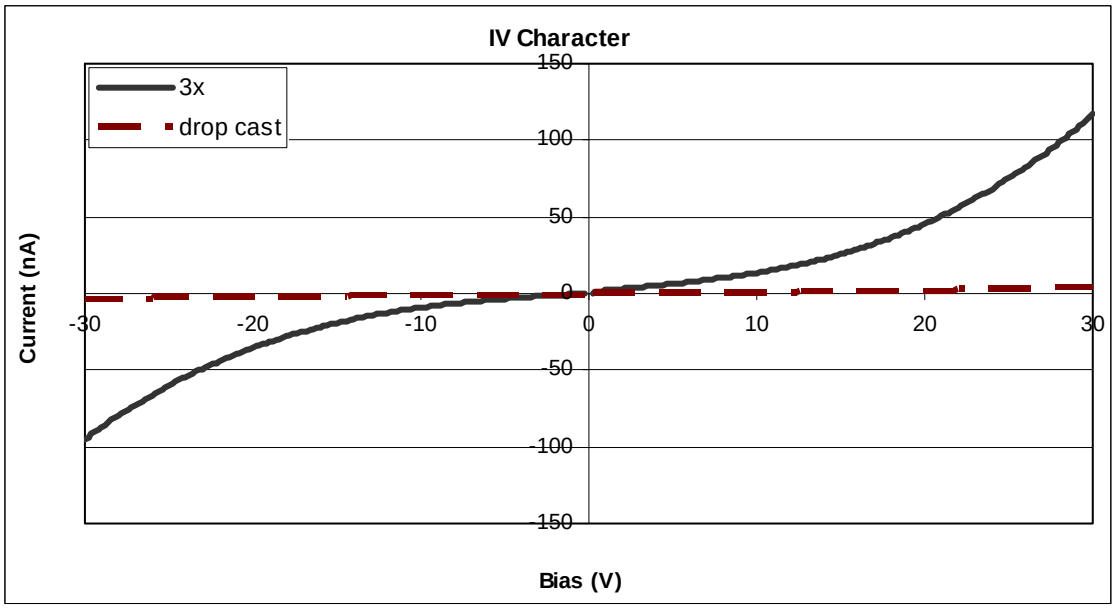

Figure 33. IV sweep with 16um IDT of drop cast and 3x films, at a rate of 0.2V/300s.

Sweeps were done from zero out to plus or minus bias, then plotted together. The samples were allowed to settle in the dark before the sweeps were started to minimize any transient effects from room lighting. The 3x film has higher current than the drop cast film, but it is still in the nanoamp range, which should be low enough for reasonable operation.

Photoconductive response was also tested on similarly prepared samples. Samples stretched to l/lo= 2.2 and 3, with the stretch orientation parallel to the field orientation, exhibited an increased photoconductive response and increased charge collection efficiency as compared to a drop cast sample with no orientation. The two stretched samples show similar photoresponse, within experimental error, which agrees with the plateau behavior seen for the Hermans orientation function. A sample with the applied field oriented orthogonally to the stretch direction shows a decreased photoresponse compared to a drop cast sample. Even when the polarization of the excitation source is rotated by 90° to align with the maximum photoresponse, the photoresponse is still weaker than in an unordered sample. Literature reports on ordered conjugated materials vary widely on electrical anisotropy ratios, from only a few to over 100, depending on material, doping, ordering method, measurement parameter and method, but with consistently improved transport in the aligned direction. It is interesting to note that decreased charge collection was observed compared to the drop cast film. The hypothesis had been that stretching would improve transport most in the stretch direction, but would improve transport also in the orthogonal direction by increasing the pi overlap between chains. It is possible that the long side chains are preventing sufficient overlap between chains to allow efficient transport in the orthogonal direction (see Figure 34).

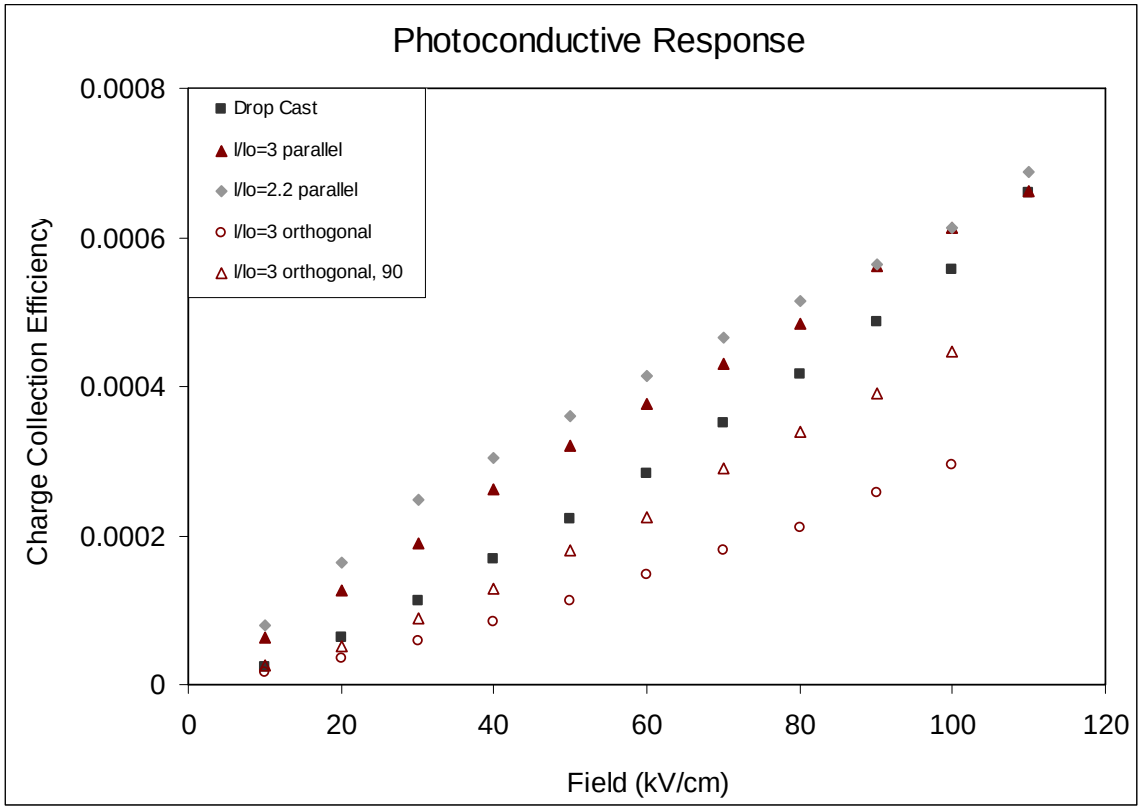

Figure 34. Charge collection efficiency for drop cast (squares) and stretched films oriented parallel (solid) and orthogonal (open) to the field direction.

6.3 Nanoparticle additives

PCBM nanoparticles were shown in Chapter 4 to not interfere in the ordering process, so next it is important to know the effects on the electrical properties. First, it is important to check that they are not acting as a dopant and significantly increasing the dark current in the material so the IV behavior was tested in complete darkness. As shown in Figure 35, the PCBM additive seems to actually slightly decrease the dark current in the material. This was tested with drop cast films at a rate of 0.1 V/ 200 s. There is some variance in the measurement so this small increase is relatively insignificant. The dark current is small enough that it should be acceptable for radiation detection purposes.

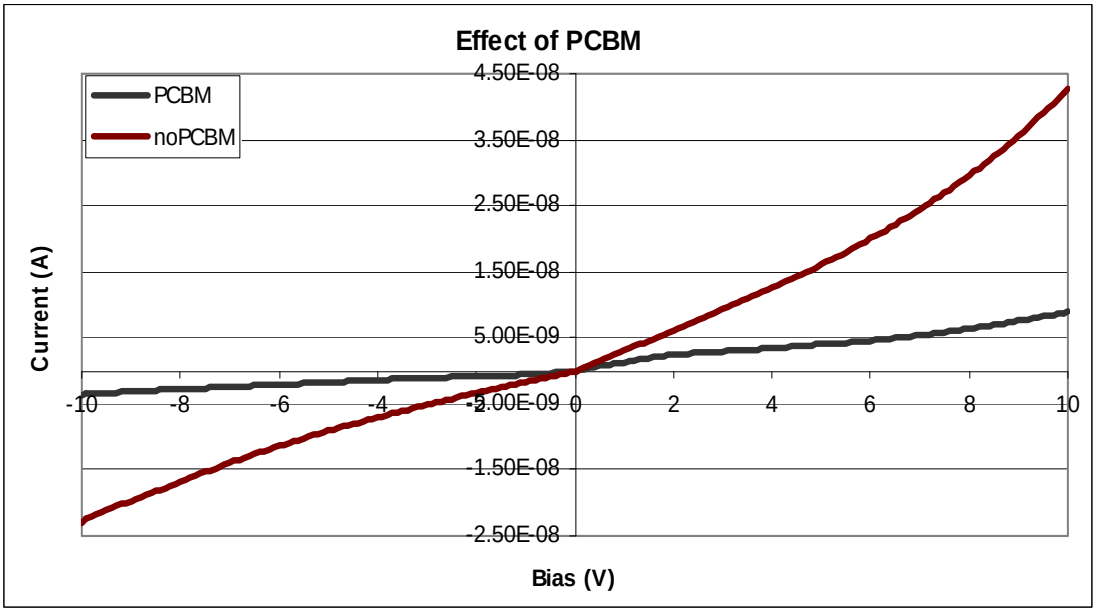

Figure 35. Dark current for films with and without PCBM.

Drop-cast films loaded with PCBM were then tested for photoconductive response. Since these were drop-cast films and not free-standing films, PCBM content as high as 50% by weight could be tested. Films with 20% and 15% were also tested, as well as drop cast films with no PCBM. The results are shown in Figure 36. The apparent discontinuity in signal for the 50% sample was caused by a change in the laser filter. At the high field, the same filter was used for all three nanoparticle samples so this is the best comparison range. This was adjusted for by using a ratio of the measured signal with the different laser filters, but there is some error in this adjustment. This should also be pointed out as an error in the true difference between the signal from the composite samples and the pure polymer sample. The composite samples used a high density filter and the polymer sample had no laser filter in place. The signals were adjusted by using a ratio of the measured intensities to account for this, and the difference is obviously so large that there is still a very dramatic effect, but there could be some absolute error due to this fact. All three samples with PCBM content showed an increase in signal of roughly two orders of magnitude over the OC10PPV film without PCBM. However, there was no apparent order to the increase in signal with the amount of PCBM content. The 50% by weight PCBM showed the highest signal, then followed by the 15% sample and the 20% sample had the lowest signal of the composite samples. This could be a morphological effect, balancing charge transfer and phase separation. The electrical performance of this composite is known to be very sensitive to morphological variations.

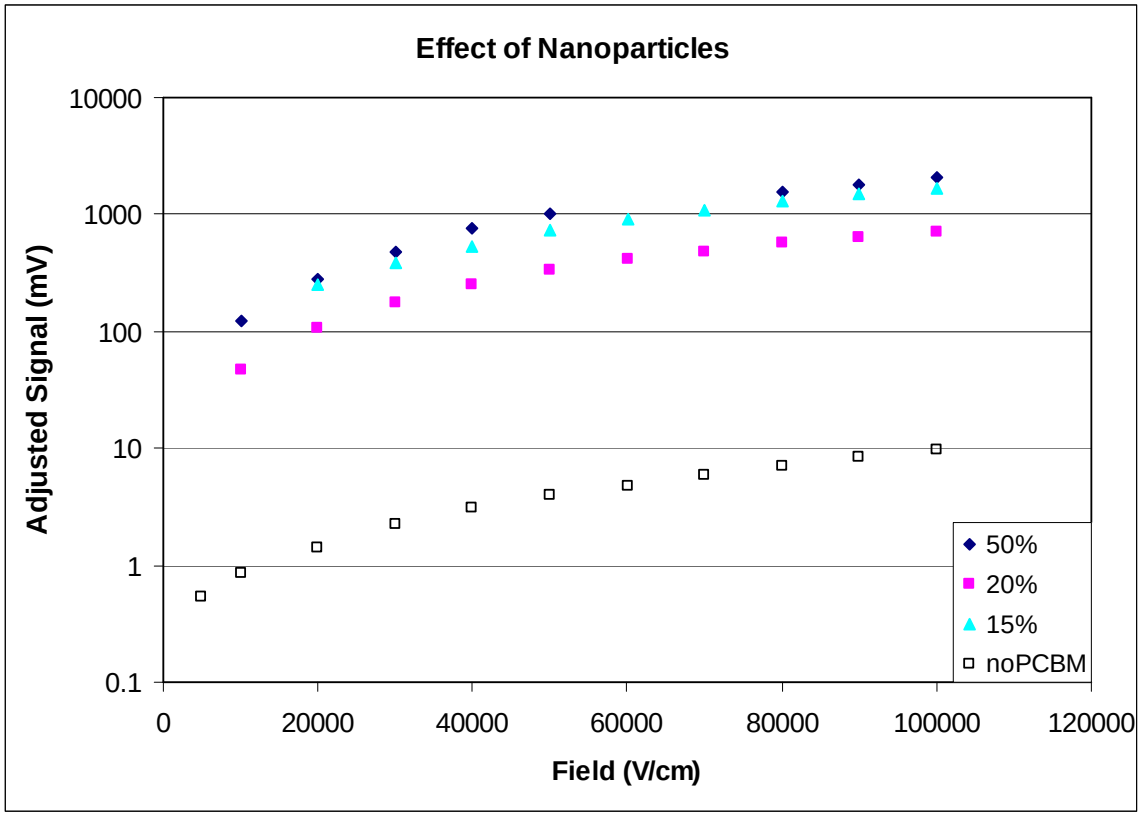

Figure 36. Photoconductive signal response from dropcast samples with different weight percentages of PCBM, from zero (open squares) to 50% (solid diamonds).

6.4 Filtered nanocomposites

In the previous chapter, analysis was shown using a 1 μm filter to remove un-dissolved polymer in order to be able to form better quality films. It was shown that this alters the average molecular weight and polydispersity of the polymer. Molecular weight and polydispersity can impact electrical properties of conjugated polymers, so this may be a relevant electrical variable both with the pure polymer and as a factor with nanocomposites. The improvement in film quality could also impact electrical properties. For the nanocomposites, the polymer was filtered separately, and then combined with nanoparticles. The nanoparticle solutions were not filtered.

First, dark current tests were done with pure polymer and with 10% by weight PCBM content on 16 μm IDTs. As shown in Figure 37, both samples without PCBM had higher dark current than those with PCBM, and the unfiltered polymer sample showed higher dark current than the filtered polymer sample. This is a good sign for the use of filtration for the application of radiation detection. However, again, the change between filtered and unfiltered samples is not large and could be within the sample variation of the test. Sweeps were taken at 0.1 V/ 200 s.

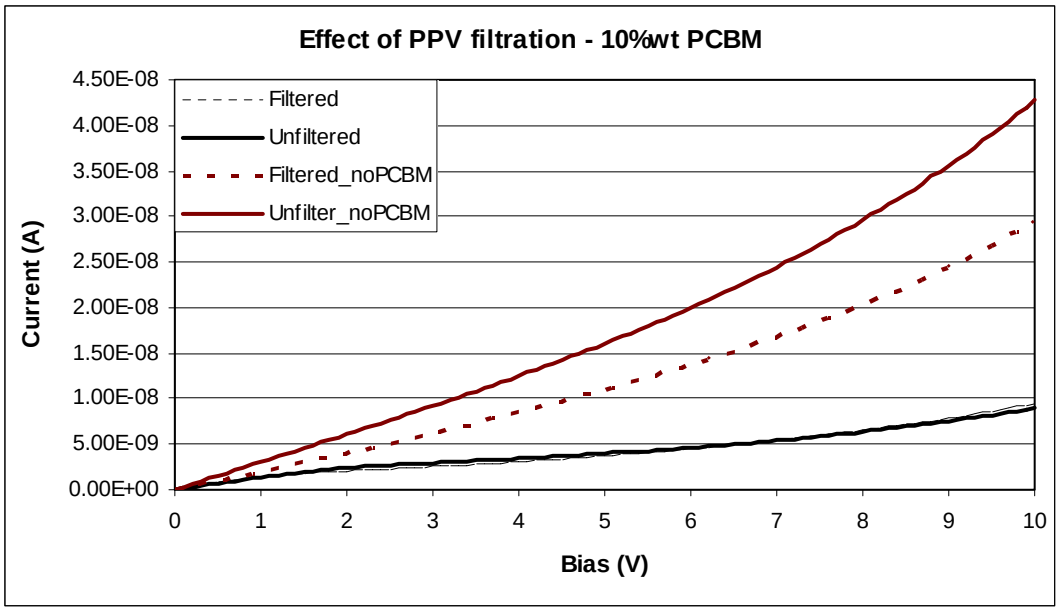

Figure 37. Dark current of filtered and unfiltered samples with no PCBM and 10 % PCBM.

Since filtration was determined to look promising from the microscopy and not be detrimental from the dark current tests, photoconductive tests were done using the same samples as the dark current tests. To minimize any differences due to laser alignment, the tests were run over two days and the test setup was not moved between tests. The results are shown in Figure 38. Although it is difficult to see in this figure, even for the samples with no PCBM, the filtered sample did show a slight increase in photoconductivity. For the samples with PCBM the difference is much more pronounced, resulting in a roughly 3x increase in photoconductive response compared to the unfiltered response. Filtering results in a lot of lost polymer which significantly increases cost, but based on this result, future solutions were filtered prior to use.

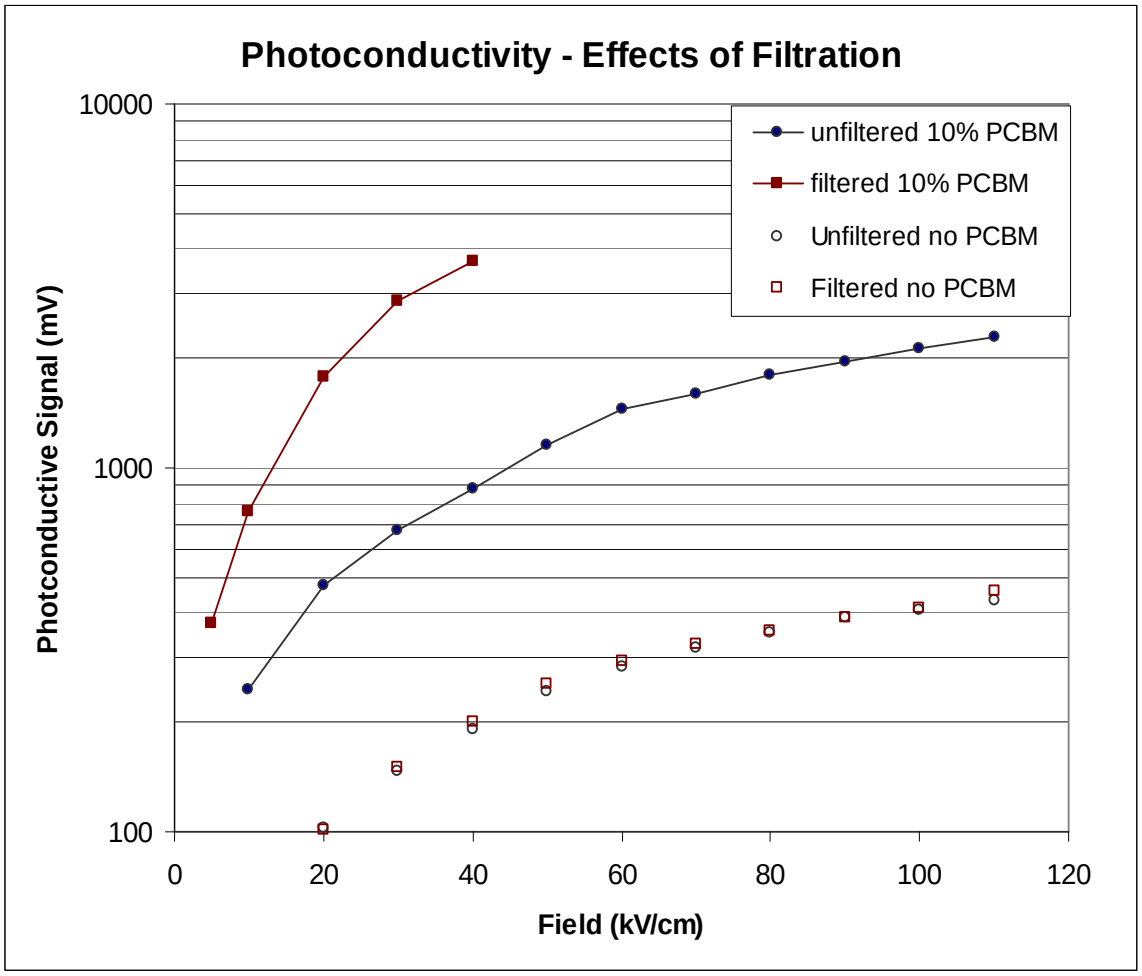

Figure 38. Photoconductive response comparing filtered and unfiltered samples with no PCBM or 10% PCBM.

6.5 Stretch-aligned nanocomposites

Next, the photoconductive signal response was examined from stretch-aligned samples with PCBM additives. Using a solution of 10% by weight PCBM, samples were stretch aligned to l/lo= 2.2 and 2.7. A drop of the same solution was cast onto an IDT for comparison with the stretch aligned films. Stretch aligned pure polymer films had shown roughly a doubling of photoconductive response with stretching, and since the nanoparticles did not impede the ordering of the polymer, one would anticipate seeing similar behavior in the nanocomposites for photoconductive testing. However, such was not the case. As shown in Figure 39, the stretch alignment actually decreased the photoconductive response significantly. The photo response for a sample stretched to l/lo=2.2 decreased by roughly 5x and for a sample stretched to l/lo =2.7 decreased about an order of magnitude.

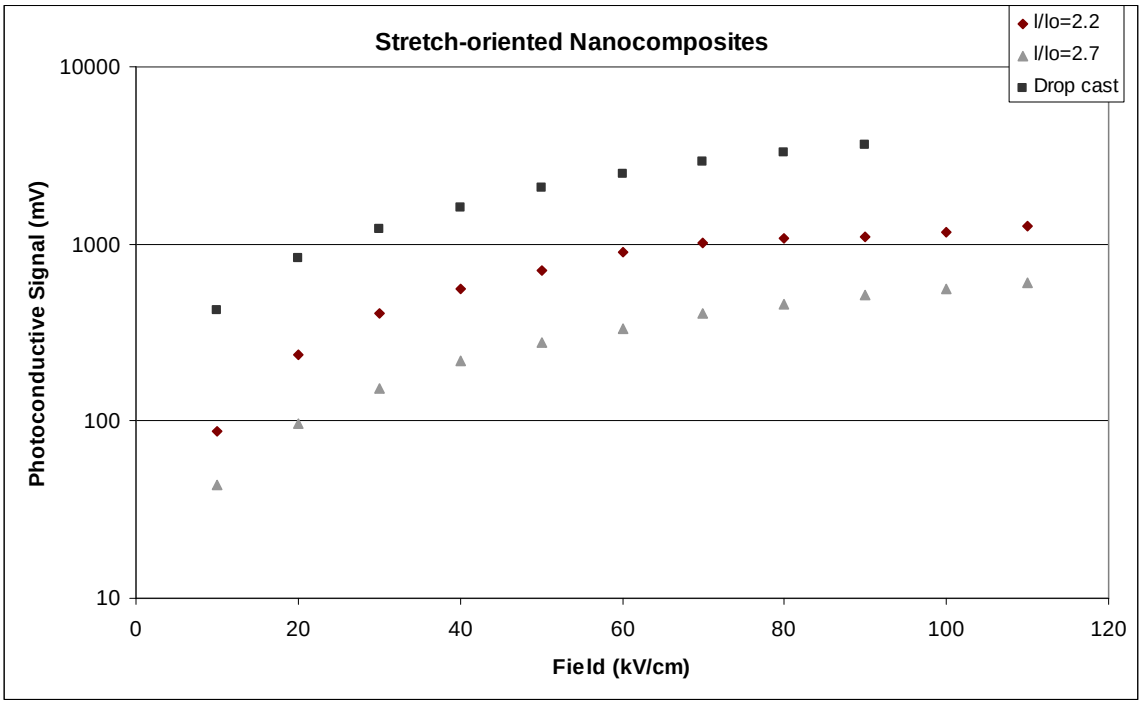

Figure 39. Photoconductive response of stretch-aligned nanocomposites.

As shown in the summary plot, Figure 40, the stretch-aligned composite still does have higher photoconductive response than the maximum response achieved with a stretch-aligned polymer without any nanoparticle additive. In order to make the testing as quantitatively comparable as possible for this plot, all samples were re-tested on the same day with the same laser alignment setup.

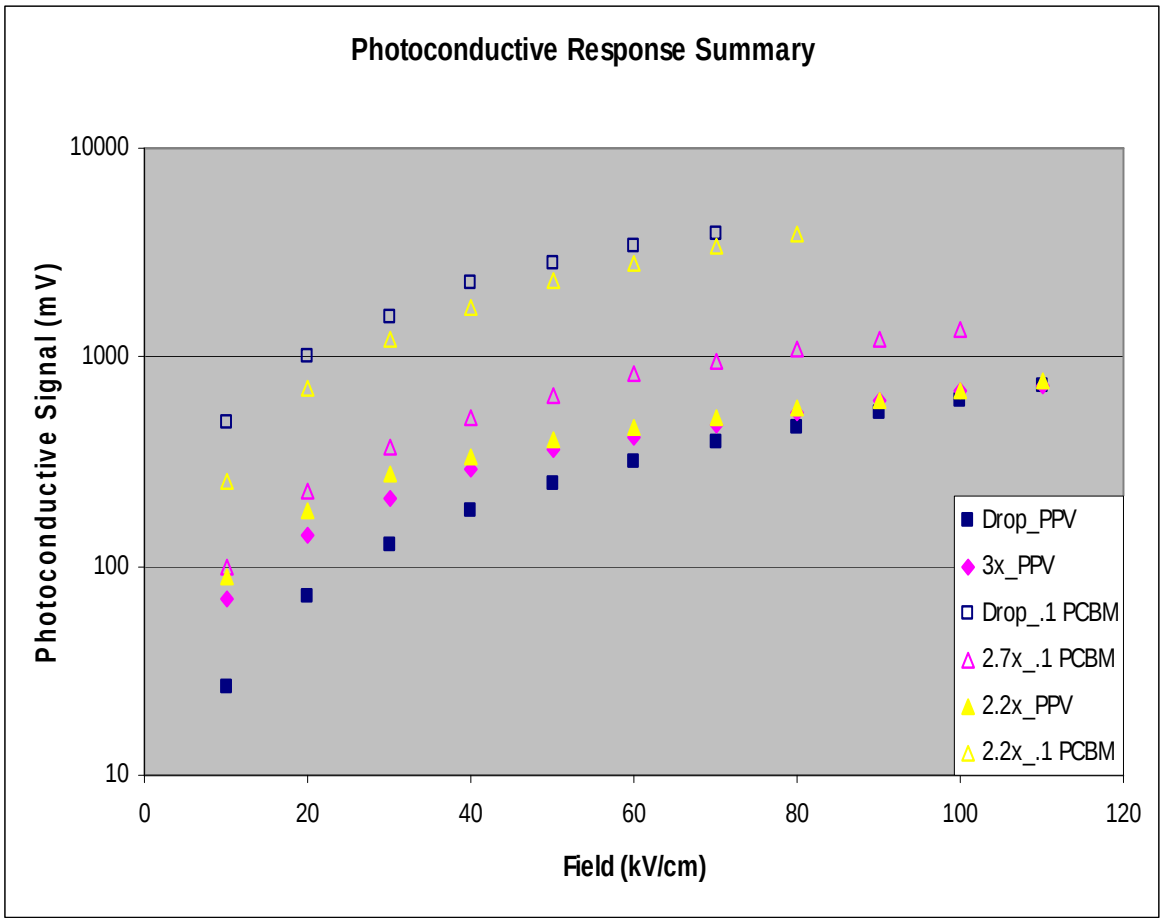

Figure 40. Photoconductive response summary of films stretched to different ratios with no PCBM (solid symbols) or 10% PCBM (open symbols).

The most likely explanation of this effect is the composite morphology, as this was likely significantly altered during the stretch alignment process. The polymer was still increasing in order, and likely still increasing in its own photoresponse, but not enough to compensate for the decreasing efficiency of the composite morphology. It is possible that the forces on the composite during the alignment are breaking apart some of the nanoparticle phases, or otherwise altering the two-phase morphology of the composite, making it less ideal. Scanning electron microscopy (SEM) analysis done of the top surfaces was inconclusive in this regard. All four samples, stretched and unstretched, with and without nanoparticles looked similar, with no striking differences in morphology at the nanoscale. There was some large scale (several μm) topography visible in the stretched samples, but this looked similar in both polymer and composite samples. SEM analysis done on samples sectioned horizontally or vertically may prove more informative. Unfortunately, there was not sufficient time and resources to investigate this further and this could be quite time consuming to investigate properly. Some representative SEM images are shown in Figure 41 and 42.

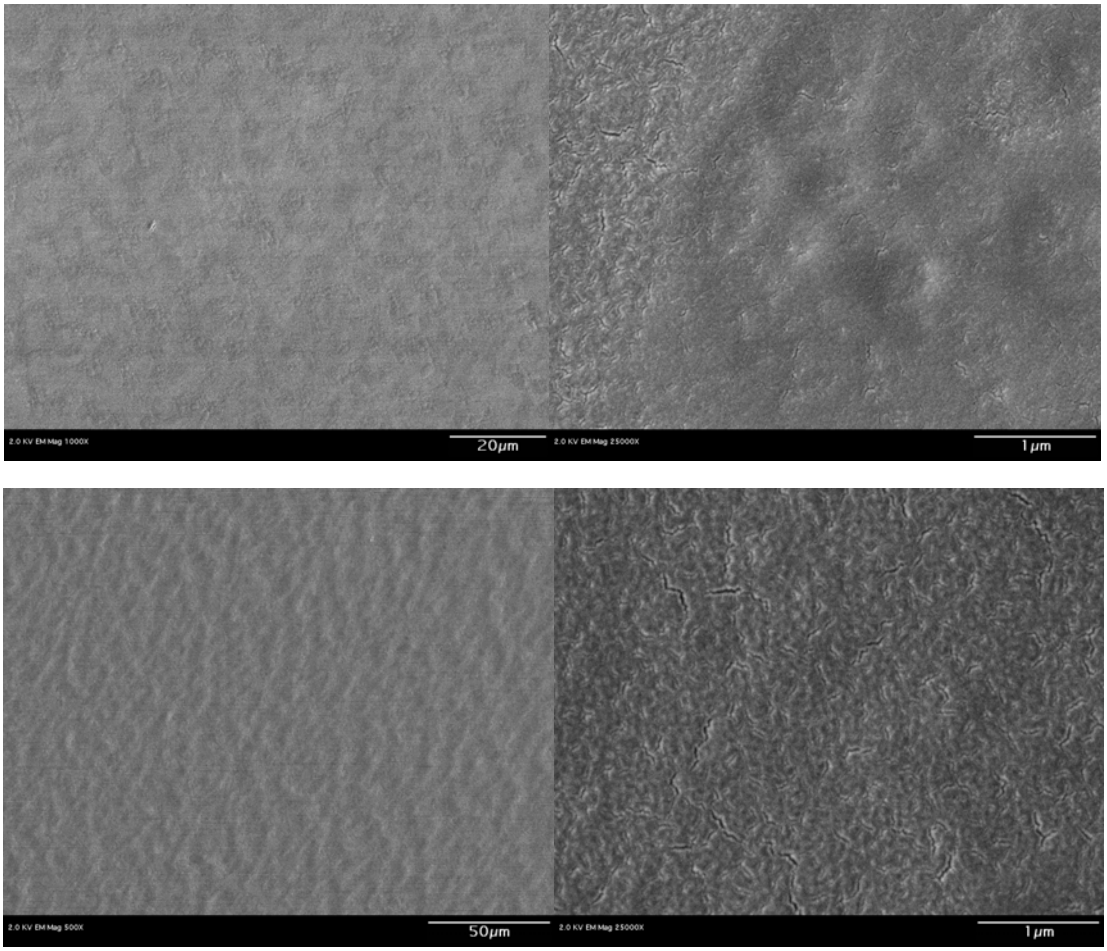

Figure 41. SEM images of (a) drop cast polymer (b) drop cast composite.

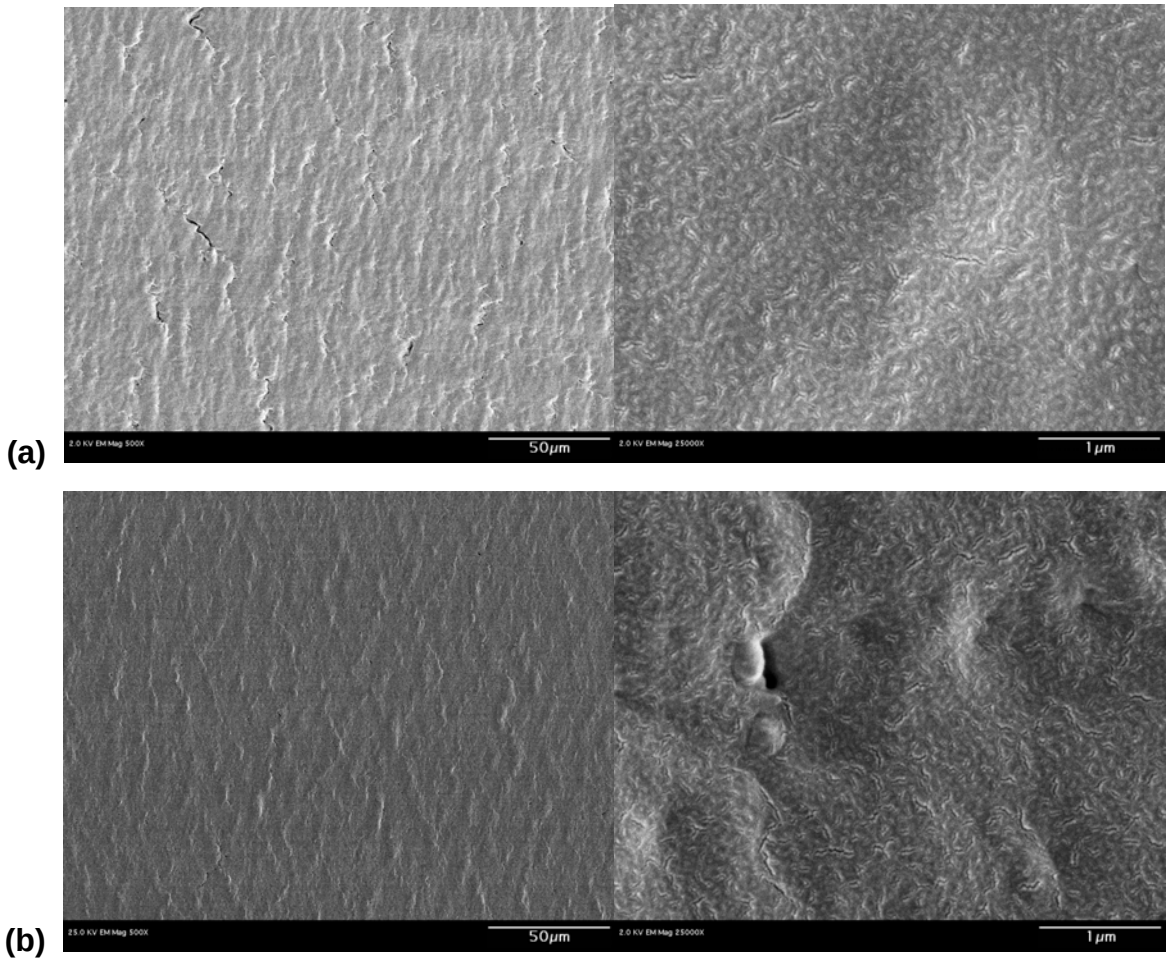

Figure 42. SEM images of (a) stretched polymer and (b) stretched composite.

The photoconductive response was also tested for its sensitivity to polarization of the excitation source. Drop cast films showed no response to polarization of the laser light, while stretched films showed a very significant change with the polarization of the laser. The laser energy was measured as a function of polarization and it changed less than a few percent over 180 degrees polarization, with 90 degrees rotation on the polarizer actually rotating the polarization 180 degrees. Figure 43 shows a summary of drop cast and stretched films with no PCBM and with 10% PCBM by weight and their sensitivity to polarization of the laser excitation. Each signal was normalized to its own maximum. The signals do not correlate particularly well with the stretch ratio, other than stretched or unstretched, and instead are all clustered together pretty closely. Readings were taken from zero degrees to 180, and some signal degradation over time is apparent which was recoverable after a few minutes with no bias and no laser, then resuming testing. This confirms an electrical impact of the order and also points to some potentially interesting applications such as possible directional sensitivity for a sensor, with the correct sensor design.

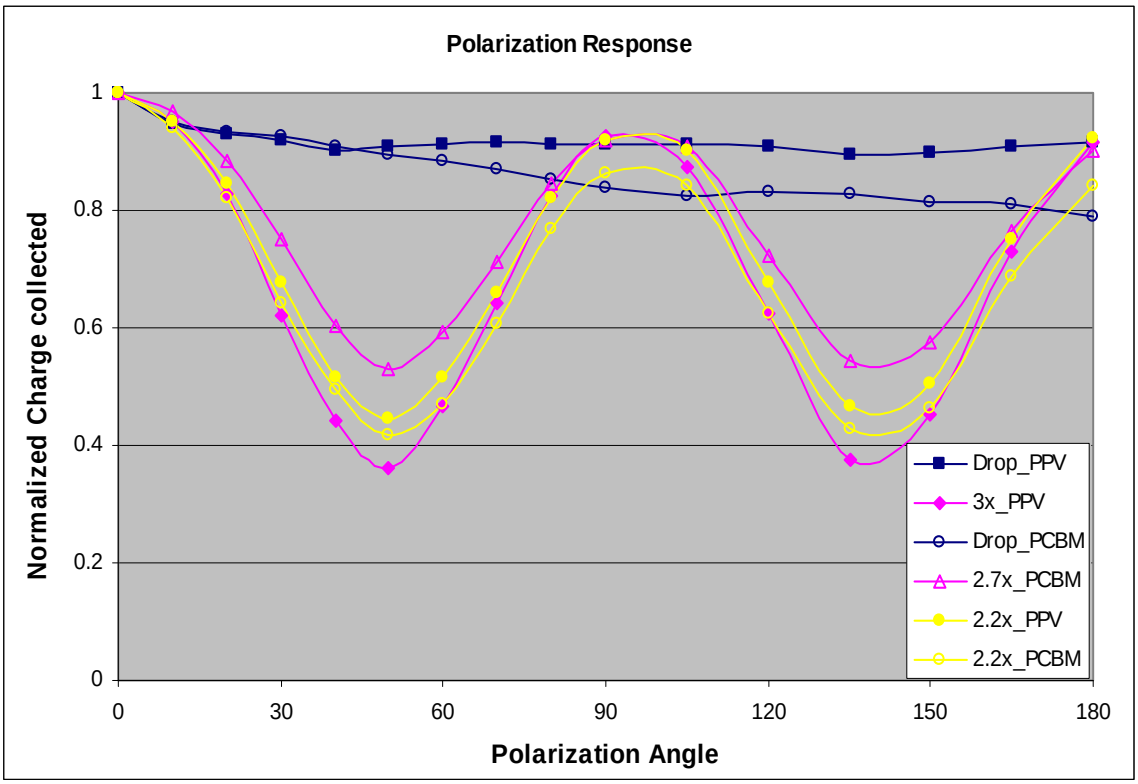

Figure 43. Photoconductive response to polarization of excitation source, OC10PPV with PCBM (open symbols) and without (solid symbols).

6.6 Other additives

Additional additives were screened for their effects on electrical properties. A similar polymer was used for initial screening efforts until promising additives were found. The polymer used was poly(2-Methoxy-5-(3,7-dimethyloctyloxy)-1,4-phenylenevinylene), referred to as MDMOPPV, obtained from Aldrich and used without further processing or filtering. This is essentially an asymmetric version of OC10PPV.

6.7 Co-solvent

The first additive screened was actually a co-solvent with a higher volatility, which could alter the drying rate of the film, having a significant effect on electrical properties in fullerene composites. This has been shown by other authors, but mostly with polythiophenes. A small amount of tetrahydrofuran (THF) was added to the existing mixture. This also serves to make the mixture much more workable with a lower viscosity, but it was necessary to ensure that this would not have any negative impacts on the properties. As shown in Figure 44, a dark current sweep at 0.5 V / 60 s showed essentially no difference with or without the volatile solvent added. To clarify the possible slight difference, this test was repeated with illumination in the same test box and same test parameters, and is shown on the same plot.

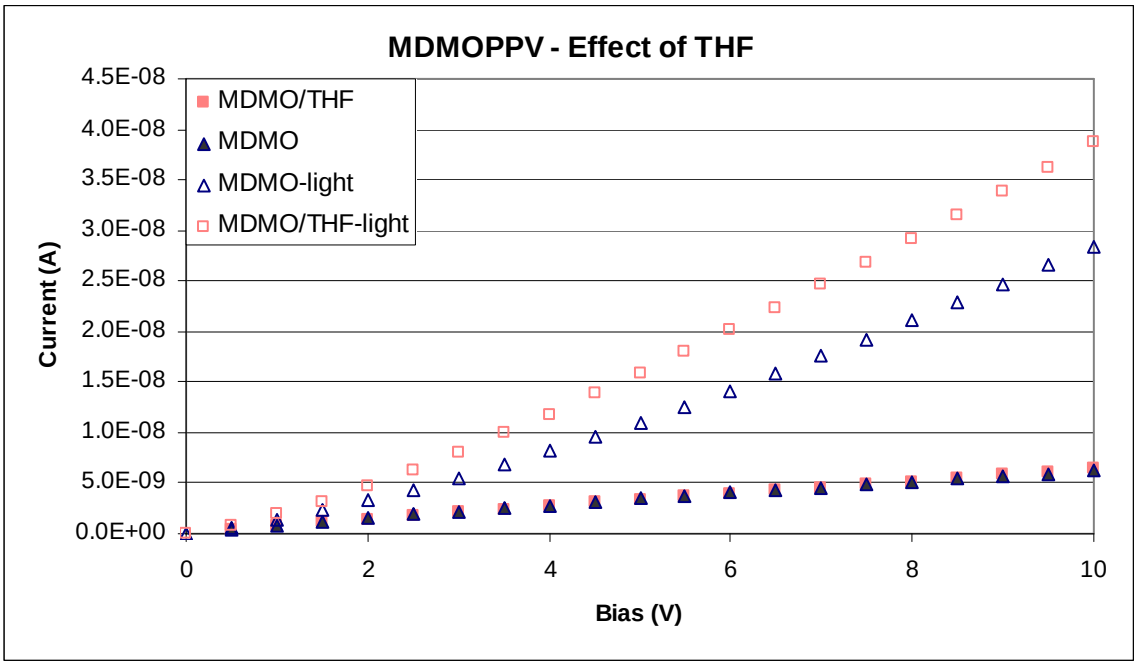

Figure 44. IV sweep of MDMOPPV in dark and illuminated with and without THF added.

The difference was enhanced and this time it does look like the sample with THF added may possibly have slightly higher dark current, but this is probably within error, particularly since the illumination conditions added some error. Once it is considered that this is under illumination, this current is still very low, and quite acceptable for radiation detection.

The IDTs were then tested for photoconductive response, as shown in Figure 45. The THF co-solvent appeared to have no significant impact on the photoconductivity of the MDMOPPV film.

The same procedure was then done with MDMOPPV/PCBM composites. THF was added and the IV behavior was analyzed under both dark and illuminated conditions. The data is shown in Figure 46. For both dark and illuminated, the THF appears to have essentially no effect on the IV behavior of the sample. The photoconductive response was tested with the same IDTs and also showed no sensitivity to the co-solvent, as shown in Figure 47. Although this did not improve the properties of the material, it also did not damage the properties, and it did decrease the viscosity of the solution, making it easier to work with, and thereby improving it from a processing standpoint.

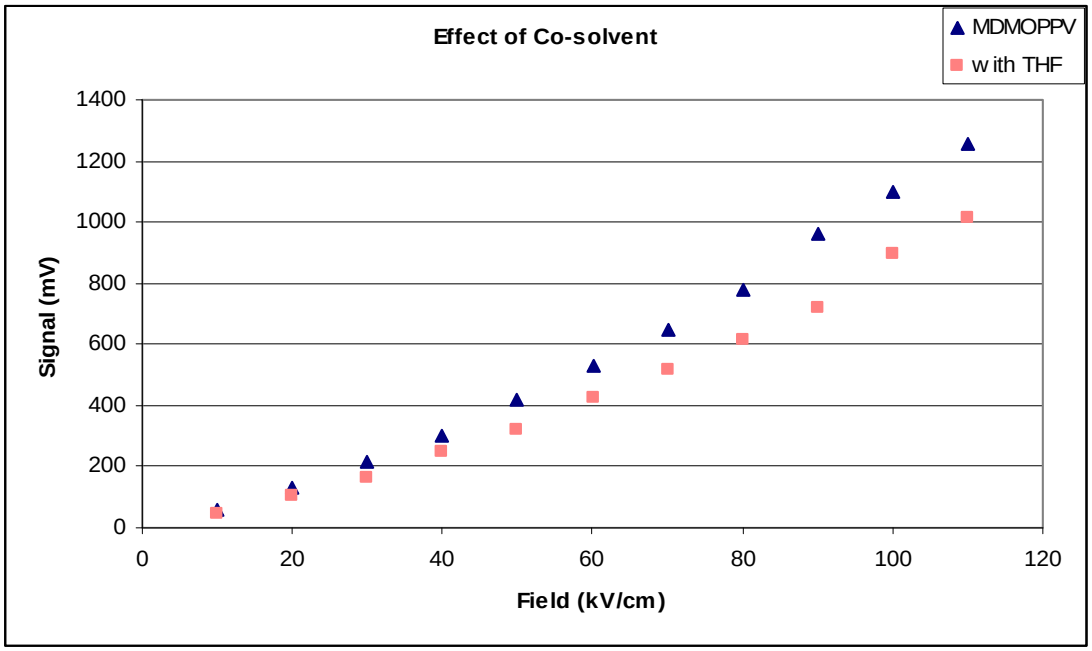

Figure 45. Photoconductive response of MDMOPPV with and without THF co-solvent.

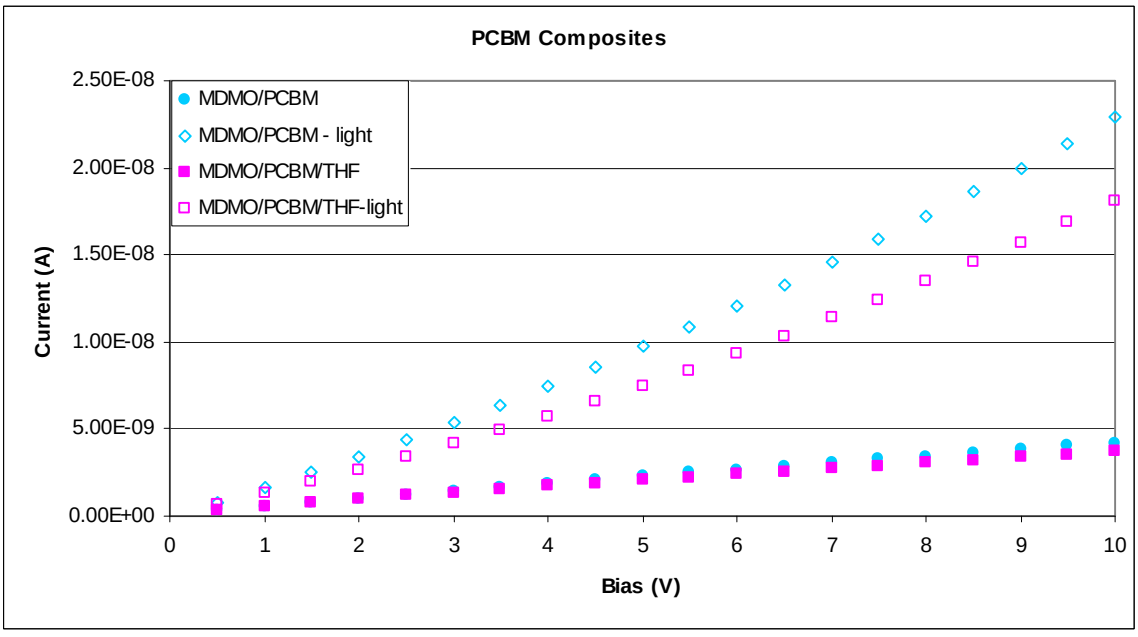

Figure 46. IV behavior for MDMOPPV/PCBM composites with and without THF.

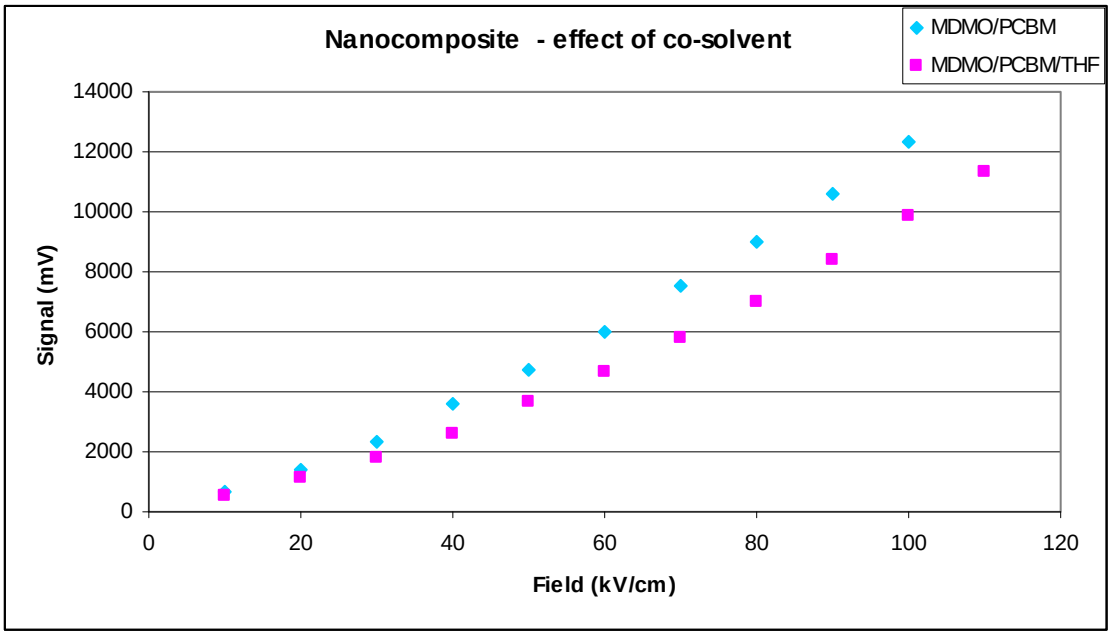

Figure 47. Photoconductive response of MDMOPPV/PCBM composites with and without THF.

6.8 Low molecular weight additive

The next additive investigated was stilbene. Stilbene is somewhat similar in structure to PPV, but with low molecular weight, so it tends to crystallize and form ordered structures. The question was if a small amount of stilbene added to PPV could act as a template to help induce order into the PPV as well. Two compositions were tried, with 10% and 20% by weight stilbene in MDMOPPV, combined from separately dissolved solutions, and drop cast onto both plain glass slides and IDTs. The drops from the 10% mixture appeared completely homogeneous to the naked eye, and no different than a pure polymer drop. However, the drops from the 20% solution were distinctly crystallized into quite large crystals. This was not entirely expected, as similar work done with a similar system of poly(3-hexylthiophene) and the small molecule dihexyl-quarterthiophene (DH4T) reported a critical concentration of 29% DH4T above which it would crystallize [8]. This was also the point at which they report a significant increase in mobility. This indicates the critical concentration for this PPV/stilbene system to be somewhere between 10% and 20% stilbene. Figure 48 shows optical microscope images of the films cast from the 10% and 20% stilbene solutions.

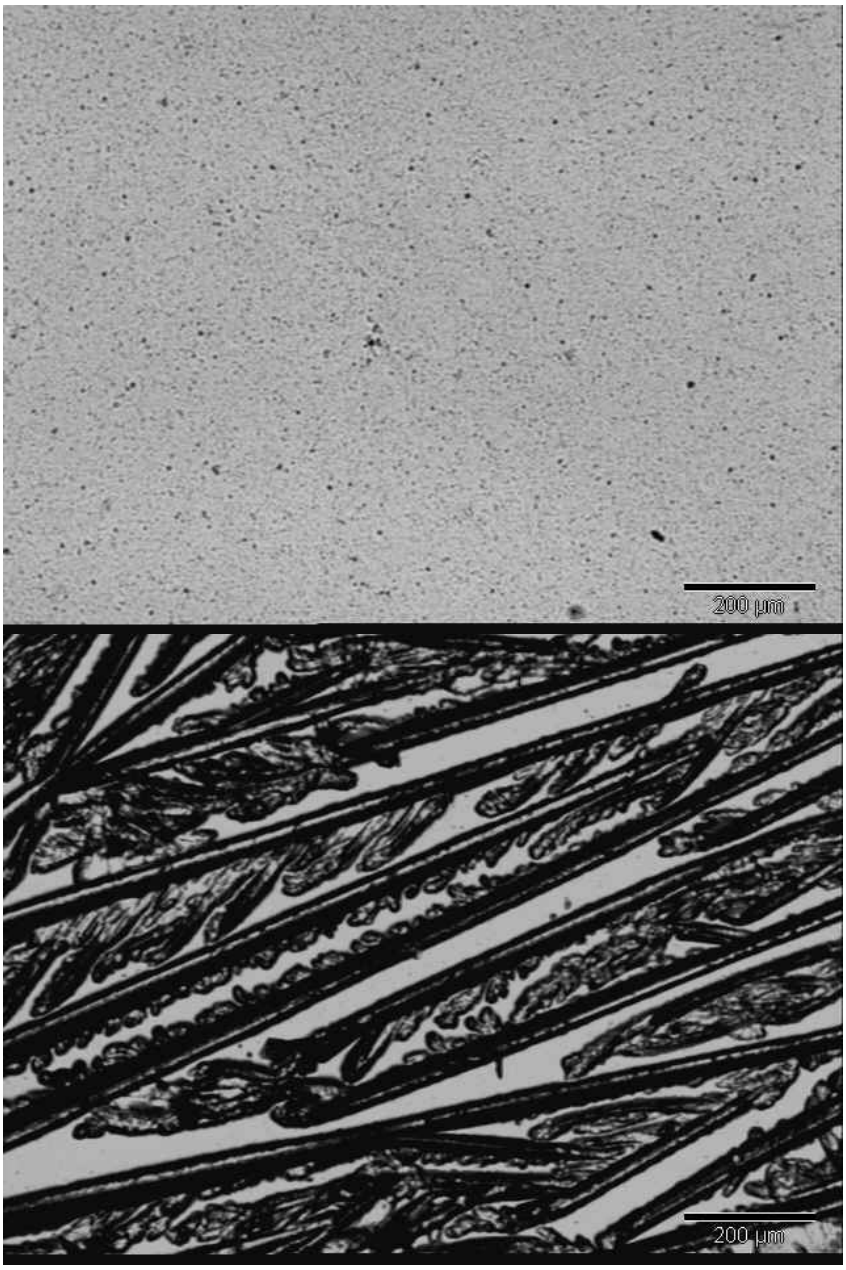

Figure 48. Optical microscope images of films cast from solutions of 10% (top) and 20% (bottom) stilbene in MDMOPPV.

The same solutions were also drop cast onto 16 µm IDTs and tested for their IV behavior under both dark and illuminated conditions and the results are shown in Figure 49. Interestingly, the two concentrations had negligible differences in their response. This could mean that the stilbene that is crystallizing is crystallizing out only on the top surface of the sample, which is not seen by the IDT and therefore not significantly altering the electrical properties.

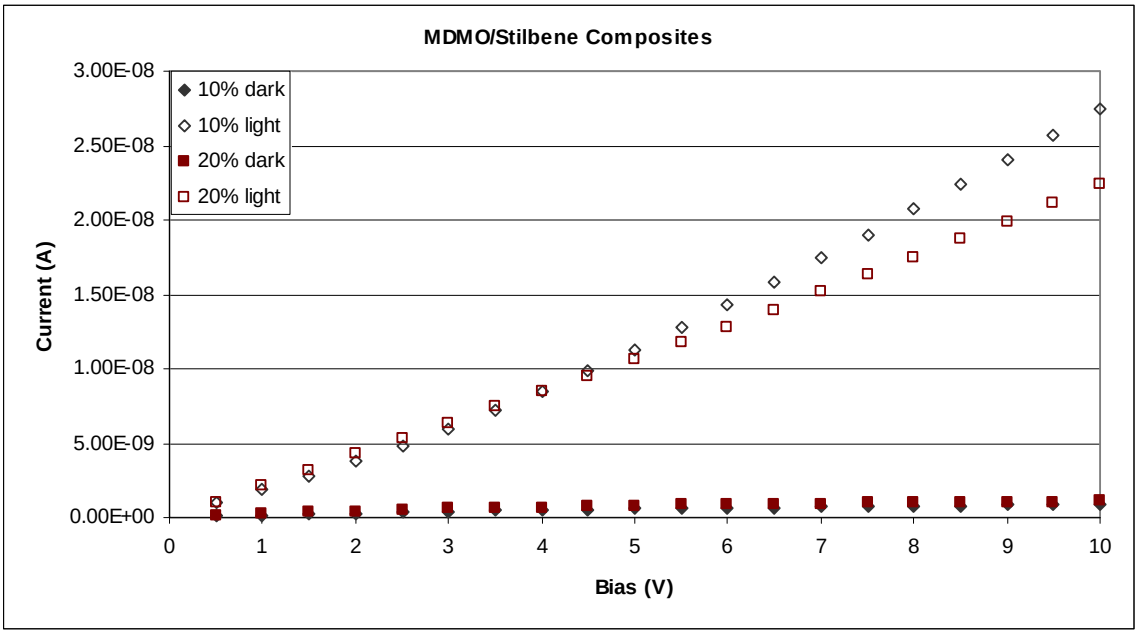

Figure 49. IV behavior of MDMOPPV with 10% and 20% stilbene.

The photoconductivity was tested on the same IDTs, and the results are shown in Figure 50. As might be expected from the IV data, the two samples showed essentially no difference. However, the literature cited saw dramatic increases in mobility above the point at which the small molecule started to crystallize within the blend, so it was unclear what to expect. The IV behavior had been essentially the same so the conductivity was not altered, but it may have been possible that some small changes were templated close enough to the electrodes to have altered mobility and affected the photoconductive response.

Figure 51 shows a summary of the photoconductivity data for the additive screening with MDMOPPV and MDMOPPV/PCBM blends. The PCBM blends show a much higher photoresponse than the MDMOPPV films without fullerenes, but this was previously shown. Interestingly, the increase is a bit less than it was for OC10PPV. Other variables showed no significant increase in photoresponse that is likely to be worth further investigation. Therefore, none of these was investigated with OC10PPV or pursued further.

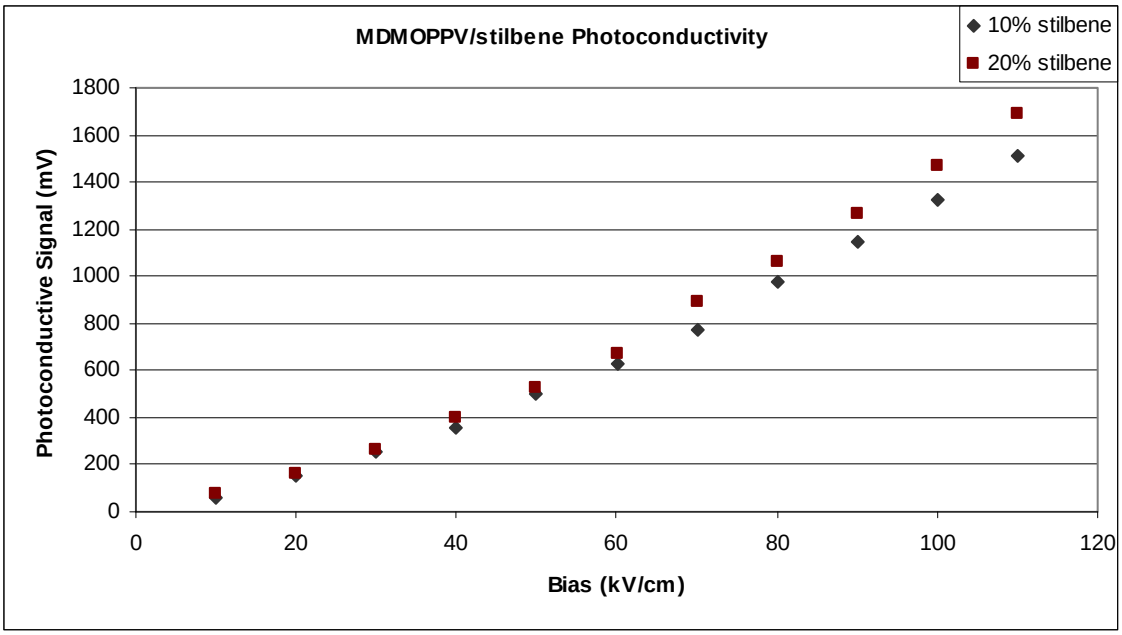

Figure 50. Photoconductive response for MDMOPPV with 10% or 20% stilbene.

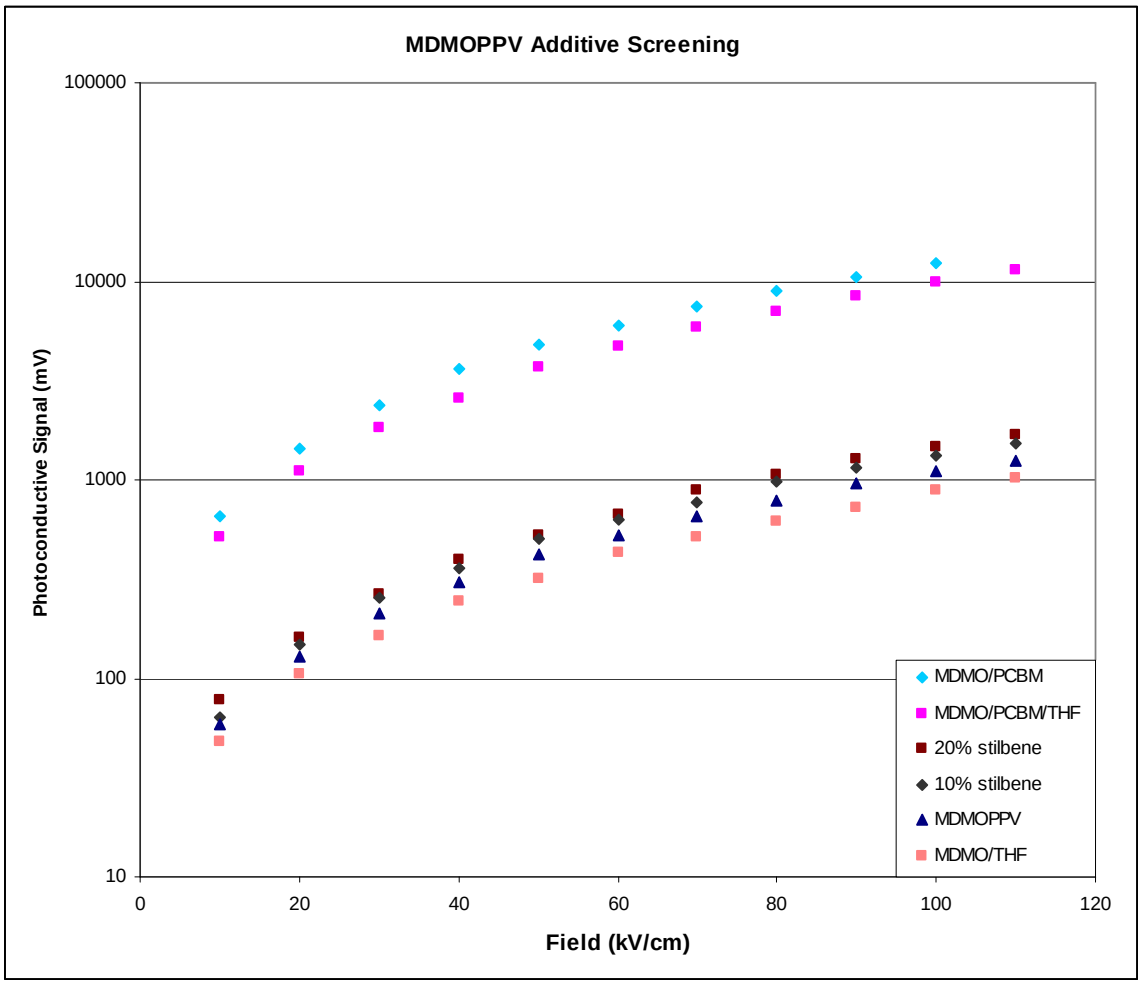

Figure 51. Summary plot of photoconductivity data for additive screening with MDMOPPV

This page intentionally left blank.

7. Particle Track Effect

Additional proton beam experiments were performed to estimate charge collection efficiency, and investigate angular response of film detectors. The experimental setup is shown in Figure 52 below. From our initial measurements it was known that subtle changes in response could be comparable to beam current variations; therefore a dual detector arrangement was built, as seen in the figure. This system employed a fixed free-standing PPV film detector in front, with a rotatable planar cast film detector in back. The fixed detector response was assumed proportional to the beam current, and the ratio of this signal to that of the device under test was used to determine the response variation with angle.

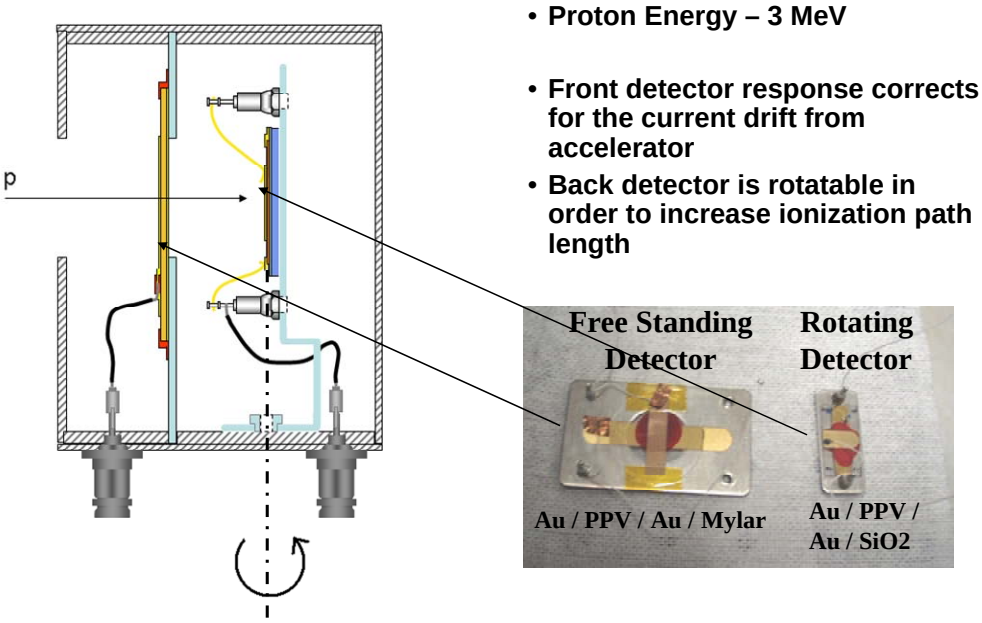

Figure 52. Experimental setup for angular response.

Results are seen in Figure 53 below. It was found that, contrary to the expected result, the signal strength decreased as the angle deviated from normal incidence. This is reasonable if it is assumed that a high mobility path is created along the particle track (i.e., traps are saturated near ionization path). In this case the charge motion will be fastest along ionization track, where the electric field component is reduced to exactly offset the increased carrier number. The signal strength is reduced, however, because only carrier motion in the z direction contributes to signal, resulting in the observed signal proportional to cos(θ).

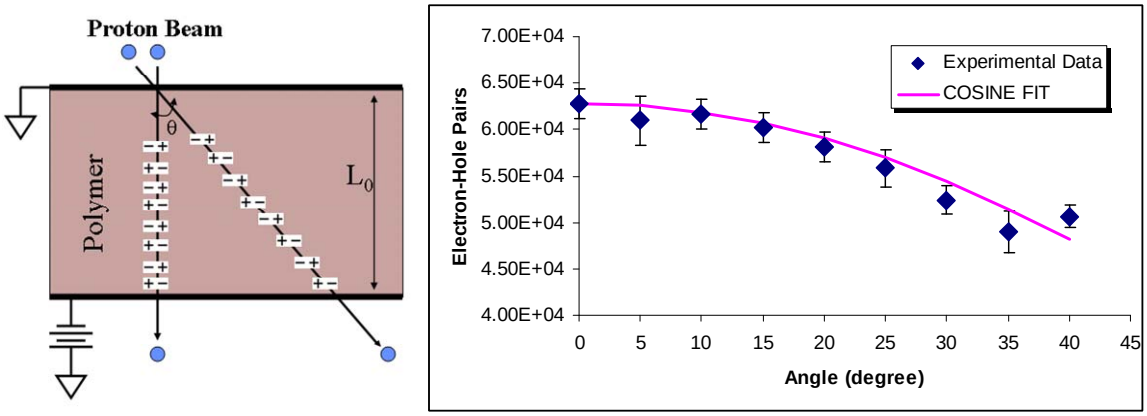

Figure 53. Results of proton beam experiments to estimate charge collection efficiency.

8. Conclusions

Conjugated polymers in the family of substituted poly(*p*-phenylene vinylene)s were investigated as detectors for ionizing radiation, primarily fission energy neutrons (0.1- 2 MeV). Semiconducting organic materials can have a high ratio of hydrogen to carbon, allowing for neutron sensitivity with no moderator, while the low Z provides minimal gamma interaction. These wide bandgap semiconductors can be selected to have high resistivity and high dielectric strength, allowing operation at high bias with low background noise. The materials can also be solution cast, allowing very different detector forms than currently available with crystalline semiconductors. Significant increases in size and reductions in cost are also possible with scale-up considerations. However, initial inquiries showed that improvements in charge collection efficiency were necessary in order to achieve the desired single particle detection with a reasonable signal-to-noise ratio. This work examines processing variables and additives to achieve that increase, as well as relevant environmental considerations.

This work demonstrated the viability of using π-conjugated organic materials for semiconducting neutron detection based on their proton-induced conductivity transient response. This further showed that the material property improvements can be tested via photoconductive response, which can be correlated to the proton response. IDT devices exhibited turn-on at biases of only 50 V, and did not show significant signal degradation until a total dose of 1 Mrad. Modeling showed that thicker films are necessary to be able to absorb much of the energy, but this is difficult to optimize with charge collection.

Films of substituted PPV, OC10PPV, were exposed to a 3 MeV proton beam and showed ion-induced transients. This showed similar shape to photo-induced transients from laser excitation. Due to the greater ease of experimentation, the laser excitation was used for further experiments. The proton exposure was also used to verify radiation hardness to a total exposure of approximately 1 Mrad, and viability of use at a bias of only 50 V. Modeling showed that the film used for testing was far too thin to include the Bragg peak of the beam, but charge collection would be difficult across such a thickness and this parameter should later be optimized for a final device.

The substituted PPV, MEHPPV, was shown to exhibit electrical sensitivity to temperature fluctuations as small as one degree Celsius. Films also showed electrical sensitivity to environmental differences of ambient air, dry air, and dry nitrogen. After storage in environments of ambient air or dry nitrogen, the excitation and emission spectra differed in intensities between the two samples, and the sample stored in air gained a significant shoulder in the emission spectrum.

Polarized FTIR was used to quantify the order in films using the Hermans orientation function. Drop cast films were found to be completely amorphous with an orientation function of zero, and films stretch-aligned post-polymerization to a ratio of 3.7 had an orientation function as high as 0.66. These values approached the theoretical Kratky function, thought to be a limiting value for constant density polymer alignment. Post-stretching annealing, at the conditions tested, did not improve alignment. The stretch rate appeared to have no impact, nor did exposure to dry methanol vapor prior to and during alignment. Addition of up to 20% by weight of PCBM

nanoparticles did not interfere with the polymer alignment. Greater amounts of nanoparticles resulted in a polymer of insufficient quality to support a freestanding film for FTIR testing. Post-polymerization alignment methods have rarely been attempted, but are appealing for scale-up.

The photoconductive response approximately doubled for stretch-aligned films with the stretch direction parallel to the electric field direction, when compared to as cast films. The response was decreased when the stretch direction was oriented orthogonally to the electric field. Stretch-aligned films also exhibited a significant sensitivity to the linear polarization of the laser excitation, whereas drop-cast films showed none. This indicates improved mobility along the backbone, but poor π-overlap in the orthogonal direction, as was hoped for.

Drop-cast composites of PPV with PCBM nanoparticles showed approximately a two order of magnitude increase in photoresponse, nearly independent of the amount of nanoparticle content. Interestingly, stretch-aligned composite films showed a substantial decrease in photoresponse with increasing stretch ratio. Other additives examined, including small molecules and co-solvents, did not cause any significant increase in photoresponse.

Finally, we discovered an inverse-geometric particle track effect wherein increased track lengths created by tilting the detector off normal incidence resulted in decreased signal collection. This is interpreted as a trap-filling effect, leading to increased carrier mobility along the track direction. Estimated collection efficiency along the track direction was near 20 electrons / micron of track length, sufficient for particle counting.

Bibliography

Barisci, J. N., C. Conn, and G. G. Wallace. "Conducting Polymer Sensors." *Trends in Polymer Science* 4, no. 9 (1996): 307-11.

Bartle, C. M., and R. C. Haight. "Small Inorganic Scintillators as Neutron Detectors." *Nuclear Instruments & Methods in Physics Research Section a-Accelerators Spectrometers Detectors and Associated Equipment* 422, no. 1-3 (1999): 54-58.

Baughman, R. H., A. A. Zakhidov, and W. A. de Heer. "Carbon Nanotubes - the Route toward Applications." *Science* 297, no. 5582 (2002): 787-92.

Bay, L., K. West, P. Sommer-Larsen, S. Skaarup, and M. Benslimane. "A Conducting Polymer Artificial Muscle with 12% Linear Strain." *Advanced Materials* 15, no. 4 (2003): 310-13.

Beckerle, P., and H. Strobele. "Charged Particle Detection in Organic Semiconductors." *Nuclear Instruments & Methods in Physics Research Section a-Accelerators Spectrometers Detectors and Associated Equipment* 449, no. 1-2 (2000): 302-10.

Berets, D. J., and D. S. Smith. "Electrical Properties of Linear Polyacetylene " *Transactions of the Faraday Society* 64, no. 543P (1968): 823-28.

Bertho, S., G. Janssen, T. J. Cleij, B. Conings, W. Moons, A. Gadisa, J. D'Haen, E. Goovaerts, L. Lutsen, J. Manca, and D. Vanderzande. "Effect of Temperature on the Morphological and Photovoltaic Stability of Bulk Heterojunction Polymer: Fullerene Solar Cells." *Solar Energy Materials and Solar Cells* 92, no. 7 (2008): 753-60.

Blom, P. W. M., and Mcjm Vissenberg. "Charge Transport in Poly(P-Phenylene Vinylene) Light-Emitting Diodes." *Materials Science & Engineering R-Reports* 27, no. 3-4 (2000): 53-94.

Bolotnikov, A. E., G. C. Camarda, G. W. Wright, and R. B. James. "Factors Limiting the Performance of Cdznte Detectors." *Ieee Transactions on Nuclear Science* 52, no. 3 (2005): 589-98.

Bozano, L., S. E. Tuttle, S. A. Carter, and P. J. Brock. "Temperature-Dependent Recombination in Polymer Composite Light-Emitting Diodes." *Applied Physics Letters* 73, no. 26 (1998): 3911-13.

Brabec, C. J., N. S. Sariciftci, and J. C. Hummelen. "Plastic Solar Cells." *Advanced Functional Materials* 11, no. 1 (2001): 15-26.

Bradley, D. D. C. "Precursor-Route Poly(P-Phenylenevinylene) - Polymer Characterization and Control of Electronic Properties." *Journal of Physics D-Applied Physics* 20, no. 11 (1987): 1389-410.

Bradley, D. D. C., R. H. Friend, T. Hartmann, E. A. Marseglia, M. M. Sokolowski, and P. D. Townsend. "Structural Studies of Oriented Precursor Route Conjugated Polymers." *Synthetic Metals* 17, no. 1-3 (1987): 473-78.

Bradley, D. D. C., R. H. Friend, H. Lindenberger, and S. Roth. "Infrared Characterization of Oriented Poly(Phenylene Vinylene)." *Polymer* 27, no. 11 (1986): 1709-13.

Briers, J., W. Eevers, P. Cos, H. J. Geise, R. Mertens, P. Nagels, X. B. Zhang, G. Vantendeloo, W. Herrebout, and B. Vanderveken. "Molecular-Orientation and Conductivity in Highly Oriented Poly(P-Phenylene Vinylene) " *Polymer* 35, no. 21 (1994): 4569-72.

Briskman, B. A. "Specificity of Proton Irradiation Effects on Polymers." *Nuclear Instruments & Methods in Physics Research Section B-Beam Interactions with Materials and Atoms* 265, no. 1 (2007): 72-75.

Brooks, F. D., and H. Klein. "Neutron Spectrometry - Historical Review and Present Status." *Nuclear Instruments & Methods in Physics Research Section a-Accelerators Spectrometers Detectors and Associated Equipment* 476, no. 1-2 (2002): 1-11.

Brutting, Wolfgang, ed. *Physics of Organic Semiconductors*. Weinheim, Germany: Wiley, 2005.

Bulle-Lieuwma, C. W. T., J. K. J. van Duren, X. Yang, J. Loos, A. B. Sieval, J. C. Hummelen, and R. A. J. Janssen. "Characterization of Poly(P-Phenylene Vinylene)/Methanofullerene Blends of Polymer Solar Cells by Time-of-Flight Secondary Ion Mass Spectrometry." *Applied Surface Science* 231-2 (2004): 274-77.

Campbell, I. H., D. L. Smith, C. J. Neef, and J. P. Ferraris. "Consistent Time-of-Flight Mobility Measurements and Polymer Light-Emitting Diode Current-Voltage Characteristics." *Applied Physics Letters* 74, no. 19 (1999): 2809-11.

Campoy-Quiles, M., T. Ferenczi, T. Agostinelli, P. G. Etchegoin, Y. Kim, T. D. Anthopoulos, P. N. Stavrinou, D. D. C. Bradley, and J. Nelson. "Morphology Evolution Via Self-Organization and Lateral and Vertical Diffusion in Polymer: Fullerene Solar Cell Blends." *Nature Materials* 7, no. 2 (2008): 158-64.

Chen, D., M. J. Winokur, M. A. Masse, and F. E. Karasz. "A Structural Study of Poly(Para-Phenylene Vinylene) " *Polymer* 33, no. 15 (1992): 3116-22.

Clough, Roger, and Shalaby W. Shalaby. *Irradiation of Polymers: Fundamentals and Technological Applications*, *Acs Symposium Series 620*: American Chemical Society, 1996.

Comoretto, D., C. Soci, F. Marabelli, A. Mikhailovsky, and D. Moses. "Polarized Optical and Photoluminescence Properties of Highly Oriented Poly(P-Phenylene-Vinylene)." *Synthetic Metals* 153, no. 1-3 (2005): 281-84.

Czirr, J. B., D. B. Merrill, D. Buehler, T. K. McKnight, J. L. Carroll, T. Abbott, and E. Wilcox. "Capture-Gated Neutron Spectrometry." *Nuclear Instruments & Methods in Physics Research Section a-Accelerators Spectrometers Detectors and Associated Equipment* 476, no. 1-2 (2002): 309-12.

Deen, A. J., M. H. Kazemeini, Y. M. Haddlara, H. F. Yu, G. Vamvounis, S. Holdcroft, and W. Woods. "Electrical Characterization of Polymer-Based Fets Fabricated by Spin-Coating Poly(3-Alkylthiophene)S." *Ieee Transactions on Electron Devices* 51, no. 11 (2004): 1892-901.

Delto, R., and R. Brenn. "Molecular Weight Distribution of Proton Irradiated Polystyrene Studied by Diffusion Experiments." *Nuclear Instruments & Methods in Physics Research Section B-Beam Interactions with Materials and Atoms* 257 (2007): 532-35.

Deng, X. Y., L. P. Zheng, C. H. Yang, Y. F. Li, G. Yu, and Y. Cao. "Polymer Photovoltaic Devices Fabricated with Blend Mehppv and Organic Small Molecules." *Journal of Physical Chemistry B* 108, no. 11 (2004): 3451-56.

Dermaut, W., T. Van den Kerkhof, B. Goderis, R. Mertens, I. Dolbnya, B. J. van der Veken, F. Blockhuys, and H. J. Geise. "A Volume-Corrected Kratky Model and the Influence of the Shape of the Orientation Distribution Function on the Molecular Orientation in Ppv and Its Precursor." *Macromolecules* 37, no. 1 (2004): 110-17.

Dermaut, W., T. Van den Kerkhof, B. J. van der Veken, R. Mertens, and H. J. Geise. "Cold Stretching of Ppv with Water as a Plasticizer." *Macromolecules* 33, no. 15 (2000): 5634-37.

Dodabalapur, A., L. Torsi, and H. E. Katz. "Organic Transistors- 2-Dimensional Transport and Improved Electrical Characteristics." *Science* 268, no. 5208 (1995): 270-71.

Doty, F. Patrick , and Douglas A. Chinn. "Organic Materials and Devices for Detecting Ionizing Radiation." United States: Sandia National Laboratories, 2007.

Dyreklev, P., G. Gustafsson, O. Inganas, and H. Stubb. "Aligned Polymer-Chain Field-Effect Transistors " *Solid State Communications* 82, no. 5 (1992): 317-20.

Fehrenbacher, G., J. Biersack, E. Cordes, and W. Wahl. "Response of Converter Semiconductor Detectors on Neutron Radiation." *Radiation Measurements* 28, no. 1-6 (1997): 429-34.

Feldman, W. C., B. L. Barraclough, K. R. Fuller, D. J. Lawrence, S. Maurice, M. C. Miller, T. H. Prettyman, and A. B. Binder. "The Lunar Prospector Gamma-Ray and Neutron Spectrometers." *Nuclear Instruments & Methods in Physics Research Section a-Accelerators Spectrometers Detectors and Associated Equipment* 422, no. 1-3 (1999): 562-66.

Forzani, E. S., H. Q. Zhang, L. A. Nagahara, I. Amlani, R. Tsui, and N. J. Tao. "A Conducting Polymer Nanojunction Sensor for Glucose Detection." *Nano Letters* 4, no. 9 (2004): 1785-88.

Gagnon, D. R., F. E. Karasz, E. L. Thomas, and R. W. Lenz. "Molecular-Orientation and Conductivity in Highly Drawn Poly(P-Phenylene Vinylene) " *Synthetic Metals* 20, no. 1 (1987): 85-95.

Geens, W., D. Tsamouras, J. Poortmans, and G. Hadziioannou. "Field-Effect Mobilities in Spin-Cast and Vacuum-Deposited Ppv-Type Pentamers." *Synthetic Metals* 122, no. 1 (2001): 191-94.

Gelinck, G. H., J. M. Warman, and E. G. J. Staring. "Polaron Pair Formation, Migration, and Decay on Photoexcited Poly(Phenylenevinylene) Chains." *Journal of Physical Chemistry* 100, no. 13 (1996): 5485-91.

Gerard, M., A. Chaubey, and B. D. Malhotra. "Application of Conducting Polymers to Biosensors." *Biosensors & Bioelectronics* 17, no. 5 (2002): 345-59.

Glidle, A., C. S. Hadyoon, N. Gadegaard, J. M. Cooper, A. R. Hillman, A. R. Wilson, K. S. Ryder, J. R. P. Webster, and R. Cubitt. "Evaluating the Influence of Deposition Conditions on Solvation of Reactive Conducting Polymers with Neutron Reflectivity." *Journal of Physical Chemistry B* 109, no. 30 (2005): 14335-43.

Gregorius, R., and F. E. Karasz. "Orientation in Poly(Arylene Vinylene) Copolymers and Blends - an Infrared Dichroism Study " *European Polymer Journal* 29, no. 2-3 (1993): 159-62.

Gustafsson, G., O. Inganas, and S. Stafstrom. "Optical Anisotropy of Neutral and Doped Poly(3-Octylthiophene) " *Solid State Communications* 76, no. 2 (1990): 203-08.

Hamada, H. M., P. R. Rela, F. E. da Costa, and C. H. de Mesquita. "Radiation Damage Studies on the Optical and Mechanical Properties of Plastic Scintillators." *Nuclear Instruments & Methods in Physics Research Section a-Accelerators Spectrometers Detectors and Associated Equipment* 422, no. 1-3 (1999): 148-54.

Hamel, L. A., L. Lessard, L. Rainville, V. Zacek, and B. Sur. "A Superheated Droplet Detector for Dark Matter Search." *Nuclear Instruments & Methods in Physics Research Section a-Accelerators Spectrometers Detectors and Associated Equipment* 388, no. 1-2 (1997): 91-99.

Hashemi-Nezhad, S. R., and L. S. Peak. "Limitation on the Response of He-3 Counters Due to Intrinsic Alpha Emission." *Nuclear Instruments & Methods in Physics Research Section a-Accelerators Spectrometers Detectors and Associated Equipment* 416, no. 1 (1998): 100-08.

Heeger, A. J. "Nobel Lecture: Semiconducting and Metallic Polymers: The Fourth Generation of Polymeric Materials." *Reviews of Modern Physics* 73, no. 3 (2001): 681-700.

Heil, H., T. Finnberg, N. von Malm, R. Schmechel, and H. von Seggern. "The Influence of Mechanical Rubbing on the Field-Effect Mobility in Polyhexylthiophene." *Journal of Applied Physics* 93, no. 3 (2003): 1636-41.

Heller, C. M., I. H. Campbell, B. K. Laurich, D. L. Smith, D. D. C. Bradley, P. L. Burn, J. P. Ferraris, and K. Mullen. "Solid-State-Concentration Effects on the Optical Absorption and Emission of Poly(P-Phenylene Vinylene)-Related Materials." *Physical Review B* 54, no. 8 (1996): 5516-22.

Hong, H. P., R. Steitz, S. Kirstein, and D. Davidov. "Superlattice Structures in Poly(Phenylenevinylene)-Based Self-Assembled Films." *Advanced Materials* 10, no. 14 (1998): 1104-08.

Huser, T., and M. Yan. "Solvent-Related Conformational Changes and Aggregation of Conjugated Polymers Studied by Single Molecule Fluorescence Spectroscopy." *Journal of Photochemistry and Photobiology a-Chemistry* 144, no. 1 (2001): 43-51.

Intel. *Intel Opens Leading-Edge 65nm, 300mm High-Volume Wafer Manufacturing Facility in Arizona* 2005 [cited April 4 2007]. Available from http://www.intel.com/pressroom/archive/releases/20051102corp.htm.

Itoga, T., M. Ishikawa, M. Baba, T. Okuji, T. Oishi, M. Nakhostin, and T. Nishitani. "Fast Response Neutron Emission Monitor for Fusion Reactor Using Stilbene Scintillator and Flash-Adc." *Radiation Protection Dosimetry* 126, no. 1-4 (2007): 380-83.

Johnston, J. H., J. Moraes, and T. Borrmann. "Conducting Polymers on Paper Fibres." *Synthetic Metals* 153, no. 1-3 (2005): 65-68.

Jordan, D. V., J. H. Ely, A. J. Peurrung, L. J. Bond, J. I. Collar, M. Flake, M. A. Knopf, W. K. Pitts, M. Shaver, A. Sonnenschein, J. E. Smart, and L. C. Todd. "Neutron Detection Via Bubble Chambers." *Applied Radiation and Isotopes* 63, no. 5-6 (2005): 645-53.

Kazukauskas, V. "Investigation of Carrier Transport and Trapping by Oxygen-Related Defects in Meh-Ppv Diodes." *Semiconductor Science and Technology* 19, no. 12 (2004): 1373-80.

Kemerink, M., J. K. J. van Duren, P. Jonkheijm, W. F. Pasveer, P. M. Koenraad, R. A. J. Janssen, H. W. M. Salemink, and J. H. Wolter. "Relating Substitution to Single-Chain Conformation and Aggregation in Poly(P-Phenylene Vinylene) Films." *Nano Letters* 3, no. 9 (2003): 1191-96.

Kennedy, Tom, and Elliott H. Lieb. "Proof of the Peierls Instability in One Dimension." *Physical Review Letters* 59, no. 12 (1987): 1309.

Kinder, L., J. Kanicki, and P. Petroff. "Structural Ordering and Enhanced Carrier Mobility in Organic Polymer Thin Film Transistors." *Synthetic Metals* 146, no. 2 (2004): 181-85.

Klein, C. A. "Bandgap Dependence and Related Features of Radiation Ionization Energies in Semiconductors " *Journal of Applied Physics* 39, no. 4 (1968): 2029-38.

Kline, R. J., M. D. McGehee, E. N. Kadnikova, J. S. Liu, and J. M. J. Frechet. "Controlling the Field-Effect Mobility of Regioregular Polythiophene by Changing the Molecular Weight." *Advanced Materials* 15, no. 18 (2003): 1519-22.

Kline, R. J., M. D. McGehee, E. N. Kadnikova, J. S. Liu, J. M. J. Frechet, and M. F. Toney. "Dependence of Regioregular Poly(3-Hexylthiophene) Film Morphology and Field-Effect Mobility on Molecular Weight." *Macromolecules* 38, no. 8 (2005): 3312-19.

Knoll, Glenn F. *Radiation Detection and Measurement*. 3 ed. New York: Wiley, 2000.

Koenig, Jack L. *Spectroscopy of Polymers*. Washington, DC: American Chemical Society, 1992.

Koerner, H., D. Jacobs, D. W. Tomlin, J. D. Busbee, and R. D. Vaia. "Tuning Polymer Nanocomposite Morphology: Ac Electric Field Manipulation of Epoxy-Montmorillonite (Clay) Suspensions." *Advanced Materials* 16, no. 4 (2004): 297-302.

Kozorezov, A. G., J. K. Wigmore, A. Owens, R. den Hartog, A. Peacock, and H. A. Al-Jawhari. "Resolution Degradation of Semiconductor Detectors Due to Carrier Trapping." *Nuclear Instruments & Methods in Physics Research Section a-Accelerators Spectrometers Detectors and Associated Equipment* 546, no. 1-2 (2005): 209-12.

Krishnamurthy, V. V., A. S. Bhandar, M. Piao, I. Zoto, A. M. Lane, D. E. Nikles, J. M. Wiest, G. J. Mankey, L. Porcar, and C. J. Glinka. "Shear- and Magnetic-Field-Induced Ordering in Magnetic Nanoparticle Dispersion from Small-Angle Neutron Scattering." *Physical Review E* 67, no. 5 (2003).

Kumar, N. D., J. D. Bhawalkar, P. N. Prasad, F. E. Karasz, and B. Hu. "Solid-State Tunable Cavity Lasing in a Poly(Para-Phenylene Vinylene) Derivative Alternating Block Co-Polymer." *Applied Physics Letters* 71, no. 8 (1997): 999-1001.

Lee, T. W., Y. Byun, B. W. Koo, I. N. Kang, Y. Y. Lyu, C. H. Lee, L. Pu, and S. Y. Lee. "All-Solution-Processed N-Type Organic Transistors Using a Spinning Metal Process." *Advanced Materials* 17, no. 18 (2005): 2180-84.

Low, H. Y. "Photo and Photo-Oxidative Degradations of Poly(Phenylene Vinylene) Derivatives." *Thin Solid Films* 413, no. 1-2 (2002): 160-66.

Ltaief, A., J. Davenas, A. Bouazizi, R. Ben Chaabane, P. Alcouffe, and H. Ben Ouada. "Film Morphology Effects on the Electrical and Optical Properties of Bulk Heterojunction Organic Solar Cells Based on Meh-Ppv/C-60 Composite." *Materials Science & Engineering C-Biomimetic and Supramolecular Systems* 25, no. 1 (2005): 67-75.

Ludwig, G. W., and R. L. Watters. "Drift and Conductivity Mobility in Silicon " *Physical Review* 101, no. 6 (1956): 1699-701.

Majkrzak, C. F. "Neutron Reflectometry Studies of Thin Films and Multilayered Materials." *Acta Physica Polonica A* 96, no. 1 (1999): 81-99.

Malliaras, G., and R. Friend. "An Organic Electronics Primer." *Physics Today* 58, no. 5 (2005): 53-58.

Martens, H. C. F., P. W. M. Blom, and H. F. M. Schoo. "Comparative Study of Hole Transport in Poly(P-Phenylene Vinylene) Derivatives." *Physical Review B* 61, no. 11 (2000): 7489-93.

Martens, T., T. Munters, L. Goris, J. D'Haen, K. Schouteden, M. D'Olieslaeger, L. Lutsen, D. Vanderzande, W. Geens, J. Poortmans, L. De Schepper, and J. V. Manca. "Nanostructured Organic Pn Junctions Towards 3d Photovoltaics." *Applied Physics a-Materials Science & Processing* 79, no. 1 (2004): 27-30.

Massardier, V., V. B. Cajipe, T. P. Nguyen, and V. H. Tran. "Molecular Orientation in Cold-Stretched Poly(Phenylene Vinylene) Films." *Synthetic Metals* 75, no. 3 (1995): 169-73.

McGregor, D. S., and J. K. Shultis. "Spectral Identification of Thin-Film-Coated and Solid-Form Semiconductor Neutron Detectors." *Nuclear Instruments & Methods in Physics Research Section a-Accelerators Spectrometers Detectors and Associated Equipment* 517, no. 1-3 (2004): 180-88.

Melcher, C. L. "Scintillation Crystals for Pet." *Journal of Nuclear Medicine* 41, no. 6 (2000): 1051-55.

Mitchell, W. J., P. L. Burn, R. K. Thomas, and G. Fragneto. "Probing the Polymer-Electrode Interface Using Neutron Reflection." *Applied Physics Letters* 82, no. 16 (2003): 2724-26.

Mitchell, W. J., P. L. Burn, R. K. Thomas, G. Fragneto, J. P. J. Markham, and I. D. W. Samuel. "Relating the Physical Structure and Optical Properties of Conjugated Polymers Using Neutron Reflectivity in Combination with Photoluminescence Spectroscopy." *Journal of Applied Physics* 95, no. 5 (2004): 2391-96.

Moses, D., A. Dogariu, and A. J. Heeger. "Mechanism of Carrier Generation and Recombination in Conjugated Polymers." *Synthetic Metals* 116, no. 1-3 (2001): 19-22.

———. "Ultrafast Detection of Charged Photocarriers in Conjugated Polymers." *Physical Review B* 61, no. 14 (2000): 9373-79.

Natali, D., and M. Sampietro. "Detectors Based on Organic Materials: Status and Perspectives." *Nuclear Instruments & Methods in Physics Research Section a-Accelerators Spectrometers Detectors and Associated Equipment* 512, no. 1-2 (2003): 419-26.

Nouh, S. A., A. A. Naby, and P. J. Sellin. "Modification Induced by Proton Irradiation in Makrofol-De Polycarbonate." *Radiation Measurements* 42, no. 10 (2007): 1655-60.

Olsen, B. D., S. Y. Jang, J. M. Luning, and R. A. Segalman. "Higher Order Liquid Crystalline Structure in Low-Polydispersity Deh-Ppv." *Macromolecules* 39, no. 13 (2006): 4469-79.

Osterbacka, R., M. Wohlgenannt, M. Shkunov, D. Chinn, and Z. V. Vardeny. "Excitons, Polarons, and Laser Action in Poly(P-Phenylene Vinylene) Films." *Journal of Chemical Physics* 118, no. 19 (2003): 8905-16.

Ou, R. Q., R. Samuels, X. W. Wang, and R. Gregory. "Characterization of Anisotropic Structure in Poly(Phenylene Vinylene) Films." *Polymer Engineering and Science* 41, no. 10 (2001): 1705-13.

Owens, A., and A. Peacock. "Compound Semiconductor Radiation Detectors." *Nuclear Instruments & Methods in Physics Research Section a-Accelerators Spectrometers Detectors and Associated Equipment* 531, no. 1-2 (2004): 18-37.

Parada, M. A., A. de Almeida, C. Muntele, I. Muntele, and D. Ila. "Effects of Mev Proton Bombardment in Thin Film Pfa and Fep Polymers." *Surface & Coatings Technology* 196, no. 1-3 (2005): 378-82.

Park, Y. W., C. Park, Y. S. Lee, C. O. Yoon, H. Shirakawa, Y. Suezaki, and K. Akagi. "Electical-Conductivity of Highly-Oriented-Polyacetylene " *Solid State Communications* 65, no. 2 (1988): 147-50.

Peurrung, A. J. "Recent Developments in Neutron Detection." *Nuclear Instruments & Methods in Physics Research Section a-Accelerators Spectrometers Detectors and Associated Equipment* 443, no. 2-3 (2000): 400-15.

Pillon, M., M. Angelone, D. Lattanzi, M. Marinelli, E. Milani, A. Tucciarone, G. Verona-Rinati, S. Popovichev, R. M. Montereali, M. A. Vincenti, and A. Murari. "Neutron Detection at Jet Using Artificial Diamond Detectors." *Fusion Engineering and Design* 82, no. 5-14 (2007): 1174-78.

Plocharski, J., W. Pukacki, and S. Roth. "Conductivity Study of Stretch-Oriented New Polyacetylene " *Journal of Polymer Science Part B-Polymer Physics* 32, no. 3 (1994): 447-51.

Russell, D. M., C. J. Newsome, S. P. Li, T. Kugler, M. Ishida, and T. Shimoda. "Blends of Semiconductor Polymer and Small Molecular Crystals for Improved-Performance Thin-Film Transistors." *Applied Physics Letters* 87, no. 22 (2005).

Safadi, B., R. Andrews, and E. A. Grulke. "Multiwalled Carbon Nanotube Polymer Composites: Synthesis and Characterization of Thin Films." *Journal of Applied Polymer Science* 84, no. 14 (2002): 2660-69.

Sandberg, H. G. O., T. G. Backlund, R. Osterbacka, S. Jussila, T. Makela, and H. Stubb. "Applications of an All-Polymer Solution-Processed High-Performance, Transistor." *Synthetic Metals* 155, no. 3 (2005): 662-65.

Santos, S. J., and I. Salazar. "High Electric Field Effect on Hopping Conduction in Molecularly Doped Polymer Systems." *Polymer* 40, no. 15 (1999): 4415-18.

Sariciftci, N. S., L. Smilowitz, A. J. Heeger, and F. Wudl. "Photoinduced Electron-Transfer from a Conducting Polymer to Buckminsterfullerene " *Science* 258, no. 5087 (1992): 1474-76.

———. "Semiconducting Polymers (as Donors) and Buckminsterfullerene (as Acceptor) - Photoinduced Electron - Transfer and Heterojunction Devices " *Synthetic Metals* 59, no. 3 (1993): 333-52.

Schlesinger, T.E., and R. B. James, eds. *Semiconductors for Room Temperature Nuclear Detector Applications*. Edited by R.K. Willardson, A.C. Beer and E. R. Weber. Vol. 43, *Semiconductors and Semimetals*. San Diego, CA: Academic Press, 1995.

Shah, J., and E. Wilkins. "Electrochemical Biosensors for Detection of Biological Warfare Agents." *Electroanalysis* 15, no. 3 (2003): 157-67.

Shaheen, S. E., C. J. Brabec, N. S. Sariciftci, F. Padinger, T. Fromherz, and J. C. Hummelen. "2.5% Efficient Organic Plastic Solar Cells." *Applied Physics Letters* 78, no. 6 (2001): 841-43.

Shi, Y., J. Liu, and Y. Yang. "Device Performance and Polymer Morphology in Polymer Light Emitting Diodes: The Control of Thin Film Morphology and Device Quantum Efficiency." *Journal of Applied Physics* 87, no. 9 (2000): 4254-63.

Singh, N. L., N. Shah, K. P. Singh, and C. F. Desai. "Electrical and Thermal Behavior of Proton Irradiated Polymeric Blends." *Radiation Measurements* 40, no. 2-6 (2005): 741-45.

Singh, T. B., S. Gunes, N. Marjanovic, N. S. Sariciftci, and R. Menon. "Correlation between Morphology and Ambipolar Transport in Organic Field-Effect Transistors." *Journal of Applied Physics* 97, no. 11 (2005).

Sirringhaus, H. "Device Physics of Solution-Processed Organic Field-Effect Transistors." *Advanced Materials* 17, no. 20 (2005): 2411-25.

Sirringhaus, H., P. J. Brown, R. H. Friend, M. M. Nielsen, K. Bechgaard, B. M. W. Langeveld-Voss, A. J. H. Spiering, R. A. J. Janssen, and E. W. Meijer. "Microstructure-Mobility Correlation in Self-Organised, Conjugated Polymer Field-Effect Transistors." *Synthetic Metals* 111 (2000): 129-32.

Smith, P. F., N. J. T. Smith, J. D. Lewin, G. J. Homer, G. J. Alner, G. T. J. Arnison, J. J. Quenby, T. J. Sumner, A. Bewick, T. Ali, B. Ahmed, A. S. Howard, D. Davidge, M. Joshi, W. G. Jones, G. Davies, I. Liubarsky, R. A. D. Smith, N. J. C. Spooner, J. W. Roberts, D. R. Tovey, M. J. Lehner, J. E. McMillan, C. D. Peak, V. A. Kudryatsev, and J. C. Barton. "Dark Matter Experiments at the Uk Boulby Mine." *Physics Reports-Review Section of Physics Letters* 307, no. 1-4 (1998): 275-82.

Soci, C., D. Moses, and A. J. Heeger. "Effects of Bimolecular Recombination and Charge-Trapping on the Transient Photoconductivity of Poly(P-Phenylene Vinylene)." *Synthetic Metals* 153, no. 1-3 (2005): 145-48.

Soci, C., D. Moses, Q. H. Xu, and A. J. Heeger. "Charge-Carrier Relaxation Dynamics in Highly Ordered Poly(P-Phenylene Vinylene): Effects of Carrier Bimolecular Recombination and Trapping." *Physical Review B* 72, no. 24 (2005).

Spreitzer, H., H. Becker, E. Kluge, W. Kreuder, H. Schenk, R. Demandt, and H. Schoo. "Soluble Phenyl-Substituted Ppvs - New Materials for Highly Efficient Polymer Leds." *Advanced Materials* 10, no. 16 (1998): 1340-43.

Tanase, C., J. Wildeman, P. W. M. Blom, M. E. Mena Benito, D. M. de Leeuw, Ajjm van Breemen, P. T. Herwig, C. H. T. Chlon, J. Sweelssen, and H. F. M. Schoo. "Optimization of the Charge Transport in Poly(Phenylene Vinylene) Derivatives by Processing and Chemical Modification." *Journal of Applied Physics* 97, no. 12 (2005).

van Breemen, Ajjm, P. T. Herwig, C. H. T. Chlon, J. Sweelssen, H. F. M. Schoo, E. M. Benito, D. M. de Leeuw, C. Tanase, J. Wildeman, and P. W. M. Blom. "High-Performance Solution-Processable Poly(P-Phenylene Vinylene)S for Air-Stable Organic Field-Effect Transistors." *Advanced Functional Materials* 15, no. 5 (2005): 872-76.

van Duren, J. K. J., X. N. Yang, J. Loos, C. W. T. Bulle-Lieuwma, A. B. Sieval, J. C. Hummelen, and R. A. J. Janssen. "Relating the Morphology of Poly(P-Phenylene Vinylene)/Methanofullerene Blends to Solar-Cell Performance." *Advanced Functional Materials* 14, no. 5 (2004): 425-34.

Vasanthan, N. "Determination of Molecular Orientation of Uniaxially Stretched Polyamide Fibers by Polarized Infrared Spectroscopy: Comparison of X-Ray Diffraction and Birefringence Methods." *Applied Spectroscopy* 59, no. 7 (2005): 897-903.

Wang, K., S. Liang, R. N. Du, Q. Zhang, and Q. Fu. "The Interplay of Thermodynamics and Shear on the Dispersion of Polymer Nanocomposite." *Polymer* 45, no. 23 (2004): 7953-60.

Webster, G. R., W. J. Mitchell, P. L. Burn, R. K. Thomas, G. Fragneto, J. P. J. Markham, and I. D. W. Samuel. "Neutron Reflection Study on Soluble and Insoluble Poly[2-(2 '-Ethylhexyloxy)-5-Methoxy-1,4-Phenylenevinylene) Films." *Journal of Applied Physics* 91, no. 11 (2002): 9066-71.

Williams, E. D., R. U. Ayres, and M. Heller. "The 1.7 Kilogram Microchip: Energy and Material Use in the Production of Semiconductor Devices." *Environmental Science & Technology* 36, no. 24 (2002): 5504-10.

Wilson, T.M.S. , F.P. Doty, D.A. Chinn, A. Talin, M.J. King, L.L. Hunter, F.E. Jones, C. Cuppoletti, H. Rouchanian, and C. Munoz. "Transport Properties of Stretch-Oriented Ppv

Films." In *Conjugated Organic Materials -- Synthesis, Structure, Device, and Applications (Materials Research Society Symposium)*, 0937-M03-04. San Francisco, CA, 2006.

Wilson, T.M.S., D. Chinn, M.J. King, and F. P. Doty. "Organic Semiconductors for Detection of Ionizing Radiation." In *Nuclear Radiation Detection Materials (Materials Research Society Symposium)*, 1038-O03-02. Boston, MA, 2008.

Wilson, T.M.S., D.A. Chinn, D.B. Robinson, and F.P. Doty. "Post-Polymerization Alignment of Bulk Conjugated Polymers." *Applied Physics Letters (accepted)* (2008).

Wilson, T.M.S., D.A. Chinn, D.H. Morse, A.J. Antolak, M.J. King, R. Olsen, and F. P. Doty. "Correlation of Proton and Photon Induced Conductivity of a Poly(P-Phenylene Vinylene) Derivative." *IEEE Transactions on Nuclear Science (submitted)* (2008).

Wilson, Tiffany M. S., F. P. Doty, Douglas A. Chinn, Michael J. King, and Blake A. Simmons. "Order and Charge Collection Correlations in Organic Materials for Neutron Detection." In *Penetrating Radiation Systems and Applications VIII*, 670710-8. San Diego, CA, USA: SPIE, 2007.

Yang, C. Y., K. Lee, and A. J. Heeger. "Tensile Drawing Induced Symmetry in Poly(P-Phenylene Vinylene) Films." *Journal of Molecular Structure* 521 (2000): 315-23.

Yang, H. C., T. J. Shin, L. Yang, K. Cho, C. Y. Ryu, and Z. N. Bao. "Effect of Mesoscale Crystalline Structure on the Field-Effect Mobility of Regioregular Poly(3-Hexyl Thiophene) in Thin-Film Transistors." *Advanced Functional Materials* 15, no. 4 (2005): 671-76.

Yu, G., J. Gao, J. C. Hummelen, F. Wudl, and A. J. Heeger. "Polymer Photovoltaic Cells - Enhanced Efficiencies Via a Network of Internal Donor-Acceptor Heterojunctions " *Science* 270, no. 5243 (1995): 1789-91.

Zbinden, Rudolf. *Infrared Spectroscopy of High Polymers*. New York: Academic Press, 1964.

Zhao, Y. S., H. Z. Zhong, and Q. B. Pei. "Fluorescence Resonance Energy Transfer in Conjugated Polymer Composites for Radiation Detection." *Physical Chemistry Chemical Physics* 10, no. 14 (2008): 1848-51.

Stopping and Range of Ions in Matter Version 2008.03.

Zucolotto, V., A. D. Faceto, F. R. Santos, C. R. Mendonca, F. E. G. Guimaraes, and O. N. Oliveira. "Molecular-Level Control of the Photoluminescence from Ppv Nanostructured Films." *Journal of Physical Chemistry B* 109, no. 15 (2005): 7063-66.

Distribution

1	MS 0959	Douglas Chinn	
1	MS 0964	Roberto Mata	
1	MS 9004	William Ballard	
1	MS 9004	Brian Damkroger	
1	MS 9004	Jill Hruby	
1	MS 9161	William Even	
1	MS 9402	John Goldsmith	
1	MS 9402	Patrick Doty	
1	MS 9406	James Lund	
1	MS 9671	Michael King	
2	MS 9018	Central Technical Files	8944
1	MS 0899	Technical Library	9536
1	MS 0123	D. Chavez, LDRD office	1011